UV RESONANCE RAMAN EXCITATION PROFILES AND DEPOLARIZATION RATIOS AS PROBES OF ELECTRONIC TRANSITIONS IN PEPTIDES

by

Bhavya Sharma

B.S. in Exercise Science/Athletic Training, SUNY at Buffalo, 1999

M.S. in Exercise Science/Biomechanics, SUNY at Buffalo, 2001

Submitted to the Graduate Faculty of

School of Arts and Sciences in partial fulfillment

of the requirements for the degree of

Doctor of Philosophy

University of Pittsburgh

2011

UNIVERSITY OF PITTSBURGH

SCHOOL OF ARTS AND SCIENCES

This dissertation was presented

by

Bhavya Sharma

It was defended on

January 21, 2011

and approved by

Lillian T. Chong, Assistant Professor, Department of Chemistry

Sunil Saxena, Associate Professor, Department of Chemistry

Ronald Wetzel, Professor, Department of Structural Biology

Dissertation Advisor: Sanford A. Asher, Distinguished Professor, Department of Chemistry

UV RESONANCE RAMAN EXCITATION PROFILES AND DEPOLARIZATION RATIOS AS PROBES OF ELECTRONIC TRANSITIONS IN PEPTIDES

Bhavya Sharma, Ph.D.

University of Pittsburgh, 2011

UV resonance Raman (UVRR) spectroscopy is well established as a technique for probing secondary structure of peptides and proteins. Excitation between 180 to 215 nm, within the $\pi \rightarrow \pi^*$ electronic transitions of the peptide backbone, results in resonance enhancement of those amide vibrations that distort the peptide bond ground state geometry towards that of the excited state. Peptide bond amide $\pi \rightarrow \pi^*$ electronic transitions show no emission and appear to be homogeneously broadened. Their broad absorption spectra provide little information about the underlying excited states. UVRR spectroscopy is unique in its ability to provide insight into electronic excited state geometry and localization of electronic transitions. We use UVRR excitation profiles and Raman depolarization ratio measurements to examine the underlying peptide bond electronic transitions.

We measured the UVRR excitation profiles and Raman depolarization ratios of peptides in different conformations to elucidate the nature of these electronic transitions. We have examined short Ala peptides which adopt β-type conformations, such as: polyproline II, β-turn, and 2.5_1 helix, and found additional electronic transitions that underlie the NV_1 $\pi \rightarrow \pi^*$ transition. For a longer, 21-residue predominantly alanine peptide (AP), $A_5(AAARA)_3A$, we identified the excitation maxima for the α-helix and poly-proline II conformations, as well as exciton splitting in both conformations. We have also examined both the excitation profiles for the arginine (Arg) residues in AP, as well as the excitation profiles for individual Arg amino acid residues, to

determine how peptide conformation affects the individual residue chromophores and to determine the electronic interactions between the Arg and the peptide bond NV_1 $\pi \rightarrow \pi^*$ transition.

We show that UVRR excitation profiles and Raman depolarization ratios can be used together to uncover electronic transitions that underlie broad peptide absorption bands. We utilized the UVRR excitation profiles and Raman depolarization ratios to discover exciton splitting of the $\pi \rightarrow \pi^*$ electronic transition in AP, charge transfer transitions in short Ala peptides, and interactions between the electronic transitions of the AP peptide backbone and individual Arg side chains in AP. We find evidence of underlying transitions and unusual excitonic interactions that have not been predicted by theory.

TABLE OF CONTENTS

LIST OF TABLES

LIST OF FIGURES

ACKNOWLEDGEMENTS

I would like to thank Professor Sanford Asher for all of his guidance, patience, and support throughout my years at the University of Pittsburgh.

I also thank the members of the Asher Group, who have made my time at Pitt both successful and enjoyable. I would especially like to thank Sharon Mansfield for being the amazing, caring person that she is, always ready to help; Dr. Sergei Bykov, Dr. Nataliya Myshakina, and Lu Ma for their scientific collaboration, as well as for being wonderful friends.

Thank you Brian Barth, for your friendship and love, pop rocks, the turtle belly, chinchilla ears, and so much more.

Thank you Gurumayi, for all of your love and guidance throughout my life.

To my family, thank you for all of your unconditional love and encouragement.

1.0 INTRODUCTION

1.1 PROTEIN STRUCTURE

Beginning with the identification of DNA as a double helix in 1953,[1] and continuing with the completion of the Human Genome Project in 2003,[2,3] great advances have been made in our understanding of the structure and function of proteins over the last 50+ years. Proteins are involved in almost every aspect of maintaining a living organism. In normal, lean adult humans 12-18% of body mass is composed of proteins.[4] Proteins have a variety of functions in the human body, including as structural elements (collagen in tissue, hair, nails, etc.), storing and transporting molecules, regulating physiological processes (as hormones), protecting the body against foreign elements (as antibodies), components of muscle tissue (actin and myosin), and regulation of biochemical reactions (as enzymes).[4,5]

Proteins evolve from a linear primary structure to a distinct three-dimensional structure.[4-6] There are four structural components involved in this evolution from linear to three-dimensional units in proteins. The first is the primary structure of a protein, which is the linear sequence of amino acids that build the protein polypeptide chain, utilizing specific combinations of the twenty amino acids that exist. With the completion of the Human Genome Project, the primary structures of most proteins produced by DNA within the human body have been determined.

Even slight changes in the primary structure of a protein can have devastating health results. Sickle cell anemia is a disease where the primary structure of hemoglobin is changed by the substitution of a non-polar valine for a polar glutamic acid, making the hemoglobin more hydrophobic. This small change in primary structure results in the formation of sickle-shaped red blood cells, which have difficulty traveling through blood vessels due to their irregular shape.[4]

Secondary structure is specified by the arrangement of the polypeptide chain into specific conformations, such as those in an α-helix or β-sheet.[4-6] The secondary structures of many proteins, such as chymotrypsin,[7,8] ribonuclease A,[9] ribonuclease S,[10] etc., have been established through techniques such as x-ray crystallography.[11] Secondary structure is stabilized by hydrogen bonding along the peptide backbone.[4] Tertiary structure is composed of the arrangement of secondary structure elements, which are often compacted into globular polypeptide domains. The final structural element of proteins is quaternary structure which is composed of organized multiple tertiary structure units. Changes in the conformation of a protein are often related to both tertiary and quaternary changes. Examples of the four structural components of a protein are shown in Figure 1.1.

Ideally, we would like to be able to predict the 3-dimensional structure of a protein from its primary structure. In some circumstances this is not currently possible, however, because there are a number of amino acid combinations that result in similar secondary structures. Also, there is little known about the energy required for the formation of the secondary structures and how a peptide or protein chooses the most energetically favorable conformation. To gain the understanding necessary to predict of 3D structure from primary structure, secondary structures and their energetic landscapes need to be determined experimentally. The most common

techniques for determining structure of proteins and peptides are x-ray crystallography,[11] NMR,[13-15] circular dichroism,[16,17] fluorescence,[18,19] and electron microscopy.[20,21] To date, in the RCSB Protein Data Bank there are more than 35,000 structures which have been defined by these techniques.[22]

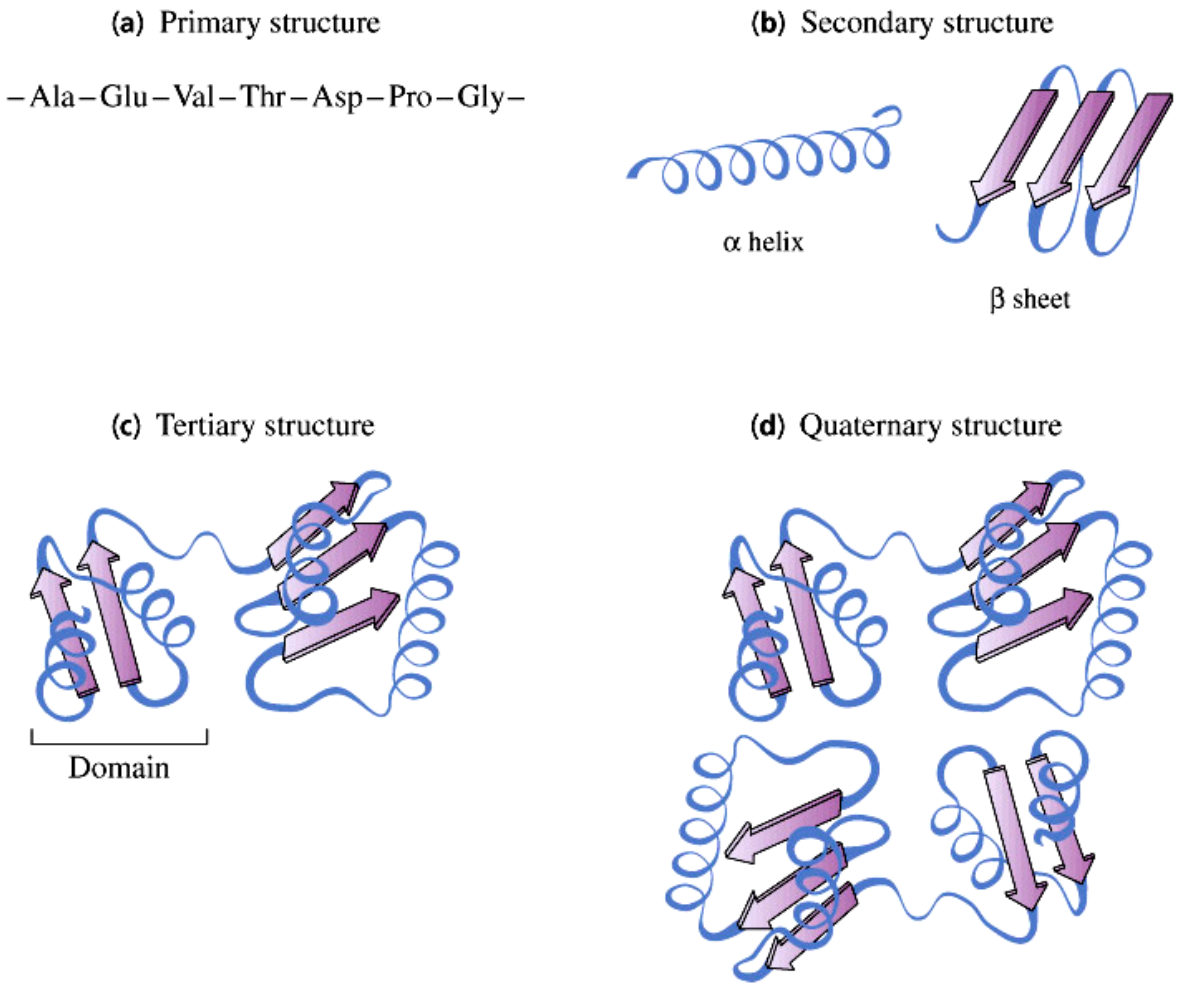

Figure 1.1 Protein structural units: (a) primary, (b) secondary, (c) tertiary, (d) quaternary (from Ref. 12).

Protein structure is built of amino acids joined together to form peptide units, which then form polypeptide chains. Examining peptide units gives further insight to how secondary structure is formed. To form a peptide bond at least two amino acids are required. The differences between the twenty amino acids arise from the side chain groups attached to their backbone. The backbone consists of a central carbon atom (C_α), which is attached to both an amino group (NH_2) and a carbonyl group (C=O; Figure 1.2a).

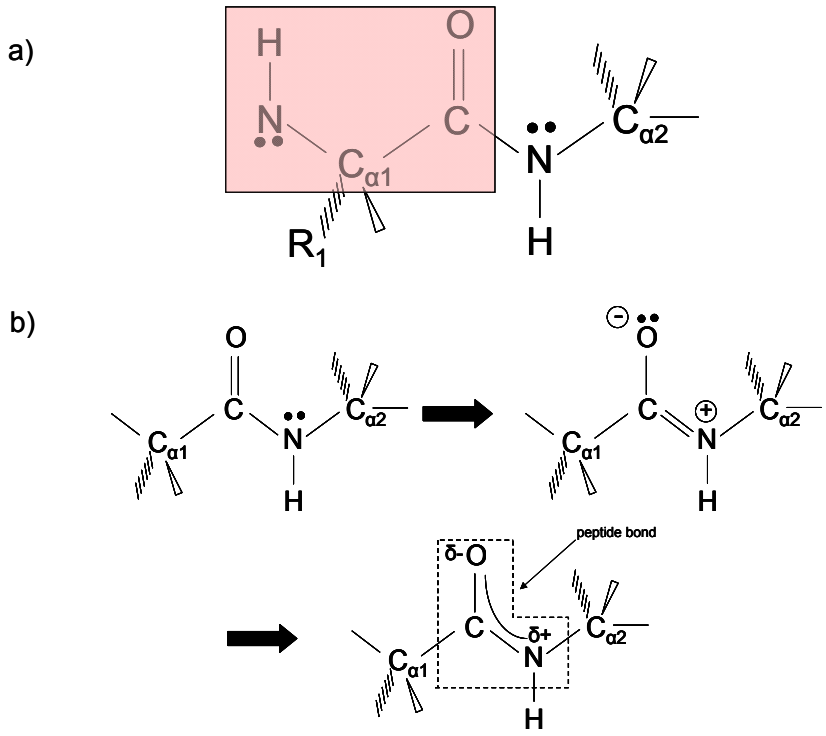

Figure 1.2 Schematic of (a) the peptide backbone, which is highlighted in pink and (b) the resonance structure of the peptide bond unit.

The amino acids can be divided into three main groups based on the characteristics of their side chains, hydrophobic, charged, and polar. The hydrophobic amino acids are alanine (Ala), cysteine (Cys), isoleucine (Ile), leucine (Leu), methionine (Met), phenylalanine (Phe), proline (Pro), tryptophan (Trp), tyrosine (Tyr), and valine (Val). Arginine (Arg), aspartic acid (Asp), glutamic acid (Glu), histidine (His), and lysine (Lys) have charged side chains; and asparagine (Asn), glutamine (Gln), serine (Ser), and threonine (Thr) are polar.[6] The peptide bond unit is formed when the carbonyl group of the first amino acid covalently bonds with the amino group of the adjacent amino acid, as shown in Figure 1.2b. This bond has partial double bond character because of competing electronegativities between the amino N and carbonyl O for π valence electrons. This partial double bond character also results in restriction of rotation about the bond, with the asymmetric distribution of electrons resulting in a dipole moment.[5,23,24] The polypeptide chain is built as successive amino acids repeat the peptide bond building process.

The peptide units are in a fixed plane with all of the peptide bond lengths and bond angles being relatively the same for the backbone. The rigidity of the backbone allows rotation only about the C_α – N bonds and the C_α – C bonds. The angles of rotation about these bonds are labeled as Φ and Ψ, respectively (Figure 1.3). One could assume that any combination of Φ and Ψ angles would be possible. Allowed conformations of structures, however, are limited by spatial restrictions due to steric interactions of the van der Waals radii of the atoms between the peptide backbone and side chain atoms.[23,24] Ramachandran et al (1963)[25] determined a set of allowed contact distances between different atoms and used these distances to establish which combinations of Φ and Ψ angles are allowed. Using these data, they then developed a conformational map of allowed conformations. The original map had angles ranging from 0 to

360° (Figure 1.4a),[25] the modern version has the two intersecting axes set as 0°, and the range goes from -180° to 0° to +180° (Figure 1.4b).[12] Within the quadrants of the map, individual secondary structures are found, as labeled in Figure 1.4b.

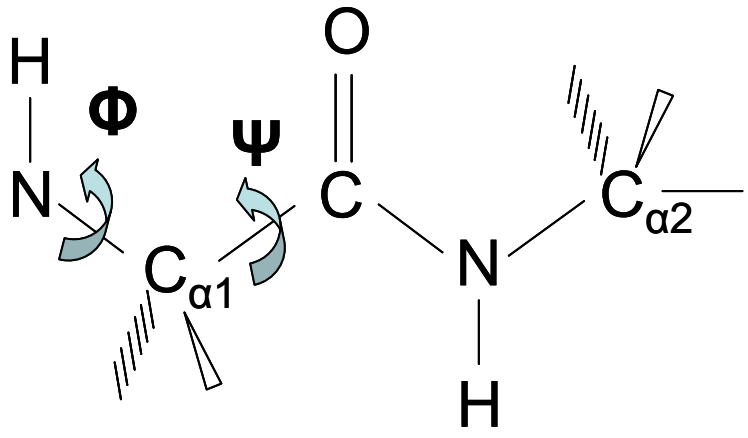

Figure 1.3 Peptide dihedral angles (Φ, Ψ) about the Cα-N and Cα-C bonds, respectively.

The two predominant secondary structures are α-helices and β-sheets. Any helical structure is built about a central axis. Two parameters define the type of helix: the number of peptide units per turn (n) and the helical rise per residue (h).[24] Ramakrishnan (1964)[26] determined a geometrical correlation between the n and h parameters and Φ and Ψ angles. Today, these parameters have been updated and include not only n and h (now referred to as r), but also helical pitch (p) which is rise (Å/turn). Table 1.1 lists the Φ and Ψ angles, n, r, and p for different types of helices and β-strands[5,24] and Figure 1.5 shows images of the different types of helices.

Table 1.1 Types of helices with (Φ, Ψ) angles, n is the number of residues per helical turn, r is the helical rise per residue, and p is the helical pitch (Å/turn). Data compiled from Ramachandran, 1968[25] and Creighton, 1993.[5]

Helix type	Phi	Psi	n	r(Å)	p(Å)	H-bond (CO, HN)	Atoms in H-bonded loop	Radius (Å) (backbone)
alpha	-57.8	-47.0	+3.6	1.5	5.5	i, i+4	13	2.3
3.10	-74.0	-4.0	+3.0	2.0	6.0	i, i+3	10	1.9
pi	-57.1	-69.7	+4.4	1.1	5.0	i, i+5	16	2.8
PPII	-75.0	145.0	+3.0	3.12	9.0			
beta strand	-139.0	135.0	+2.0	3.4	6.8			

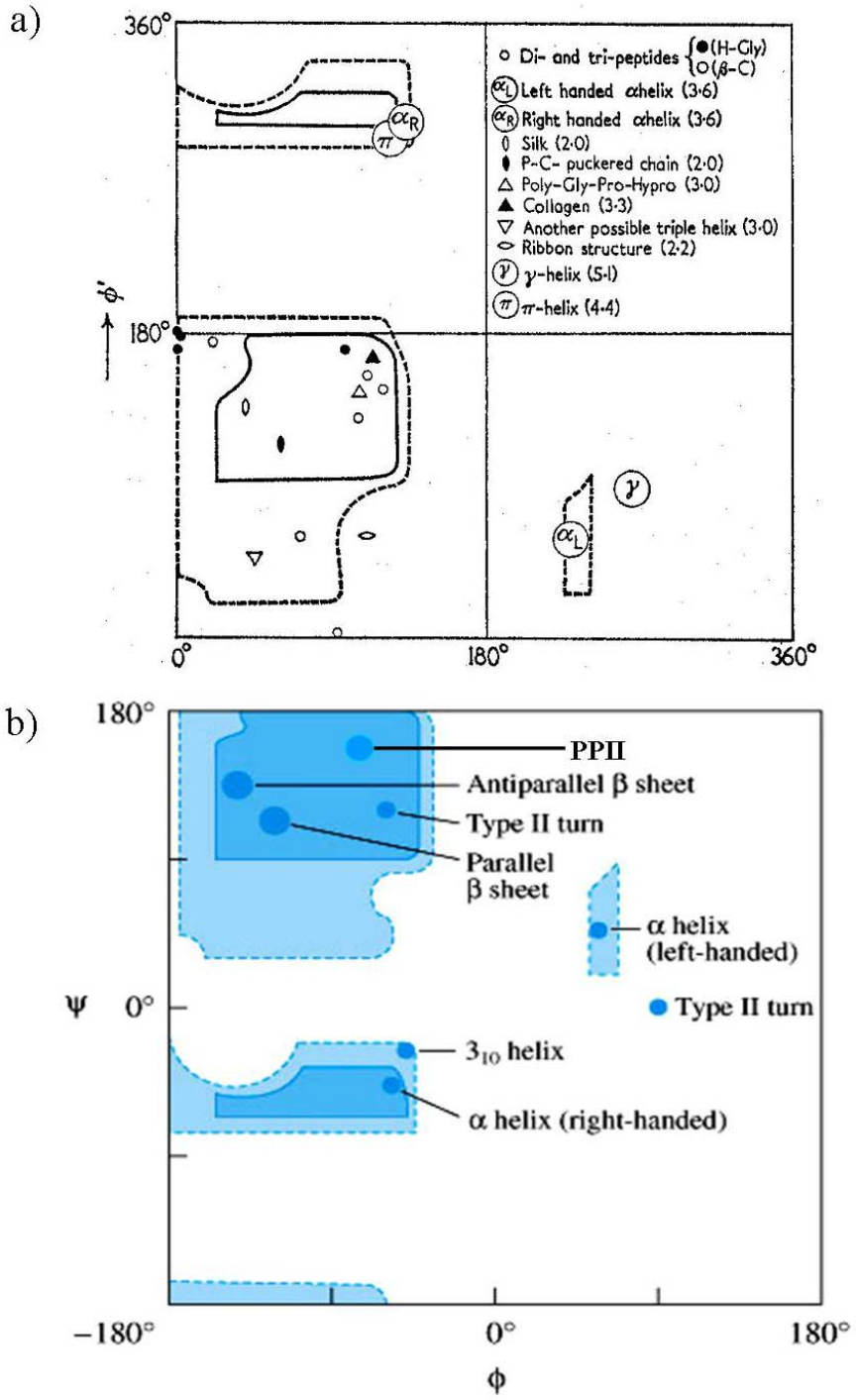

Figure 1.4 (a) Original Ramachandran plot.[25] (b) Modern version of the Ramachandran plot with various secondary structures labeled according to their (Φ, Ψ) dihedral angles.[12]

The α-helix was first proposed by Pauling and Corey in 1950,[27] and fully characterized in 1951.[28,29] They based their predicted structure on parameters such as interatomic distances, bond angles, and other configurational parameters derived from the crystal structure of amino acids.28 The α-helix has (Φ, Ψ) = (-58°, -47°), with 3.6 residues per turn, and the i^{th} residue hydrogen bonded to the $i+4^{th}$ residue. This bonding pattern results in all of the hydrogen bonds pointing in the same direction, with the peptide units aligned in the same orientation along the helical axis.[5,6] With the peptide units aligned in the same direction, the dipole moments of the units also align in the same direction. This results in a net dipole moment aligned along the helical axis, with the partial positive charge at the amino terminus and the partial negative charge at the carboxy terminus.[5,6]

In 1951, Pauling and Corey also described the structure of a pleated sheet structure, now known as a β-sheet.[30] The elementary unit of a β-sheet is the β-strand, a fully extended polypeptide chain. A β-sheet is built of adjacent β-strands which are hydrogen-bonded together. The β-sheet can be either parallel, with the strands running in the same direction, from amino terminal to carboxy terminal; or anti-parallel, with the strands running in opposite directions.[5,6] β-sheets have proven to be difficult to study because the structures do not readily dissolve and they have a tendency to aggregate at experimental concentrations.[5] β-hairpins more readily dissolve in solution, so they present an alternative to studying β-sheets.

There are other, less prevalent secondary structures which exist, including the 3_{10} helix and the π helix, which are variations on the α-helix motif (Table 1.1). The 3_{10} helix is more tightly coiled than the α-helix, with the i^{th} residue bonding to the $i+3^{rd}$ residue.[5] The (Φ, Ψ) for the 3_{10} helix are (-74°, -4°).[5,24] The π helix is less tightly wound than the α-helix, with the i^{th} residue bonding to the $i+5^{th}$ residue.[5] The (Φ, Ψ) for the π helix are (-57°, -70°).[5,24] The final

secondary structure to be discussed here (although others do exist) is what was previously referred to as "random coil," but is now accepted to be a mainly poly-proline II (PPII) helix.[32-36] The difference in designation will be discussed later. Although the name implies that the helical structure is obtained only with prolines, it has been shown that this structure exists for other amino acids. The PPII helix is a left-handed helix with 3.3 residues/turn (Table 1.1). The (Φ, Ψ) for the PPII helix are (-145°, -75°).

1.2 ELECTRONIC TRANSITIONS

Experiments performed with absorption spectroscopy, circular dichroism, and optical rotatory dispersion in the 1950s and 1960s helped to determine the classical electronic transitions found in peptides.[37-59] The present theoretical consensus is that three electronic transitions occur in simple amides in the 230 to 130 nm range (Figure 1.5). These electronic transitions include the weak n→π* transition (210 to 230 nm), the strong NV_1 π→π* transition (170 to 195 nm), and a second, weaker NV_2 π→π* transition (135 to 160 nm).[37,41-48,55,56] Along with the classically defined transitions, other transitions have been reported that include charge transfer electronic transition states (Figure 1.6),[47,48,57,58,60] as well as Rydberg transitions.[37,41-43,49]

In α-helices a weak n→π* electronic transition is thought to occur at ~ 220 nm while a higher frequency NV_1 π→π* electronic transition occurs at ~ 190 nm. This π→π* transition in the α-helix is understood to undergo exciton splitting which gives rise to two dipole-allowed transitions: one perpendicular to the helical axis at 190 nm and the second parallel to the axis at 205 nm.[38,50-54] α-helices have been demonstrated by our group, as well as others, to melt to a predominantly left-handed polyproline II (PPII) helix-like conformation and not a random coil

conformation.[33-36,39] The transitions in PPII helices involve an n→π* transition at ~ 220 nm and a π→π* transition at ~ 200 nm. Theory has not yet been able to accurately model the excited states found in a PPII helix such that they can predict circular dichroism (CD) and absorption spectra.[54] It has been suggested that, for the PPII conformation, a mixing of the π→π* transition with higher energy transitions must be included in calculations to accurately reproduce the CD and absorption experimental data.[54] For β-sheets, the π→π* transition occurs at ~ 194 nm for parallel sheets and ~196 nm for anti-parallel sheets. The n→π* transition occurs at ~217 nm, regardless of strand orientation in the sheet.[40] The electronic transitions for other conformations, such as β-turns, 3_{10}-helix, π-bulge/helix and 2.5_1 helix, have not been clearly defined.

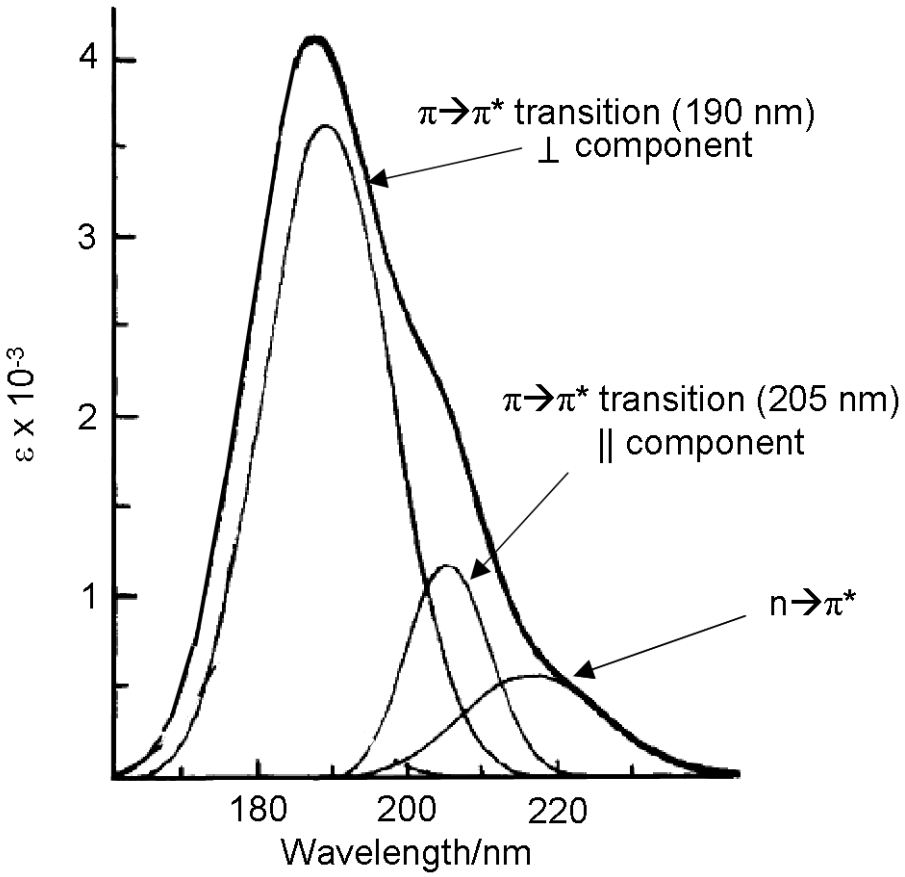

Figure 1.5 Poly-alanine absorption spectrum with the three classical electronic transitions labeled (Figure adapted from Ref. 59).

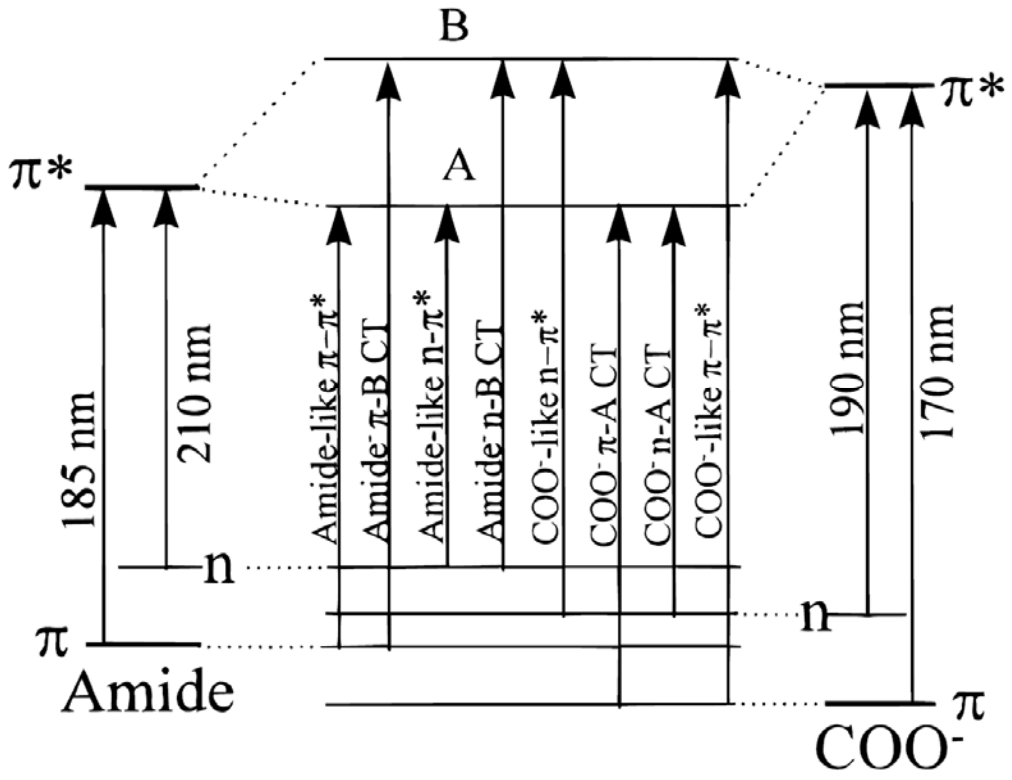

Figure 1.6 Energy level diagram of the isolated orbitals of the amide and carboxylate groups with the classical transitions labeled. Also shown are the levels A and B, which are molecular orbitals that result from the interaction of the amide and carboxyl group π.

1.3 UNDERSTANDING EXCITED STATES

Often when investigating the electronic states of molecules, only the ground electronic state is considered. People think in the framework of how the properties of the molecule in its ground electronic state will change when it is perturbed by mechanical strain, an electric field, etc. It is important however, to understand the nature of the electronic excited states of biomolecules because the excited state geometries determine how the ground state can assume unusual ground

electronic state geometries and dynamics. The effect of an applied perturbation is best understood by knowing what the electronic excited state looks like, since these states enable changes in the ground electronic state structure and dynamics.

In perturbation theory, we calculate how the energy of a system changes in response to an applied perturbation. This is calculated as a sum over the electronic excited states, and is weighted by a denominator that gives information about how far in energy the electronic excited state is from the ground electronic state. We study electronic excited states because we gain insight into how a biological molecule will respond to a perturbation.

In biology, it is essential to characterize the electronic excited states of molecules in order to fully understand their role in biological function, especially molecules involved in respiration, in photosynthesis, as photoreceptors, and in energy transduction pathways.[61-65] Charge transfer is an important process in photosynthesis, where light-harvesting and photo-protection involve energy transfer between singlet and triplet excited states.63, [65, 66] Electron transfer processes are also essential elements of energy transduction pathways, specifically across protein-protein interfaces.[63] Proteins such as photoactive yellow protein and rhodopsin are photoreceptors, which initiate a signal transduction cascade upon exposure to light.[64] Numerous theoretical and experimental studies have been performed to characterize the complex excited states of these proteins.[64]

1.4 REFERENCES

1. Watson, J.D. and Crick, F.H.C. *Nature*, **1953**, *171*, 737.

2. International Human Genome Mapping Consortium *Nature,* **2001**, *409***,** 934.

3. Collins, F.S., Green, E.D., Guttmacher, A.E., and Guyer, M.S. *Nature,* **2003,** *422***,** 835.

4. Tortora, G.J. and Grabowski, S.R. Principles of Anatomy and Physiology 8th ed. New York: HarperCollins College Publishers, **1996**.

5. Creighton, T.E. Proteins: Structures and Molecular Properties, 2nd ed. New York: W.H. Freeman & Co., **1993**.

6. Branden, C. and Tooze, J. Introduction to Protein Science. New York: Garland Publishing, Inc., **1991**.

7. Matthews, B.W., Sigler, P.B., Henderson, R., and Blow, D.M. *Nature*, **1967**, ***214***, 652.

8. Kraut, J., Wright, H.R., Kellerman, M., and Freer, S.T. *Proc. Natl. Acad. Sci. USA*, **1967**, *58*, 304.

9. Kartha, G., Bello, J., and Harker, D. *Nature*, **1967**, *213*, 862.

10. Wyckoff, H.W., Hardman, K.D., Allewell, N.M., Inagami, T., Johnson, L.N., and Richards, F.M. *J. Biol. Chem.,* **1967**, *242*, 3984.

11. Stryer, L. *Ann. Rev. Biochem.,* **1968**, *37***,** 25.

12. Horton, H.R., Moran, L.A., Ochs, R.S., Rawn, J.D., and Scrimgeour, K.G. Principles of Biochemistry, 3rd ed., New Jersey: Prentice Hall, **2002**.

13. Smurnyy, Y. and Opella, S.J. *Magn. Reson. Chem.,* **2006**, *44*, 283.

14. Jennings, P.A. and Wright, P.E. *Science,* **1993**, *262*, 892.

15. Hughson, F.M., Wright, P.E., and Baldwin, R.L. *Science,* **1990**, *249*, 1544.

16. Kelly, S.M. and Price, N.C. *Curr. Protein Pept. Sc.,* **2000**, *1*, 349.

17. Wallace, B.A. *J. Synchrotron Rad.,* **2000**, *7*, 289.

18. Engelborghs, Y. (2003) *J. Fluoresc.,* **2003**, *13*, 9.

19. Teale, F.W.J. *Biochim. Biophys. Acta,* **1959**, *35*, 5.

20. Topf, M. and Sali, A. *Curr. Opin. Struc. Biol.,* **2005**, *15*, 578.

21. McGuire, N.K. *Modern Drug Discovery,* **2002**, *5*, 43.

22. Berman, H.M., Westbrook, J., Feng, Z., Gilliland, G., Bhat, T.N., Weissig, H., Shindyalov, I.N., and Bourne, P.E. *Nucleic Acid Res.,* **2000**, *28*, 235.

23. Pauling, L. The Nature of the Chemical Bond, 3rd ed., Ithaca, NY: Cornell University Press, **1960**.

24. Ramachandran, G.N. and Sasisekharan, V. *Adv. Prot. Chem.,* **1968**, *23*, 283.

25. Ramachandran, G.N., Ramakrishnan, C., and Sasisekharan, V. *J. Mol. Biol.,* **1963**, *7*, 95.

26. Ramakrishnan, C. *Indian Acad. Sci. Section A,* **1964**, *59*, 327.

27. Pauling, L. and Corey, R.B. *J. Am. Chem. Soc.,* **1950**, *72*, 5349.

28. Pauling, L., Corey, R.B., and Branson, H. R. *Proc. Natl. Acad. Sci. USA,* **1951**, *37*, 205.

29. (a) Pauling, L. and Corey, R.B. *Proc. Natl. Acad. Sci. USA,* **1951**, *37*, 235.

30. (b) Pauling, L. and Corey, R.B. *Proc. Natl. Acad. Sci. USA,* **1951**, *37*, 729.

31. Mikhonin, A. V.; Bykov, S. V.; Myshakina, N. S.; Asher, S. A. *J. Phys. Chem. B* **2006,** *110*, 1928.

32. Asher, S. A.; Mikhonin, A. V.; Bykov, S. *J. Am. Chem. Soc.* **2004,** *126*, 8433.

33. Blanch, E. W.; Morozova-Roche, L. A.; Cochran, D. A. E.; Doig, A. J.; Hecht, L.; Barron, L. D. *J. Molec. Biol.* **2000,** *301*, 553.

34. Shi, Z.; Woody, R. W.; Kallenbach, N. R. *Adv. Prot. Chem.* **2002,** *62*, 163.

35. Ramakrishnan, V.; Ranbhor, R.; Durani, S. *J. Am. Chem. Soc.,* **2004,** *126,* 16332.

36. Asciutto, E. K.; Mikhonin, A. V.; Asher, S. A.; Madura, J. D. *Biochemistry*, **2008,** *47,* 2046.

37. Hunt, H. D.; Simpson, W. T. *J. Am. Chem. Soc.,* **1953**, *75*, 4540.

38. Moffitt, W. *J. Chem. Phys.*, **1956**, *25*, 467.

39. Asher, S.A.; Mikhonin, A.V.; Bykov, S.V. *J. Am. Chem. Soc.* **2004**, *126*, 8433.

40. Woody, R.W. *Tetrahedron: Asymmetry* **1993**, *4*, 529.

41. Peterson, D. L.; Simpson, W. T. J. *Am. Chem. Soc.* **1957**, *79,* 2375.

42. Basch, H.; Robin, M. B.; Kuebler, N. A. *J. Chem. Phys.* **1967**, *47*, 1201.

43. Basch, H.; Robin, M. B.; Kuebler, N. A. *J. Chem. Phys.* **1968**, *49*, 5007.

44. Schellman, J. A.; Nielsen, E. B. *J. Phys. Chem.* **1967**, *71*, 3914.

45. Barnes, D. G.; Rhodes, W. *J. Chem. Phys.* **1968**, *48*, 817.

46. Serrano-Andres, L.; Fuelscher, M. P. *J. Am. Chem. Soc.* **1998**, *120*, 10912.

47. Serrano-Andres, L.; Fuelscher, M. P. *J. Phys. Chem. B* **2001**, *105*, 9323.

48. Clark, L. B. *J. Am. Chem. Soc.* **1995**, *117*, 7974.

49. Robin, M. B. Higher Excited States of Polyatomic Molecules, vol. III; Academic Press, Inc.: New York, 1985.

50. Rosenheck, K.; Doty, P. *Proc. Natl. Acad. Sci. U.S.A.* **1961**, *47*, 1775.

51. Brahms, J.; Pilet, J.; Damany, H.; Chandrasekharan, V. *Proc. Natl. Acad. Sci. U.S.A.* **1968**, *60*, 1130.

52. Brahms, S.; Brahms, J. *J. Molec. Biol.* **1980**, *138*, 149.

53. Mandel, R.; Holzwarth, G. *J. Chem. Phys.* **1972**, *57*, 3469.

54. Woody, R. W. *Monatshefte fur Chemie* **2005**, *136*, 347.

55. Johnson, W. C., Jr.; Simpson, W. T. *J. Chem. Phys.* **1968**, *48*, 2168.

56. Moffitt, W. *J. Chem. Phys.* **1956**, *25*, 467.

57. Kaya, K.; Nagakura, S. *Theor. Chim. Acta* **1967**, *7*, 117.

58. Nagakura, S. *Mol. Phys.* **1960**, *3*, 105.

59. Quadrifoglio, F.; Urry, D.W. *J. Am. Chem. Soc.*, **1968**, *90*, 2755.

60. Chen, X. G.; Li, P.; Holtz, J. S. W.; Chi, Z.; Pajcini, V.; Asher, S. A.; Kelly, L. A. *J. Am. Chem. Soc.* **1996**, *118*, 9716

61. Hsu, C.-P. *Acct. Chem. Res.* **2009**, *42*, 509.

62. Alarcon, E.; Gonzalez-Bejar, M.; Gorelsky, S.; Ebensperger, R.; Lopez-Alarcon, C.; Netto-Ferreira, J. C.; Scaiano, J. C. *Photochem. Photobiol. Sci.*, **2010**, *9*, 1378.

63. Gray, H. B.; Winkler, J. R. *Quart. Rev. Biophys.* **2003**, *36*, 341.

64. Ma, Y.; Rohlfing, M.; Molteni, C. *Phys. Rev. B*, **2009**, *80*, 241405(R).

65. McLendon, G.; Hake, R. *Chem. Rev.*, **1992**, *92*, 481.

66. Cogdell, R. J.; Howard, T. D.; Bittl, R.; Erberhard, S.; Geisenheimer, I.; Lubitz, W. *Phil.Trans. R. Soc. Lond. B* **2000,** *355*, 1345.

2.0 THEORY OF RAMAN SCATTERING

2.1 INTRODUCTION

Ultraviolet (UV) resonance Raman spectroscopy (UVRRS) has been shown to be a powerful technique for probing the molecular structure of polypeptides and proteins.[1-15] Raman spectroscopy derives from the coupling that occurs between the applied electromagnetic radiation and the polarizability of a molecule. The resonance Raman effect becomes prevalent when the wavelength of the applied electromagnetic radiation falls within an electronic absorption band, which causes the vibrations of the absorbing molecule to be selectively enhanced. In UVRRS, this excitation can be within the $\pi \rightarrow \pi^*$ electronic transitions of peptide bonds, which occur between 180-215 nm. Excitation in this region results in UVRRS dominated by peptide bond amide vibrations, which differ for the different types of secondary structure of a protein or polypeptide.

The vibrational Raman frequencies provide information about the geometry and electronic structure of a molecule in the ground state, whereas the intensities of the Raman lines provide information about the symmetry, equilibrium geometry, and dynamics of the resonant excited state.[16] Although the relationship between Raman intensities and the excited state is known, little has been done to utilize experimental intensities to gain quantitative information about the resonant excited state. This is partly due to the complexity of the theory of resonance Raman scattering where, even with simple approximations, there is no *direct* relationship

between intensities and properties of the excited state. While different theories attempt to explain resonance Raman scattering, only the Kramers-Heisenberg-Dirac theory involving summation over all states, will be discussed here.

2.2 KRAMERS-HEISENBERG-DIRAC APPROACH

Placzek [17] first introduced the concept of polarizability with respect to Raman scattering in 1934. This work contributed significantly to the understanding of the Raman Effect which was experimentally discovered by C. V. Raman in 1928. Placzek's theory is related to excitation in areas of the spectrum which lie far from the absorption bands, and involves examining polarizability (α) as a function of normal coordinates (Q). A fundamental component of Raman theory is the Kramers-Heisenberg dispersion equation,[18] which is derived from second-order time dependent perturbation theory.[16,19-21] The total radiated power from a Raman transition from an initial state $|I\rangle$ to another state $|F\rangle$ is given as:

$$P_{I \to F} = I \cdot \sigma_{I \to F}(E_L) \qquad \textbf{(2.1)}$$

where the probability of Raman scattering from I to F is proportional to the Raman cross section $\sigma_{I \to F}$,

$$\sigma_{I \to F}(E_L) = \frac{8\pi e^4 E_s^3 E_L}{9\hbar^4 c^4} \sum_{\rho,\lambda} |\,(\alpha_{\rho\lambda})_{I \to F}\,|^2 \qquad \textbf{(2.2)}$$

with E_s and E_L are the scattered and incident light, respectively, and $\alpha_{\rho\lambda}$ is the polarizability tensor, with the incident (λ) and scattered (ρ) light polarization.

Theoretically, the intensity of a Raman band is give as:[22]

$$I_{IF} = c \cdot I_o \cdot (\nu_o - \nu_{IF})^4 \sum_{\rho,\lambda} \left| (\alpha_{\rho\lambda})_{IF} \right|^2 \qquad \textbf{(2.3)}$$

where c is a constant, I_o is the incident laser beam of frequency ν_o, $(\nu_o - \nu_{IF})^4$ is the difference between the incident laser frequency (ν_o) and the frequency of the transition (ν_{IF}), and $(\alpha_{\rho\lambda})_{IF}$ is the Raman polarizability for the I → F transition.

The second-order perturbation theory equation for polarizability is given in a sum over eigenstates as:

$$(\alpha_{\rho\lambda})_{I\to F} = \sum_V \frac{\langle F|m_\rho|V\rangle\langle V|m_\lambda|I\rangle}{E_V - E_I - E_L - i\Gamma_V} + \frac{\langle F|m_\lambda|V\rangle\langle V|m_\rho|I\rangle}{E_V - E_F + E_L - i\Gamma_V} \qquad \textbf{(2.4)}$$

where E_L is incident photon energy; $|I\rangle$, $|V\rangle$, $|F\rangle$ are the initial, intermediate, and final vibronic states, respectively, with the sum being over all intermediate states; m_ρ and m_λ are the vector components of the transition dipole moment operators, Γ_v are the homogeneous linewidths of the electronic transitions, and $i\Gamma_v$ is the damping constant related to the lifetime of the intermediate states $|V\rangle$.[22]

Several approximations can be made to simplify eqn. 2.2 and 2.3. The first is application of the Born-Oppenheimer approximation in which the vibronic states are factored into products of the electronic and vibrational states. This simplifies the dipole moment matrix elements. The second approximation applied is the Condon approximation, where it is assumed that since during resonance the strong electronic transition occurs on a time scale that is significantly shorter than the nuclear motion, the nuclear coordinate can be neglected. Resonance occurs when the incident photon energy (E_L) approaches the energy of an allowed transition ($E_0 + \varepsilon_v - \varepsilon_i$), at which the first term (the resonant term) in equation 2.4 becomes dominant, so the second

term (non-resonant term) can be neglected. Taking the approximations into account, the polarizability becomes

$$\alpha_{I\to F}(E_L) = M^2 \sum_V \frac{\langle f|v\rangle\langle v|i\rangle}{\varepsilon_v - \varepsilon_i + E_0 - E_L - i\Gamma} \qquad \textbf{(2.5)}$$

and the Raman cross section is given by

$$\sigma_{I\to F} = (5.87x10^{-19}) M^4 E_S^3 E_L \left| \sum_V \frac{\langle f|v\rangle\langle v|i\rangle}{\varepsilon_v - \varepsilon_i + E_0 - E_L - i\Gamma} \right|^2 \qquad \textbf{(2.6)}$$

Here, E_0 is the zero-zero energy separation between the lowest vibrational levels of the ground and excited states; M is the electronic transition moment matrix element; $|v\rangle$ and $|i\rangle$ are vibrational states with energies ε_v and ε_I (Figure 2.1). Equations 2.5 and 2.6 are related to the Albrecht A-term expression for excitation within an allowed absorption band (electronic transition).[23]

In Albrecht's A-term scattering mechanism[23] excitation which results in scattering couples the ground state and the excited state.[24] Initially the treatment of resonance Raman scattering is restricted to a single resonant state. The A-term is non-zero if two conditions are fulfilled: (i) the transition dipole moments are non-zero and (ii) the products of the vibrational overlap integrals (Franck-Condon factors) are non-zero for some of the excited vibronic states. Condition (i) is fulfilled if the resonant electronic transition is electric dipole-allowed.

Strong A-term resonance Raman scattering is observed for excitation within intense electronic absorption bands;[16,23] e.g., a charge transfer or a $\pi\rightarrow\pi^*$ transition. Weak absorption bands, such as ligand-field bands and those arising from other forbidden transitions do not produce significant A-term enhancement. When there is a difference between the nuclear

geometry of the ground and the electronic excited states, it results in strong A-term resonance enhancement.[23,24]

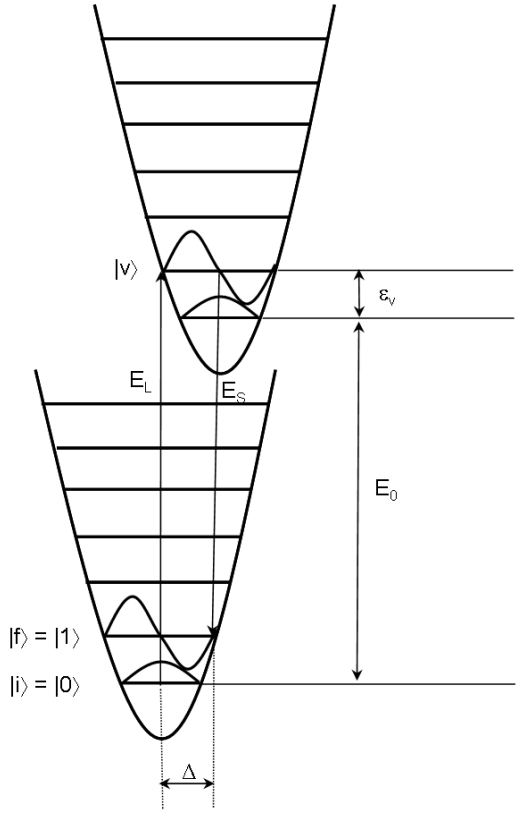

Figure 2.1 Raman scattering in a harmonic system. |i⟩ is excited by the incident light with energy E_L to a virtual levels |v⟩. It returns to a final level |f⟩, emitting a photon with energy E_S. Δ is the displacement of the potential between the ground and excited states.[16,19]

The enhanced vibrational modes are localized on the atoms whose electrons contribute to the electronic transitions, namely in our case the peptide bonds. Relative Raman intensities depend on both oscillator strengths and the Franck-Condon overlaps. To evaluate the Franck-Condon factors, ⟨f | v⟩ in equation 2.6, the Franck-Condon principle is applied, which is an approximation that the ground and excited state surfaces are harmonic and differ only in

equilibrium position (Figure 2.1).[16,22,23,25] Based on this assumption, the vibrational frequencies and normal coordinates are identical in the ground and excited states. Thus, the vibrational modes (N) can now be treated as N harmonic oscillators, as in Figure 2.1. This assumption can then be used to simplify the Franck-Condon factors into one-dimensional overlaps:

$$\langle f | v \rangle = \prod_{j=1}^{N} \langle f_j | v_j \rangle \qquad \textbf{(2.7)}$$

Based on these one-dimensional overlaps the fundamental Raman scattering can then be re-written as:

$$\alpha_{i \to i+1} = M^2 \sum_{v_1}^{\infty} \sum_{v_2}^{\infty} \cdots \sum_{v_N}^{\infty} \frac{\langle (i+1)_1 | v_1 \rangle \langle v_1 | i_1 \rangle \prod_{j=2}^{N} \langle i_j | v_j \rangle \langle v_j | i_j \rangle}{\sum_{j=1}^{N} \hbar\omega(v_j - i_j) + E_0 - E_L - i\Gamma} \qquad \textbf{(2.8)}$$

Recursion relations were determined for the one-dimensional Franck-Condon factors.[16,25] When the assumption is made that the frequencies are equal, these factors are then:

$$\langle 0 | 0 \rangle = \exp \frac{-\Delta^2}{4} \qquad \textbf{(2.9)}$$

$$\langle m+1 | n \rangle = \left(\frac{n}{m+1} \right)^{1/2} \langle m | n-1 \rangle - \Delta [2(m+1)]^{-1/2} \langle m | n \rangle \qquad \textbf{(2.10)}$$

$$\langle m | n+1 \rangle = \left(\frac{m}{n+1} \right)^{1/2} \langle m-1 | n \rangle + \Delta [2(n+1)]^{-1/2} \langle m | n \rangle \qquad \textbf{(2.11)}$$

where m and n are vibrational levels of the excited and ground states, respectively. Assuming that the initial state is the ground vibrational state, eqn. 2.9-2.11 can then be further manipulated to give the products of one-dimensional overlaps (eqn. 2.12-2.14). These products will then aid in the calculation of absorption, Raman fundamentals, and overtone frequencies. At this point, the problem of evaluating Raman cross sections for a given set of excited state parameters has

been eliminated. There remains, however, a problem of summing over the excited vibrational levels.

$$\langle 0|m\rangle\langle m|0\rangle = \left[\left(\frac{\Delta^2}{2}\right)^m \frac{1}{m!}\right]\exp\left(-\frac{\Delta^2}{2}\right) \qquad \textbf{(2.12)}$$

$$\langle 1|m\rangle\langle m|0\rangle = \left(\frac{\Delta}{2}\right)^{1/2}\left[\langle 0|m\rangle\langle m|0\rangle - \langle 0|m-1\rangle\langle m-1|0\rangle\right] \qquad \textbf{(2.13)}$$

$$\langle 2|m\rangle\langle m|0\rangle = \left(\frac{1}{2}\right)^{1/2}\left[\frac{\Delta^2}{2} - 2m + \frac{2m^2}{\Delta}\langle 0|m\rangle\langle m|0\rangle - \langle 0|m-1\rangle\langle m-1|0\rangle\right] \qquad \textbf{(2.14)}$$

Utilizing the separable harmonic approximation, the Raman intensities only depend on the magnitude of displacement along the normal coordinates.

If the restriction of equivalent ground and excited state frequencies is not placed on the system, a separable harmonic approximation can still be achieved because the normal coordinates are assumed to be the same.[16,19,21] With different ground and excited states the products of the one-dimensional overlaps become:

$$\langle 0|0\rangle = \left[\frac{2\left(\frac{\omega_g}{\omega_e}\right)^{1/2}}{\frac{\omega_g}{\omega_e}+1}\right]\exp\left(-\frac{\Delta^2}{2\left(1+\frac{\omega_g}{\omega_e}\right)}\right) \qquad \textbf{(2.15)}$$

$$\langle m+1|n\rangle = -\left(\frac{m}{m+1}\right)^{1/2}\left(\frac{\frac{\omega_g}{\omega_e}-1}{\frac{\omega_g}{\omega_e}+1}\right)\langle m|n-1\rangle + \left(\frac{n}{m+1}\right)^{1/2}\left[\frac{2\left(\frac{\omega_g}{\omega_e}\right)^{1/2}}{\frac{\omega_g}{\omega_e}+1}\right]\langle m|n-1\rangle - (m+1)^{-1/2}\left(\frac{\Delta\left(\frac{2\omega_g}{\omega_e}\right)^{1/2}}{1+\frac{\omega_g}{\omega_e}}\right)\langle m|n\rangle$$

(2.16)

$$\langle m|n+1\rangle = \left(\frac{n}{n+1}\right)^{1/2}\left(\frac{\frac{\omega_g}{\omega_e}-1}{\frac{\omega_g}{\omega_e}+1}\right)\langle m|n-1\rangle + \left(\frac{m}{n+1}\right)^{1/2}\left[\frac{2\left(\frac{\omega_g}{\omega_e}\right)^{1/2}}{\frac{\omega_g}{\omega_e}+1}\right]\langle m-1|n\rangle - (n+1)^{-1/2}\left(\frac{\Delta(2^{1/2})}{1+\frac{\omega_g}{\omega_e}}\right)\langle m|n\rangle \quad \textbf{(2.17)}$$

where ω_g and ω_e are the ground and excited state frequencies, respectively and Δ is the displacement in the ground state.

Electronic excitation results in changes of equilibrium geometry as well as vibrational frequencies. It has been found that that the compositions of normal modes of vibration also change with electronic excitation. This is known as the Duschinsky (rotation) effect.[16,26] These effects can be included in the absorption and Raman calculations, however, the calculations become much more complex. The Duschinsky effect is included as mixed second derivatives of the excited state electronic energy with respect to the ground state, resulting in Franck-Condon factors which are no longer able to be expressed as products of one-dimensional overlap. Ideally, including the full Duschinsky effect would lead to more accurate profiles of the ground and excited state.

Another factor which needs to be taken into consideration is the dependence of the electronic transition length matrix (M) on the normal coordinate (Q). Using a Taylor series, M(Q) can be evaluated beginning with the ground-state geometry (Q_0):

$$M(Q) = M_0 + \sum_j \left(\frac{\delta M}{\delta q_j}\right)_0 q_j + \frac{1}{2}\sum_{j,k}\left(\frac{\delta 2M}{\delta q_j \delta q_k}\right)_0 q_j q_k + \cdots \quad \textbf{(2.18)}$$

The derivatives of this series are most commonly evaluated using a Herzberg-Teller expansion of the coordinate-dependent excited state based on the ground state geometry.[23] This makes calculation of the cross section more involved, but provides valuable information

regarding the transition lengths. From the calculations it can be shown that coordinates with large transition displacement derivatives are most likely to couple the resonant electronic state to an allowed neighboring state. As a result of the coordinate dependence of the transition length, Franck-Condon factors can no longer be considered to be purely vibrational overlaps, and instead have to be represented as electronic transition matrix elements.

Finally, considerations need to be made for the broadening that results from thermal effects. In Raman scattering, molecules scatter radiation independently of each other, and therefore, scattering must be considered as a sum of probabilities. The scattering molecules can lie in different initial states due to thermal excitation in the vibrational levels. This can lead to inhomogeneous broadening of bands in the resonance Raman spectra. If the inhomogeneous broadening is considered to be a Gaussian distribution of zero-zero energies, it can be incorporated into the equation for the resonance Raman cross sections as θ:[16,19,21]

$$\sigma_{i\to f}(E_L) \propto \frac{1}{\theta(2\pi)^{1/2}} \int_0^\infty dE_0 \exp\left[\frac{-(E_0-\overline{E}_0)^2}{2\theta^2}\right] \left| \sum_v \frac{\langle f|v\rangle\langle v|i\rangle}{\varepsilon_v - \varepsilon_i + E_0 - E_L - i\Gamma} \right|^2 \quad \textbf{(2.19)}$$

where θ is the standard deviation of the zero-zero energies and $\overline{E}_0$ is the average zero-zero energy. A Gaussian distribution is used because it most accurately represents the distribution of the various broadening effects on the range of transition energies.

In resonance Raman spectroscopy, laser excitation wavelengths that are resonant within an electronic transition are used to excite a sample. This significantly enhances the vibrational modes, resulting in resonance Raman cross sections 10^3-10^6 times greater than normal Raman cross sections, allowing for samples with low concentrations to be studied.[19] These factors make UV resonance Raman an ideal tool for studying protein and polypeptide systems.

Usually, proteins are difficult to investigate with spectroscopy due to the immense number of vibrational normal modes that exist, (3N-6), where N is the number of atoms in the protein molecule. With UVRRS, however, it is possible to selectively excite within the $\pi \rightarrow \pi^*$ electronic transitions of peptide bonds and to selectively study a limited number of vibrational modes that give direct information on structure. With this data, information can be gained about the amide backbone, secondary structure, and dynamics of protein folding.

2.3 REFERENCES

1. Mix, G., Schweitzer-Stenner, R. & Asher, S. A. *J. Am. Chem. Soc.* **2000**, *122*, 9028.
2. Ianoul, A., Boyden, M. N. & Asher, S. A. *J. Am. Chem. Soc.* **2001**, 123, 7433.
3. Asher, S. A.; Ianoul, A.; Mix, G.; Boyden, M. N.; Karnoup, A.; Diem, M.; Schweitzer-Stenner, R. *J. Am. Chem. Soc.* **2001**, *123*, 11775.
4. Chi, Z., Chen, X. G., Holtz, J. S. W. & Asher, S. A. *Biochemistry* **1998**, *37*, 2854.
5. Sieler, G., Schweitzer-Stenner, R., Holtz, J. S. W., Pajcini, V. & Asher, S. A. *J. Phys. Chem. B* **1999**, *103*, 372.
6. Holtz, J. S. W., Holtz, J. H., Chi, Z. & Asher, S. A. *Biophys. J.* **1999**, *76*, 3227.
7. Ozdemir, A., Lednev, I. K. & Asher, S. A. *Biochemistry* **2002**, *41*, 1893.
8. Holtz, J. S. W., Lednev, I. K. & Asher, S. A. *Biopolymers* **2000**, *57*, 55.
9. Boyden, M. N. & Asher, S. A. *Biochemistry* **2001**, *40*, 13723.
10. Chi, Z. & Asher, S. A. *J. Phys. Chem. B* **1998**, *102*, 9595.
11. Ianoul, A., Mikhonin, A., Lednev, I. K. and Asher, S. A. *J. Phys. Chem. A* **2002**, *106*, 3621.
12. Asher, S. A., Mikhonin, A. V. and Bykov, S. B. *J. Am. Chem. Soc.* **2004**, *126*, 8433.

13. Mikhonin, A. V., Ahmed, Z., Ianoul, A. and Asher., S. A. *J. Phys. Chem. B* **2004**, *108*, 19020.

14. Mikhonin, A. V., Bykov, S. V., Myshakina, N. S. and Asher, S. A. *J. Phys. Chem. B,* **2006**, *110***,** 1928.

15. Mikhonin, A. V., Myshakina, N. S., Bykov, S. V. and Asher, S. A. *J. Am. Chem. Soc.* **2005**, *127*, 7712.

16. Myers, A.B. and Mathies, R.A. *In* Spiro, T.G. (ed.) Biological Applications of Raman Spectroscopy, Vol 2: Resonance Raman Spectra of Polyenes and Aromatics. New York: John Wiley & Sons, **1987**.

17. Placzek, G. Rayleigh-Streuung und Raman Effekt. Marx, Leipzig, 1934. [Rayleigh and Raman scattering**.** U.S. Atomic Energy Commission Translation, **1955**].

18. Kramers, H.A. and Heisenberg, W. *Z. Phys.,* **1925**, *31*, 681.

19. Myers, A. B. & Rizzo, T.R. (eds.) Laser Techniques in Chemistry Vol. XXIII. New York: John Wiley & Sons, **1995**.

20. Shorygin, P.P. & Krushinskij, L.L. *J. Raman Spec.,* **1997**, *28*, 383.

21. Myers, A.B. *J. Raman Spec.,* **1997**, *28*, 389.

22. Ferraro, J.R., Nakamoto, K., and Brown, C.W. Introductory Raman Spectroscopy, 2nd ed. Amsterdam: Academic Press, **2003**.

23. Albrecht, A. *J. Chem. Phys.*, **1961**, *34*, 1476.

24. Smith, E. & Dent, G. (eds.) Modern Raman Spectroscopy: a Practical Approach. Hoboken: John Wiley, **2005**.

25. IUPAC, *Compendium of Chemical Terminology* **1996**, *68*, 2243.

26. Manneback, C. *Physica,* **1951**, *17*, 1001.

27. Neugebauer, J. & Hess, B. A. *J. Chem. Phys.,* **2004**, *120*, 11564.

3.0 UV RESONANCE RAMAN SPECTROSCOPY

3.1 EXAMINING PEPTIDE STRUCTURE

Unlike NMR or x-ray crystallography, UV resonance Raman spectroscopy (UVRRS) yields spectra which can be interpreted to gain information about the structure or a peptide or protein. The spectral features are sensitive to even slight changes in structure. It is known that excitation in the UV, from 180 to 215 nm occurs within the $\pi \rightarrow \pi^*$ electronic transitions of the peptide backbone. [1-4, 9, 11-15, 27-29] This excitation results in resonance enhancement of the transition. It has been previously shown that UV excitation results in high intensity Raman spectra for peptides and proteins. [1, 2, 5, 8, 12, 13, 30-32] The sensitivity of the technique allows for examination of the frequencies, intensities, and cross sections of the Raman bands to gain information about the molecular structure of a system. [1-3, 5, 8, 10, 12, 13, 27, 31, 32]

Early studies of peptide and protein behavior relied on a simple peptide model, N-methylacetamide (NMA). NMA is often used to model peptide behavior because it contains the equivalent of a single peptide bond unit. Studies have indicated that the amide bands of NMA are resonantly enhanced by the first dipole-allowed transition at approximately 190 nm, and the Raman excitation profiles indicate the presence of destructive interference from the second dipole-allowed transition at ~165 nm.[33,34] Raman excitation profiles are used to gain information about the excited state of a molecule.[33] For peptides, the amide $\pi \rightarrow \pi^*$ transitions are homogeneously broadened, resulting in absorption spectra which are also broad, providing little

information about the structure. It is believed that the excitation profiles of any given secondary structure will be identical, but that different secondary structures should have different profiles. This difference arises from the differences in absorption bands between conformations and the differences in homogenous broadening.

The amide vibrations that arise from excitation of the $\pi \rightarrow \pi^*$ transition of the peptide bond are clearly defined (Figure 3.1). These vibrations include the amide I (AmI) vibration which is mainly a C=O stretch (st). In NMA the AmI vibration has been found to couple with the bending motion of water molecules hydrogen bonded to the backbone.[35,36] The amide II (AmII) vibration is composed of a C-N st with an in-plane N-H bend (b). The AmIII vibration also involves the C-N st with an in-plane N-H b, and has been shown by our group to be the most sensitive to peptide conformation.[50] The final vibration, a C_α-H symmetric bend, is only seen with certain β-type secondary structures, and is not found in the α-helix spectrum.

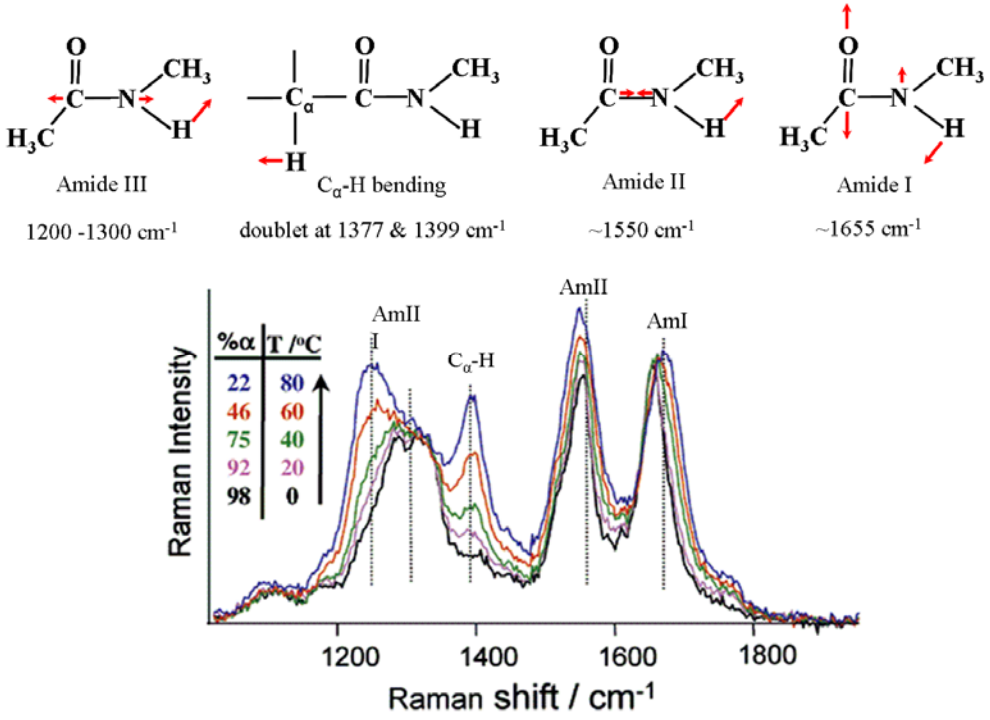

Figure 3.1 Amide vibrations (upper panel); Raman spectrum of poly-glutamic acid with amide vibrations labeled (lower panel).

Due to the complexity in analyzing protein structures, many researchers examine isolated secondary structures with the hopes of applying the information gained about behavior of the secondary structures to understanding whole proteins. One of the peptides frequently studied is a 21-residue poly-alanine peptide (AP). This peptide is known to have a predominantly α-helical structure at low temperatures and unfolds at higher temperatures.[37] This unfolded state was previously considered to be a random coil, but recent studies have shown that the unfolded state is actually a poly-proline II (PPII) helix, and not a random disordered state.[12, 38-47] This discovery is forcing changes in the way people understand α-helix melting. Up to this point, all of the existing models for α-helix melting assumed a two-state transition, from ordered to disordered. These models are now being questioned since it has been shown that the right-handed α-helix melts to a left-handed PPII, requiring that a turn conformation must exist at the junction between the two structures.[48, 49]

Further examination of AP shows that amide vibrations independently scatter, with negligible coupling occurring between adjacent peptide bonds, in both the PPII and α-helix. The AmI vibration shows evidence of coupling between adjacent bonds for the α-helix, but not the PPII conformation.[31] The difference for the AmI band between the two conformations is believed to be due to the position of the C=O in the α-helix, where they are intra-amide hydrogen bonded and are parallel to the helical axis. It was also noted that the AmI band intensity increases with decreasing α-helical length, so using the AmI for conformational studies of α-helices need to be performed with care.[31]

The AmIII region is the most sensitive amide vibration to conformation. A correlation has been established between the $AmIII_3$ band frequency (which is sensitive to the backbone conformation[33]), Ψ angle, and hydrogen-bonding.[12, 50] The conformational dependence of the

$AmIII_3$ band results from the coupling between the C_α-H and N-H bending motions. In an α-helix, the C_α-H bonds are in a *trans* position, whereas in the PPII helix and β-strands, they are in a *cis* position which results in increased coupling of the C_α-H bending with the N-H bending mode.[2] The normal modes for each band in the AmIII region have been assigned.[13] In a PPII conformation, the $AmIII_3$ band (1245 cm^{-1}) is assigned to the N-H b coupled to C_α-H b and C-N st. The $AmIII_2$ band (1303 cm^{-1}) is composed of mainly a C_α-C st, N-C st, and C-N st. In the α-helix, the $AmIII_3$ band is shifted in frequency (1261 cm^{-1}) and the included motions are N-H b, C-N st, and maybe C_α-C st. The $AmIII_2$ band is also slightly shifted in frequency (1306 cm^{-1}) and is composed of C_α-C st, N-C st, and a small amount of C-N st. The $AmIII_1$ band (1337 cm^{-1}) also includes C_α-C st, N-C st, and a small amount of C-N st.

The latest work with AP has resulted in the determination that the "pure" α-helix spectrum is actually composed of not only α-helix, but also 3_{10} and π helices at low temperatures.[50] This experimental data has been supported by recent molecular dynamics (MD) simulations which found similar results.[51] The MD simulations suggest that the 3_{10} and π helices are intermediates in the folding process and can also exist as defects in the α-helix structure. Spectrally these additional helices are found as components of the $AmIII_3$ band, with their frequency determined by equations given by Mikhonin et al. (2006).50 These findings reinforce the idea that α-helix structure and formation is a complex process, and that further investigations need to be carried out in order to fully understand the α-helix behavior.

3.2 REFERENCES

1. Mix, G., Schweitzer-Stenner, R. & Asher, S. A. *J. Am. Chem. Soc.* **2000**, *122*, 9028.

2. Ianoul, A., Boyden, M. N. & Asher, S. A. *J. Am. Chem. Soc.* **2001**, *123*, 7433.

3. Asher, S. A.; Ianoul, A.; Mix, G.; Boyden, M. N.; Karnoup, A.; Diem, M.; Schweitzer-Stenner, R. *J. Am. Chem. Soc.* **2001**, *123*, 11775.

4. Chi, Z., Chen, X. G., Holtz, J. S. W. & Asher, S. A. *Biochemistry* **1998**, *37*, 2854.

5. Sieler, G., Schweitzer-Stenner, R., Holtz, J. S. W., Pajcini, V. & Asher, S. A. *J. Phys. Chem. B* **1999**, *103*, 372.

6. Holtz, J. S. W., Holtz, J. H., Chi, Z. & Asher, S. A. *Biophys. J.* **1999**, *76*, 3227.

7. Ozdemir, A., Lednev, I. K. & Asher, S. A. *Biochemistry* **2002**, *41*, 1893.

8. Holtz, J. S. W., Lednev, I. K. & Asher, S. A. *Biopolymers* **2000**, *57*, 55.

9. Boyden, M. N. & Asher, S. A. *Biochemistry* **2001**, *40*, 13723.

10. Chi, Z. & Asher, S. A. *J. Phys. Chem. B* **1998**, *102*, 9595.

11. Ianoul, A., Mikhonin, A., Lednev, I. K. and Asher, S. A. *J. Phys. Chem. A* **2002**, *106*, 3621.

12. Asher, S. A., Mikhonin, A. V. and Bykov, S. B. *J. Am. Chem. Soc.* **2004**, *126*, 8433.

13. Mikhonin, A. V., Ahmed, Z., Ianoul, A. and Asher., S. A. *J. Phys. Chem. B* **2004**, *108*, 19020.

14. Mikhonin, A. V., Bykov, S. V., Myshakina, N. S. and Asher, S. A. *J. Phys. Chem. B,* **2006**, *110*, 1928.

15. Mikhonin, A. V., Myshakina, N. S., Bykov, S. V. and Asher, S. A. *J. Am. Chem. Soc.* **2005**, *127*, 7712.

16. Myers, A.B. and Mathies, R.A. *In* Spiro, T.G. (ed.) Biological Applications of Raman Spectroscopy, Vol 2: Resonance Raman Spectra of Polyenes and Aromatics. New York: John Wiley & Sons, **1987**.

17. Placzek, G. Rayleigh-Streuung und Raman Effekt. Marx, Leipzig, 1934. [Rayleigh and Raman scattering**.** U.S. Atomic Energy Commission Translation, 1955].

18. Kramers, H.A. and Heisenberg, W. *Z. Phys.,* **1925**, *31*, 681.

19. Myers, A. B. & Rizzo, T.R. (eds.) Laser Techniques in Chemistry Vol. XXIII. New York: John Wiley & Sons, **1995**.

20. Shorygin, P.P. & Krushinskij, L.L. *J. Raman Spec.,* **1997**, *28*, 383-388.

21. Myers, A.B. *J. Raman Spec.,* **1997**, *28*, 389.

22. Ferraro, J.R., Nakamoto, K., and Brown, C.W. Introductory Raman Spectroscopy, 2nd ed. Amsterdam: Academic Press, **2003**.

23. Albrecht, A. *J. Chem. Phys.*, **1961**, *34*, 1476.

24. IUPAC, *Compendium of Chemical Terminology* **1996**, *68*, 2243.

25. Manneback, C. *Physica,* **1951**, *17*, 1001.

26. Neugebauer, J. & Hess, B. A. *J. Chem. Phys.,* **2004**, *120*, 11564.

27. Cho, N. and Asher, S. A. *Biospectrosc.* **1996**, *2*, 71.

28. Asher, S. A. *Anal. Chem.* **1993**, *65*, 201A.

29. Chen, X. G., Asher, S. A., Schweitzer-Stenner, R., Mirkin, N. G. and Krimm, S. *J. Am. Chem. Soc.* **1995**, *117*, 2884.

30. Beeler, J. A.; Yan, S.-Z.; Bykov, S.; Murza, A.; Asher, S.; Tang, W.-J. *Biochemistry* **2004**, *43*, 15463.

31. Mikhonin, A. V. and Asher, S. A. *J. Phys. Chem. B* **2005**, *109*, 3047.

32. Pimenov, K. V., Bykov, S. V., Mikhonin, A. V. and Asher, S. *J. Am. Chem. Soc.* **2005**, *127*, 2840.

33. Dudik, J.M., Johnson, C.R., and Asher, S.A. *J. Phys. Chem.,* **1985**, *89*, 3805.

34. Asher, S.A., Chi, Z., and Li, P. *J. Raman Spectr.,* **1998**, *29***,** 927.

35. Chen, X.G., Schweitzer-Stenner, R., Asher, S.A., Mirkin, N.G., and Krimm, S. *J. Phys. Chem.,* **1995**, *99*, 3074.

36. Chen, X.G., Schweitzer-Stenner, R., Krimm, S., Mirkin, N.G., and Asher, S.A. *J. Am. Chem. Soc.,* **1994**, *116*, 11141.

37. Lednev, I.K., Karnoup, A.S., Sparrow, M.C., and Asher, S.A. *J. Am. Chem. Soc.,* **1999**, *121*, 8074.

38. Pappu, R. V. and Rose, G. D. *Protein Sci.* **2002**, *11*, 2437.

39. Rucker, A. L. and Creamer, T. P. *Protein Sci.* **2002**, *11*, 980.

40. Shi, Z., Olson, C. A., Rose, G. D., Baldwin, R. L. and Kallenbach, N. R. *Proc. Natl. Acad. Sci. USA* **2002**, *99*, 9190.

41. Zagrovic, B., Lipfert, J., Sorin, E. J., Millett, I. S., Van Gunsteren, W. F., Doniach, S. and Pande, V. S. *Proc. Natl. Acad. Sci. USA* **2005**, *102*, 11698.

42. Chellgren, B. W. and Creamer, T. P. *J. Am. Chem. Soc.* **2004**, *126*, 14734.

43. Chellgren, B. W. and Creamer, T. P. *Biochemistry* **2004**, *43*, 5864.

44. Chen, K., Liu, Z. and Kallenbach, N. R. *Proc. Natl. Acad. Sci. USA* **2004**, *101*, 15352.

45. Eker, F., Griebenow, K., Cao, X., Nafie, L. A. and Schweitzer-Stenner, R. *Proc. Natl. Acad. Sci. USA* **2004**, *101*, 10054.

46. Ferreon, J. C. and Hilser, V. J. *Protein Sci.* **2003**, *12*, 447.

47. Fleming, P. J., Fitzkee, N. C., Mezei, M., Srinivasan, R. and Rose, G. D. *Protein Sci.* **2005**, *14*, 111.

48. Daggett, V. and Levitt, M. *J. Mol. Biol.* **1992**, *223*, 1121.

49. Hirst, J. D. and Brooks, C. L., III. *Biochemistry* **1995**, *34*, 7614.

50. Mikhonin, A.V. and Asher, S.A. *J. Phys. Chem. B,* **2006**, *110,* 1928.

51. Sorin, E.J., Rhee, Y.M., Shirts, M.R., and Pande, V.S. *J. Mol. Biol.,* **2006**, *356***,** 248.

4.0 UV RESONANCE RAMAN INVESTIGATION OF ELECTRONIC TRANSITIONS IN A-HELICAL AND POLYPROLINE II-LIKE CONFORMATIONS

UV resonance Raman (UVRR) excitation profiles and Raman depolarization ratios were measured for a 21-residue predominantly alanine peptide, AAAAA(AAARA)$_3$A (AP), excited between 194 and 218 nm. Excitation within the $\pi \rightarrow \pi^*$ electronic transitions of the amide group results in UVRR spectra dominated by amide vibrations. The Raman cross sections and excitation profiles provide information about the nature of the electronic transitions of the α-helix and PPII-like peptide conformations. AP is known to be predominantly α-helical at low temperatures and takes on a polyproline II (PPII) helix-like conformation at high temperatures. The PPII-like and α-helix conformations show distinctly different Raman excitation profiles. The PPII-like conformation cross sections are approximately twice those of the α-helix. This is due to hypochromism that results from excitonic interactions between the NV_1 transition of one amide group with the higher energy electronic transitions of other amide groups, which decreases the α-helical NV1 ($\pi \rightarrow \pi^*$) oscillator strengths. Excitation profiles of the α-helix and PPII-like conformations indicate that highest signal-to-noise Raman spectra of α-helix and PPII-like conformations are obtained at excitation wavelengths of 194 and 198 nm, respectively. We also see evidence of at least two electronic transitions underlying the Raman excitation profiles of both the α-helical and PPII-like conformations. In addition to the well known ~190 nm $\pi \rightarrow \pi^*$ transitions, the Raman excitation profiles and Raman depolarization ratio measurements show

features between 205-207 nm, which in the α-helix likely results from the parallel excitonic component. The PPII-like helix appears to also undergo excitonic splitting of its $\pi \rightarrow \pi^*$ transition which leads to a 207 nm feature. (This work was published in the *J. Phys. Chem. B* **2008**, 112, 11762-11769.)

4.1 INTRODUCTION

UV resonance Raman (UVRR) spectroscopy is well established as a technique for probing secondary structure of peptides and proteins.[1-29] Excitation between 180 to 215 nm, within the $\pi \rightarrow \pi^*$ electronic transitions of the peptide backbone, results in the enhancement of amide vibrations.[1-29] Amide $\pi \rightarrow \pi^*$ electronic transitions show no emission and appear to be homogeneously broadened. Their broad absorption spectra provide little information about the underlying excited states. UVRR excitation profiles and Raman depolarization ratios are utilized here to examine the underlying amide electronic transitions.[25,26,29] The present consensus is that predominantly three electronic transitions occur in simple amides in the 130 to 230 nm range. These electronic transitions are the weak $n \rightarrow \pi^*$ transition (210 to 230 nm), the strong $\pi \rightarrow \pi^*$ transition (170 to 195 nm), and a second, weaker $\pi \rightarrow \pi^*$ transition (135 to 160 nm).[30-37] Along with the classically defined transitions, other transitions reported include charge transfer electronic transition states,[36,37] as well as Rydberg transitions found in gas phase spectra.[30-32,39,40]

In α-helices a weak $n \rightarrow \pi^*$ electronic transition occurs at ~ 220 nm while a higher frequency $\pi \rightarrow \pi^*$ electronic transition occurs at ~ 190 nm. This $\pi \rightarrow \pi^*$ transition is understood to

undergo exciton splitting which gives rise to two dipole-allowed transitions: one perpendicular to the helical axis at 190 nm and the second parallel to the axis at 205 nm.[41-46]

The melted state of α-helices has been demonstrated by our group, as well as others, to predominantly be a conformation closely related to the left-handed polyproline II (PPII) helix,[12,47-50] and not a random coil, although there is some disagreement with this result.[51,52] The high temperature AP spectra are identical to the spectra of the peptide XAO, which Shi et al., determined to be ~90% PPII helix.[48] We treat the non-α-helical conformation of AP as being a predominantly PPII helix, which means that the PPII structure is found primarily along the peptide chain, but also may include some β-turn like structures.[12] The transitions in pure PPII helices involve an $n\rightarrow\pi^*$ transition at ~ 220 nm and a $\pi\rightarrow\pi^*$ transition at ~ 200 nm. Theory has not yet been able to accurately model the excited states found in a PPII helix such that it can predict circular dichroism (CD) and absorption spectra.[46] It has been suggested that, for the PPII conformation, a mixing of the $\pi\rightarrow\pi^*$ transition with higher energy transitions must be included in calculations to accurately reproduce the CD and absorption experimental data. [46]

In this study, we characterize the UVRR excitation profiles and depolarization ratios of aqueous solutions of a 21-residue, mainly alanine peptide (AP) from 194 to 229 nm and at 5°C and 60°C. AP has been shown to be a mixture of α-helix and polyproline II (PPII) helix conformations at low temperatures (<25°C) and predominantly PPII helix-like at high temperatures (>25°C).[26,50,54] This high temperature PPII-like conformation is often referred to as the peptide unfolded state.

We observe the two exciton split classically defined components of the $\pi\rightarrow\pi^*$ transition in the α-helix. In the PPII-like helix, however, we also observe two strong electronic transitions in the 190 to 230 nm range, which also likely derive from excitonic interactions.

4.2 MATERIALS AND METHODS

4.2.1 Sample Preparation

The 21-residue poly-alanine peptide AAAAA(AAARA)$_3$A (AP) was prepared by AnaSpec (San Jose, CA) using solid-state peptide synthesis (HPLC pure). We used 2 mg/ml (1.13 mM) solutions for the UVRRS measurements, which contained sodium perchlorate (0.2 M) as an internal standard. For the circular dichroism (CD) spectra AP was used at 2.7 mM concentrations and for the absorption spectra, AP was used at 0.15 mM concentrations. The UVRR, CD, and absorption spectral measurements were taken at both 5 °C ± 0.5 °C (where AP is a mixture of α-helical and PPII conformations; Figure 4.1) and at 60 °C ± 0.5 °C (the PPII-like conformation dominates).

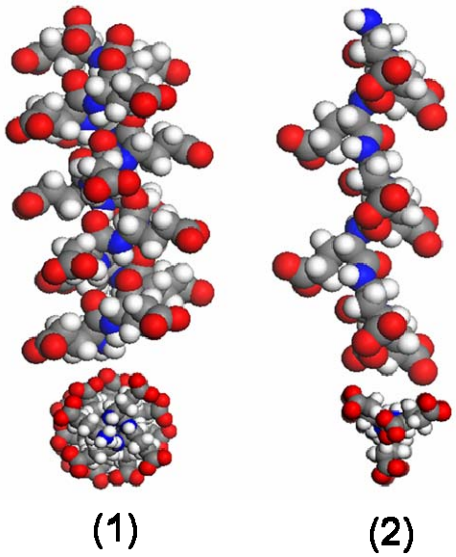

Figure 4.1 Examples of conformations adopted by AP (shown here for poly-glutamic acid). (1) α-helix: a right-handed helix with (Φ, Ψ) = (-58°, -47°), and an *i – i+4* hydrogen bonding pattern; (2) poly-proline II-like (PPII): a left-handed helix with (Φ, Ψ) = (-75°, +145°) which hydrogen bonds to water and does not undergo intramolecular hydrogen bonding.

4.2.2 Raman Instrumentation

The UVRR spectroscopic instrumentation has previously been described in detail.[54] In brief, the laser sources were two Positive Light Co. Indigo-S Ti:Sapphire laser systems. The Indigo-S systems both utilize intra-cavity frequency doubled, Q-switch pulsed Nd:YLF Evolution 15 lasers (527 nm wavelength, 5 kHz repetition rate, 10 W average power) to pump Ti:Sapphire oscillators generating tunable radiation from 772 to 840 nm and 840 to 960 nm. These tunable Ti:Sapphire lasers are frequency quadrupled and mixed utilizing two different harmonic crystal packages. The 210 nm laser utilizes two successive frequency doublers to convert the fundamental (840-960 nm) to the UV (210-240 nm). The 193 nm laser harmonics package mixes the third harmonic with the fundamental to produce tunable radiation between 193 and 210 nm. The average powers in the UV were between 2-5 mW (193-210 nm) and ~10 mW (210-220 nm).

The laser beam was focused into a temperature-controlled, circulating flow stream which was purged with N_2 to eliminate Raman scattering from the O_2 band at 1555 cm^{-1}. The 20-mL sample of AP was irradiated for a maximum of 15 min. The scattered light was directed into the subtractive double monochromator[54] and the Raman scattered light was detected by a liquid nitrogen-cooled CCD (Princeton Instruments, Spec-10:400B). The Raman intensities were normalized to the 932 cm^{-1} perchlorate (ClO_4^-) symmetric stretch vibration band. The spectra were analyzed and deconvoluted using Grams/32 AI software from Thermo Electron Corporation (Waltham, MA).

UV Raman depolarization ratios (ρ) were measured by using a 180° scattering geometry. The light scattered from the sample was directed through a UV linear dichroic polarizer (Oriel Instruments, Stratford, CT) and a crystalline quartz scrambler (Spex Industries, Edison, NJ)

directly before the monochromator entrance slit. The depolarization ratios were collected at: 198, 202, 204, 206, 210 and 218 nm (Indigo S, Coherent, Santa Clara, CA), as well as 229 nm (intracavity frequency doubled-Ar^+, Coherent). The incident beams were highly polarized. ρ was calculated as a ratio of the perpendicularly polarized light ($I_\perp$) to the parallel polarized light ($I_\parallel$):

$$\rho = \frac{I_\perp}{I_\parallel} \qquad \textbf{(4.1)}$$

The accuracy of the depolarization ratios was verified using the depolarization ratios of ClO4- and cyclohexane as standards.[55]

4.2.3 Spectrometer Efficiency

The spectrometer we used is a modified Spex 1401 double monochromator that operates in the 193-270 nm range.[54] Since the throughput efficiency of the spectrometer varies over this range, we corrected for the differences in throughput efficiency by recording the scattering of a standard intensity UV-deuterium lamp (Optronics Laboratories Inc., Orlando, FL) from the surface of packed $BaSO_4$ powder to determine the efficiency curve.[54] The efficiency factors determined by Bykov et al., 2005 were used for the absolute Raman cross section calculations.[54]

4.2.4 Absorption and CD Measurements

The UV absorbance spectra between 190 and 260 nm were measured by using a Cary 5000 Varian UV-Vis-NIR spectrophotometer. The CD spectra were measured using a Jasco J-710

spectropolarimeter. The spectra were measured in a temperature-controlled 0.2 mm path-length cell.

4.3 RESULTS AND DISCUSSION

4.3.1 Absorption Spectrum

The absorption spectra and the structure of AP are shown in Figure 4.2. As the wavelength decreases from 260 to 190 nm, the absorbance increases. The broad band at 190 nm derives from the amide $\pi \rightarrow \pi^*$ transition(s). The conventional understanding of amide electronic transitions indicates that for pure α-helices, exciton splitting leads to two dipole-allowed transitions, one centered at 190 nm which is perpendicular to the helical axis,[43] and a second transition dipole occurs parallel to the helical axis[44] and appears as a shoulder at 205 nm.[42] The band assignments are confirmed by CD data, with a strong positive band at 190 nm and weaker negative bands at 205 nm and 222 nm, which is assigned to the $n \rightarrow \pi^*$ transition.[46]

For a "pure" PPII conformation, previously referred to as random coil, an absorption maximum is found at 192 nm, slightly red-shifted from the α-helix maximum.[42] This absorption maximum for the "pure" PPII conformation is significantly larger than that of the "pure" α-helix conformation. The increase in absorbance of the AP sample with increasing temperature results from the loss of α-helix hypochromism upon the conversion to the PPII-like conformation at 60 °C. In the CD of peptides containing a large amount of PPII, a strong negative band is observed at ~196 nm and a weak positive band at 215 nm (not observed for AP).[46]

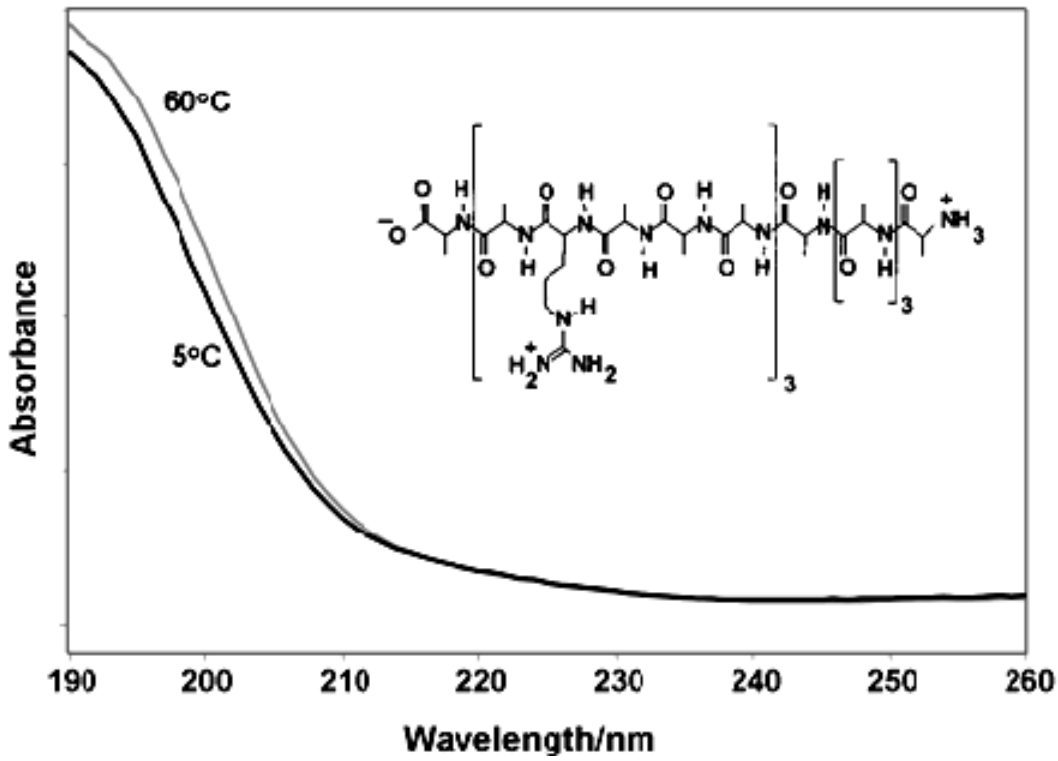

Figure 4.2 UV-vis absorption spectrum of AP at 5 °C, where it is predominantly α-helical, and at 60 °C, where it is in a mainly PPII-like conformation. Inset: Structure of AP.

4.3.2 UV Resonance Raman Spectra

At 5°C, AP is approximately 55% α-helical and 45% PPII.[26] AP melts to a predominantly PPII-like conformation by 60 °C. Figure 4.3 shows the UVRRS of AP at 60 °C in the PPII-like conformation excited between 218 to 194 nm. The spectra shown are normalized with respect to the 932 cm^{-1} ClO_4^- band, but are not corrected for self absorption or spectrometer efficiency. The enhanced amide vibrations for the PPII-like conformation include the Amide I (AmI) band at 1659 cm^{-1}, which originates primarily from C = O stretching (st). The Amide II (AmII) band, which results from coupling of C – N st and N –H in-plane bending (b), is located at 1548 cm^{-1}. The doublet from the C_α – H symmetric b vibration occurs at 1377 cm^{-1} (C_α – H_1) and 1399 cm^{-1}

($C_\alpha - H_2$). The Amide III_3 ($AmIII_3$) and Amide III_2 ($AmIII_2$) bands at 1261 cm^{-1} and 1303 cm^{-1}, respectively, derive from vibrations where C – N st couples with the N – H in-plane b. The relative intensities of the Raman bands in the UVRR spectra of AP increase as the laser excitation wavelength is decreased from 218 to 194 nm (Figure 4.3). The spectrum at 198 nm shows the highest relative band intensities. A comparison of the AP PPII-like spectra across the entire excitation wavelength range demonstrates very similar enhancement patterns with essentially identical bands enhanced. The similarity of these spectra suggests that very similar or identical electronic transitions span this spectral region.

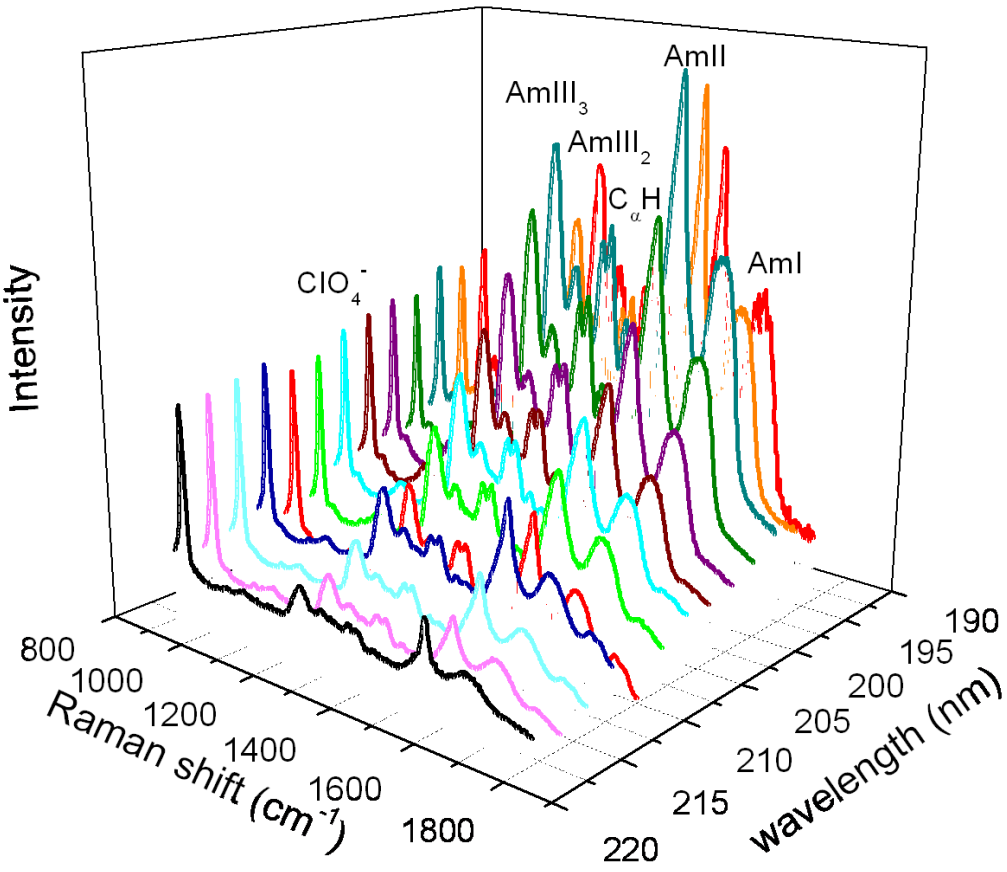

Figure 4.3 Observed UVRR spectra of AP in the PPII-like conformation at 60 °C between 218 and 194 nm. The spectra were collected for 15 min at each wavelength. The spectral resolution is between 7 cm^{-1} at 218 nm and 5.9 cm^{-1} at 194 nm. All spectra were normalized to the ClO_4^- internal standard.

To determine the excitation profile of the α-helix spectra at 5 °C, we numerically removed the contributions from the 45% concentration of the PPII conformation.[26] We calculated the spectra of the PPII conformation at 5 °C for excitation between 218 and 194 nm (Figure 4.4) using Lednev et al.'s methodology, which modeled the temperature dependence of the frequencies, intensities, and bandwidths of PPII at 5 °C from the high temperature PPII-like spectra.[26] As discussed above, the relative intensities within spectra between different excitation wavelengths are very similar again suggesting similar electronic transitions span the 190 to 215 nm spectral region.

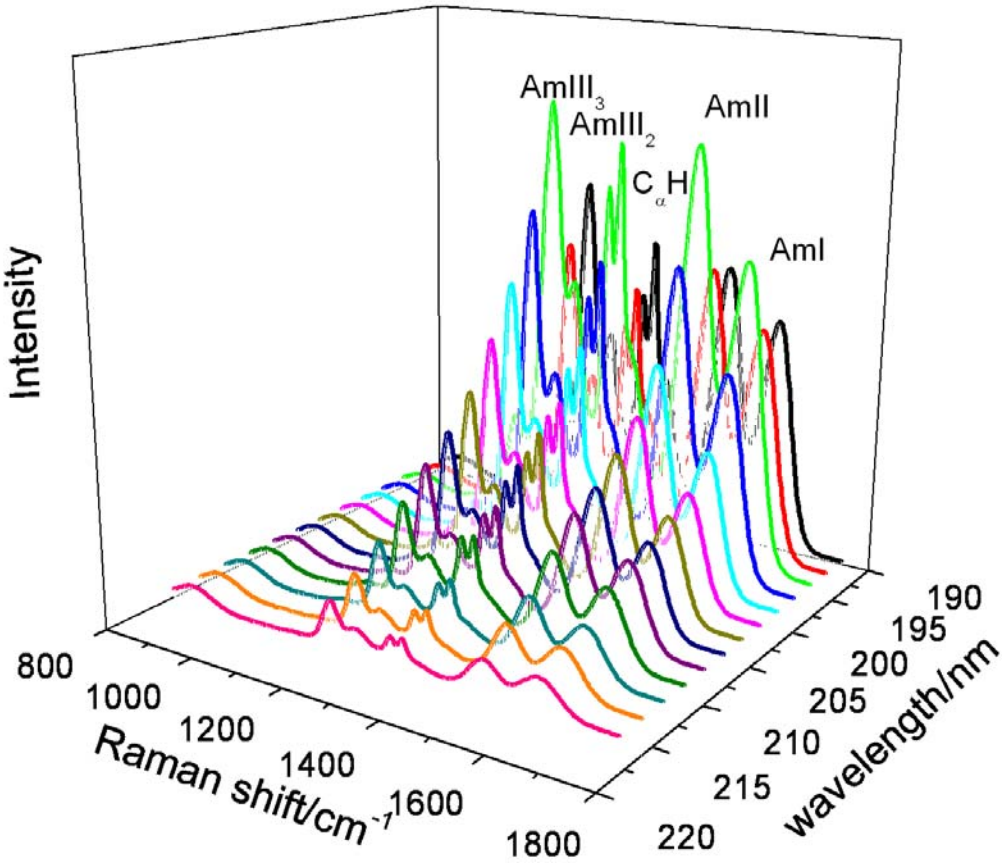

Figure 4.4 Calculated Raman spectra of AP in the PPII conformation at 5 °C between 218 to 194 nm. See text for details.

These calculated PPII spectra were subtracted from the measured 5 °C AP spectra to yield the pure 5 °C AP α-helical Raman spectra. Figure 4.5 compares the 204 nm excited AP mixed α-helix/PPII spectrum at 5 °C to the calculated 5°C PPII-helix spectrum and to the resulting "pure" α-helix spectrum.

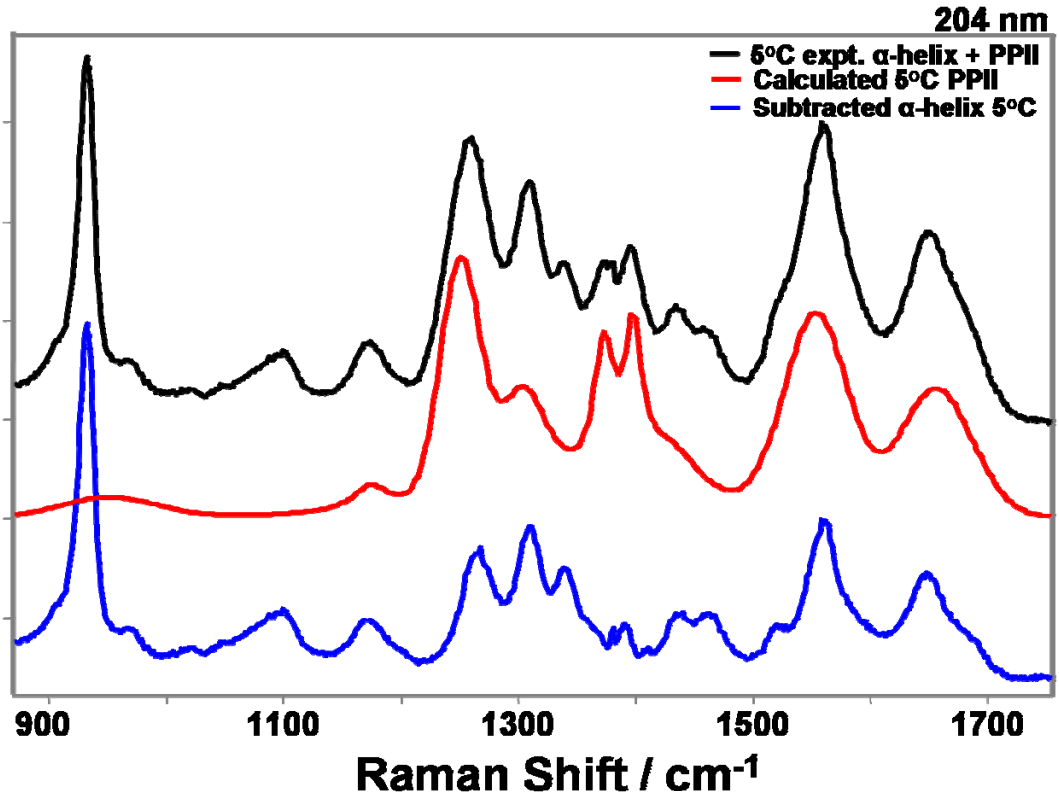

Figure 4.5 UVRR spectra of AP at 204 nm. Observed 5° C spectrum (black), calculated 5° C PPII spectrum (red), and subtracted 5° C α-helix spectrum (blue).

Figure 4.6 shows the calculated α-helical Raman spectra excited between 218 and 194 nm. The intensities of the Raman bands increase almost monotonically with decreasing excitation wavelengths from 218 to 194 nm. Comparing the PPII-like and α-helix spectra, we find that the PPII-like conformation Raman spectral intensities are greater than that of the α-helix. The $AmIII_3$ and $AmIII_2$ bands of the PPII-like conformation are broader and occur at

lower frequency compared to those in the α-helix. In the α-helix there is a third AmIII band present at 1337 cm^{-1} ($AmIII_1$). The AmII and AmI bands in the PPII-like conformation are also at lower frequency than in the α-helix.

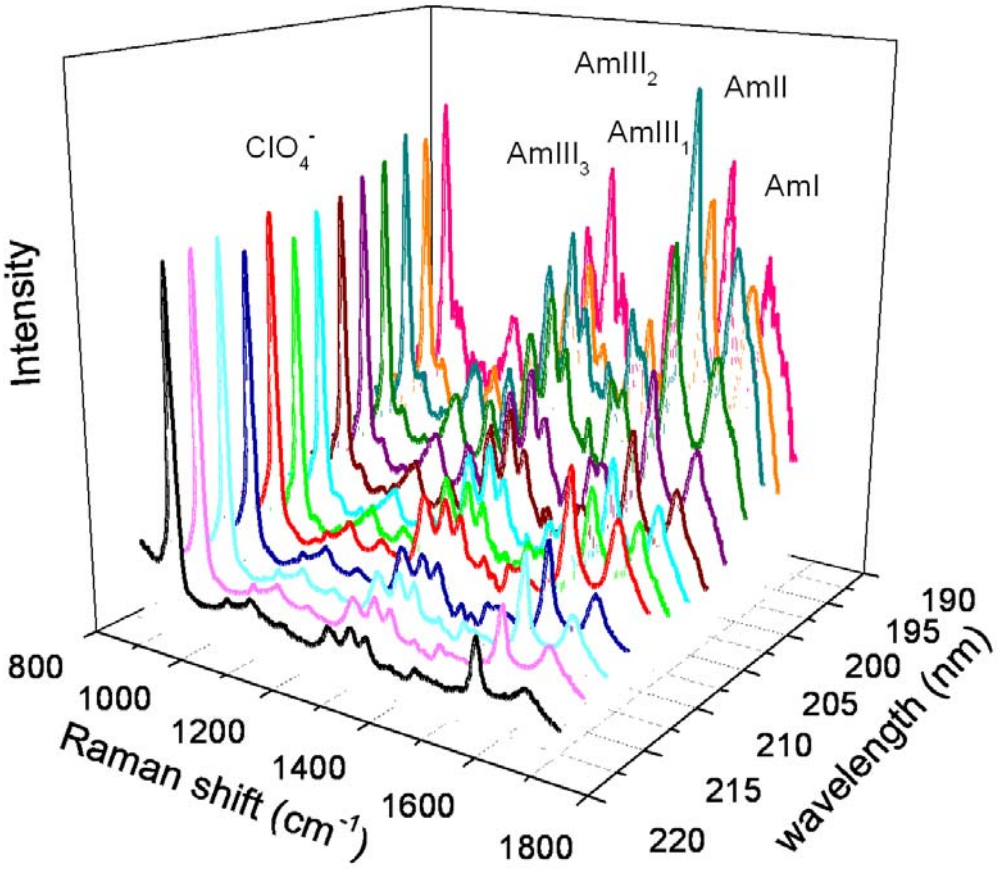

Figure 4.6 Subtracted UVRR spectra of α-helix conformation of AP at 5° C between 218 and 194 nm. The spectral resolution is between 7 cm^{-1} at 218 nm and 5.9 cm^{-1} at 194 nm.

4.3.3 Absolute Raman Cross Sections

We calculated the Raman cross sections using ClO_4^- as an internal standard. We previously showed that the ClO_4^- Raman cross section dependence on excitation frequency is well modeled by:[22]

$$\sigma_R = K_2 \nu_o \left(\nu_o - \nu_{mn}\right)^3 \left[\frac{1}{1 - \quad} \right]^2 \quad \textbf{(4.2)}$$

Error! Bookmark not defined.

where K_2 is a constant, ν_o is the incident laser excitation frequency (cm^{-1}), ν_{mn} corresponds to the frequency of the Raman vibrational mode (cm^{-1}), and ν_e is the frequency of the transition to the resonant excited state (cm^{-1}). Dudik et al. found that the ClO_4^- symmetric stretching band shows an Albrecht A-term frequency dependence for excitation wavelengths from the visible to the UV to 220 nm.[22] We assume this cross section frequency dependence occurs down to 194 nm.

We normalized our AP UVRR spectra with respect to the ClO_4^- 932 cm^{-1} band. The absolute Raman cross sections (with correction for self absorption) of AP in both the PPII-like and α-helix conformations were calculated as:

$$\sigma_{AP} = \frac{I_{band} \cdot k(\lambda_{ClO4}) \cdot C_{ClO4} \cdot \sigma_{ClO4}}{I_{ClO4} \cdot k(\lambda_{band}) \cdot C_{AP} \cdot n_A} \cdot \left[\frac{\varepsilon_s + \varepsilon_o}{\varepsilon_r + \varepsilon_o} \right] \quad \textbf{(4.3)}$$

where I_{band} and I_{ClO4} are the relative intensities of the amide bands and ClO_4^-, respectively; $k(\lambda_{band})$ and $k(\lambda_{ClO4})$ are the spectrometer efficiencies at the specific wavelengths of the bands; C_{AP} and C_{ClO4} are the concentrations (M) of the AP and perchlorate; σ_{ClO4} is the calculated ClO_4^- cross section at the specific wavelength; n_A is the number of amide bonds in the peptide; ε_o is the extinction coefficient for AP at the laser frequency; ε_s is the extinction coefficient for AP at each Raman band position; and ε_r is the extinction coefficient for ClO_4^- at each wavelength. The expression in the brackets corrects the Raman intensities for self absorption. We apply this small correction for self absorption to account for the differences in absorbance of AP at the various excitation and Raman scattered wavelengths.[56,57]

4.3.4 Excitation Profiles

4.3.4.1 Polyproline II (PPII)-like Conformation

Figure 4.7 shows the absolute Raman cross section excitation profiles for the AP amide bands in the PPII-like conformation. The Raman cross sections monotonically increase from 220 nm, reaching an excitation maximum at 198 nm. Interestingly, the $AmIII_3$, $AmIII_2$, and C_α-H vibration cross sections increase again at excitation wavelengths shorter than 194 nm.

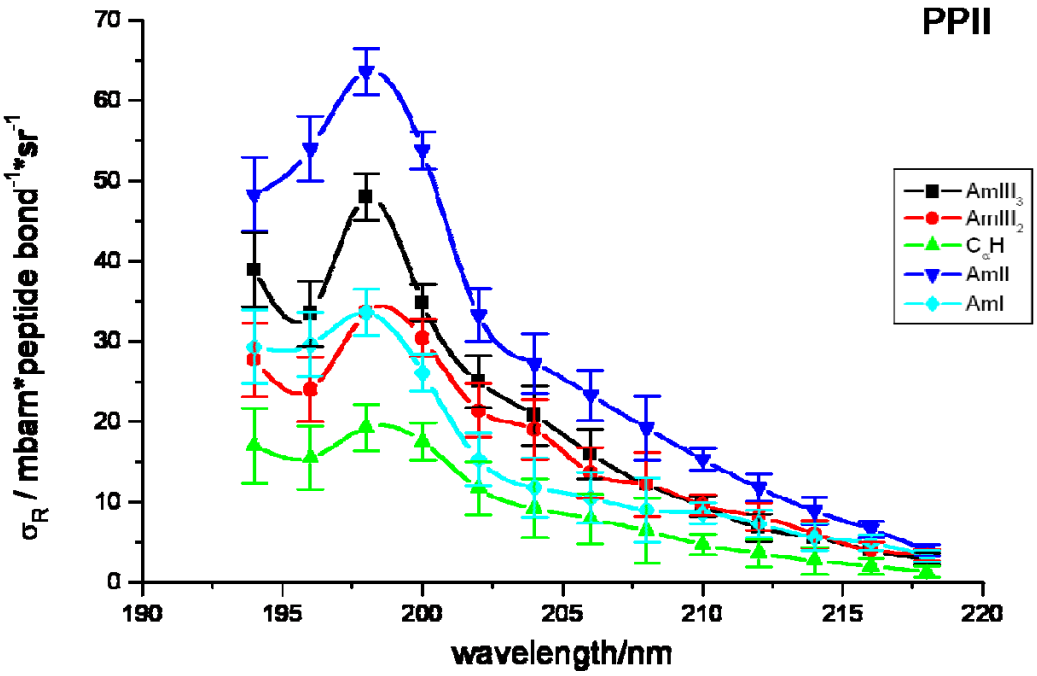

Figure 4.7 PPII-like conformation absolute Raman cross sections (mbarn*peptide bond^{-1}*sr^{-1}) excitation profiles between 194 to 218 nm.

The largest cross sections occur for the AmII vibration, which is comprised of C-N st coupled with N-H in-plane b. The AmII vibration was previously shown to be the most enhanced vibration in N-methylacetamide (NMA), because the large component of C-N st in the AmII vibration couples to the large ππ* excited state C-N bond length expansion.[18] It, thus,

appears that the AP amide $\pi \rightarrow \pi^*$ transitions for the PPII-like conformation (as well as for the α-helix as shown below) are similar to that in NMA.

The AmIII vibration is the next most intense vibration because it also contains a large amount of C-N bond stretching. In the PPII-like conformation of AP, two bands occur in the AmIII region. These $AmIII_3$ and $AmIII_2$ bands have Raman cross sections which are considerably less than that of the AmII vibration. This is consistent with previous data on the normal modes of a polyalanine peptide that indicate that the C-N motion contribution to the AmII vibration is two times greater than that of the AmIII vibrations.[58]

In order to accurately examine the behavior of the AmI vibration in AP, we corrected for the contribution to the AmI band of the 1669 cm^{-1} Arg band by removing the overlapping Arg contribution to this spectral region.[4] To estimate the contribution of this underlying Arg band to the integrated area of the AmI band, a spectrum of free Arg in solution was used to calculate the cross section of the 1669 cm^{-1} Arg band. The Arg cross section was then subtracted from the AmI cross sections. The Arg band at 1669 cm^{-1} accounts for ~ 39% of the AmI band intensity. The small cross section for the AmI (C=O st) vibration compared to the AmII vibration is similar to that in NMA, presumably because the C=O bond in AP also exhibits only a minimal excited state expansion.[18] This weak AmI enhancement is also observed in the difference spectrum between Ala_5 (A_5) and Ala_3 (A_3), which displays the spectrum of the interior two peptide bonds in a PPII-like conformation.

In the PPII-like conformation there are two C_α-H bending bands at 1377 and 1399 cm^{-1} which show almost identical excitation profiles. We calculated the average cross sections by integrating over both bands. In AP, the C_α-H bend couples with N-H bending motion to produce an excitation profile that is similar to that of the other amide bands. For the PPII-like

conformation, the C_α-H bending bands show an excitation profile maximum at the same wavelength as all the other amide bands, λ_{max} = 198 nm.

4.3.4.2 α-helix Conformation

For the AP α–helical conformation, we see a broad excitation profile where the Raman cross sections increase continuously from 218 to 194 nm (Figure 4.8). It is not clear whether the maximum occurs at 194 nm or at lower wavelength. As in the PPII-like excitation profile, the AmII band has the largest Raman cross section, indicating again, as in NMA, that the α-helix ππ* excited state displacement is mainly along the C-N bond, just as in for the PPII-like conformation. In the AmI region, the α-helix 1669 cm^{-1} Arg band contribution was also subtracted to calculate the pure AmI cross sections. The $AmIII_3$, $AmIII_2$, AmII and AmI vibrations show very similar excitation profiles. The $AmIII_1$ vibration, however, shows a somewhat different profile than the $AmIII_3$ and $AmIII_2$ vibrations.

The different excitation profile maxima for the PPII-like and α-helix conformations indicate different electronic transition frequencies for the underlying electronic transitions. Comparing the Raman cross section data for AP in both PPII-like (Table 4.1) and α-helical (Table 4.2) conformations, we find cross sections for PPII-like conformation are in general significantly larger than the α-helix, presumably due to hypochromism for the NV_1 ($\pi \rightarrow \pi^*$) absorption band of the α-helix.[59, 60] For both conformations we find a shoulder in the excitation profile between 205-~207 nm which is suggestive of an underlying electronic transition. The spacing between this shoulder and the ~190-198 nm absorption maximum is too large to be consistent with a vibronic progression.

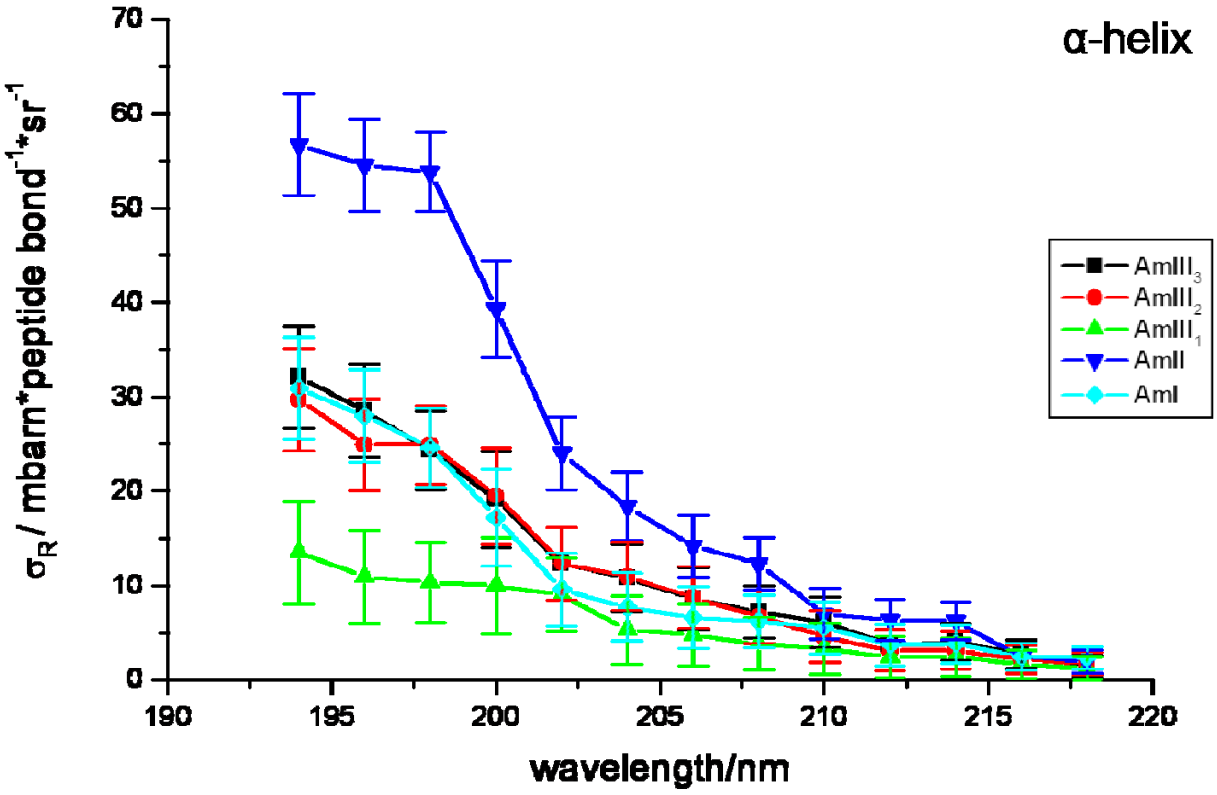

Figure 4.8 α-helix conformation absolute Raman cross sections (mbarn*peptide bond^{-1}*sr^{-1}) excitation profiles of AP between 194 to 218 nm.

Table 4.1 PPII-like conformation absolute Raman cross sections (mbarn*peptide bond^{-1}*sr^{-1})

Wavelength (nm)	AmIII$_3$ 1247 cm^{-1}	AmIII$_2$ 1311 cm^{-1}	C_α- H (ave) 1377 & 1399 cm^{-1}	AmII 1548 cm^{-1}	AmI 1659 cm^{-1}
194	38.9	27.7	17.0	48.3	29.3
196	33.4	24.0	15.5	54.0	29.6
198	48.0	33.6	19.3	63.6	33.6
200	34.8	20.4	17.5	53.8	26.1
202	25.0	21.4	11.7	33.3	15.3
204	20.8	19.0	9.2	27.2	11.8
206	16.0	13.6	7.9	23.3	10.5
208	12.2	12.2	6.4	19.2	9.0
210	9.5	9.6	4.7	15.3	8.6
212	6.8	8.2	3.6	11.8	7.3
214	5.6	6.0	2.7	8.9	5.6
216	4.0	4.0	2.0	6.6	4.9
218	2.9	3.4	1.3	4.0	3.2

Table 4.2 α-helix conformation absolute Raman cross sections (mbarn*peptide bond^{-1}*sr^{-1})

Wavelength (nm)	$AmIII_3$ 1261 cm^{-1}	$AmIII_2$ 1303 cm^{-1}	$AmIII_1$ 1337 cm^{-1}	AmII 1538 cm^{-1}	AmI 1657 cm^{-1}
194	32.1	29.7	13.5	56.7	30.9
196	28.5	24.9	10.9	54.5	28.0
198	24.3	24.9	10.3	53.8	24.6
200	19.1	19.5	10.0	39.3	17.2
202	12.3	12.3	9.0	24.0	9.6
204	10.8	10.9	5.3	18.4	7.7
206	8.6	8.7	4.8	14.2	6.6
208	7.2	6.7	3.8	12.3	6.2
210	6.1	4.6	3.3	7.0	5.5
212	3.7	3.1	2.4	6.3	3.7
214	4.0	3.1	2.4	6.2	3.8
216	2.7	2.2	1.6	2.4	2.4
218	1.4	1.7	1.2	1.9	2.3

4.3.5 Comparison between UV Raman Excitation Profiles, Absorption and CD Spectra and Raman Depolarization Ratios

The excitation profiles of the α-helix and PPII-like conformations both reveal a shoulder centered at ~207 nm, which suggests the presence of a second electronic transition. No similar feature is evident in the absorption spectrum, nor is there a clear 207 nm feature in the CD spectrum shown in Figure 4.9a (although there is a minimum in the CD spectrum at 204 nm) which compares the averaged AP Raman excitation profiles of the α-helix conformation with the measured absorption and CD spectrum at 5 °C (where the α-helix dominates).

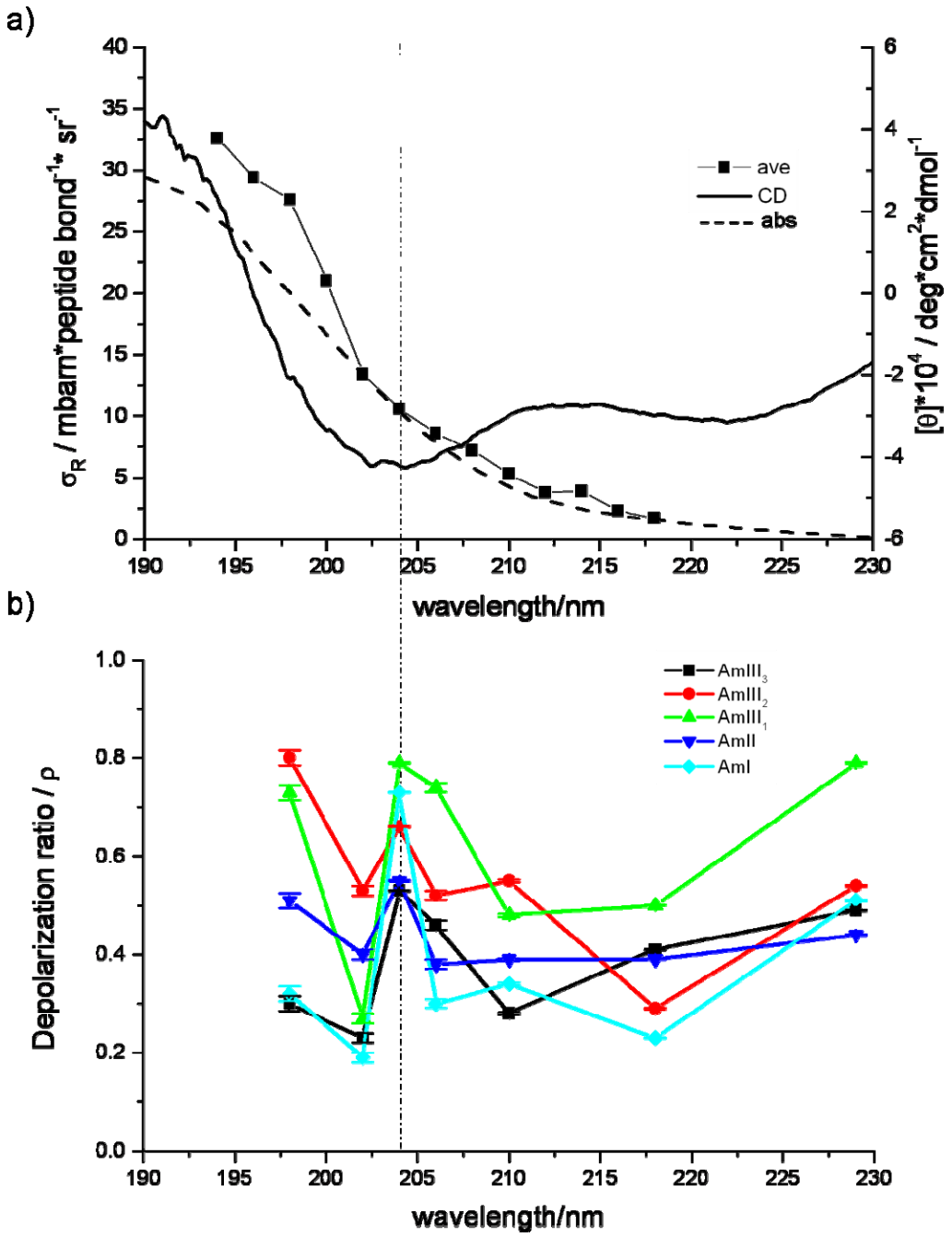

Figure 4.9 (a) The average amide band excitation profile for the α-helix conformation, excluding the AmI cross section; CD spectrum of AP at 5 °C; absorption spectrum of AP at 5 °C. (b) Raman depolarization ratios of AP at 5 °C. The dashed line indicates the presence of the shoulder in the excitation profile.

4.3.5.1 α-helix Conformation

In the α-helix it is well established that the $\pi \rightarrow \pi^*$ transition undergoes excitonic splitting to result in two delocalized dipole-allowed transitions, one is perpendicular (190 nm) and the other parallel (205 nm) to the helical axis.[42-44, 46] The parallel component of the $\pi \rightarrow \pi^*$ transition presents in the CD spectrum as a strong negative band at ~205 nm.[46] Thus, we straightforwardly assign the shoulder centered at ~207 nm in the α-helix excitation profile as the parallel component of the α-helix $\pi \rightarrow \pi^*$ transition.

The Raman depolarization ratio measurements support this conclusion. A single, non-degenerate electronic transition will cause a single resonance Raman tensor element to dominate, giving a Raman depolarization ratio, $\rho = 0.33$ independent of excitation wavelength.[24,27,61] For values of $\rho \neq 0.33$ the resonance enhancement must arise from at least two diagonal elements of the Raman tensor. If $\rho > 0.33$, and if there are only two components of the Raman tensor, they must be of opposite sign. For $\rho < 0.33$, where only two elements contribute, the two diagonal elements must be of the same sign.[24,27,61] Thus, $\rho \neq 0.33$ requires that at least two electronic transitions contribute.

Two nondegenerate electronic transitions with different transition moment orientations near one another which give rise to similar resonance Raman polarizability values (and which have the same sign, which is typical) in preresonance will give rise to $\rho < 0.33$ in preresonance at an excitation energy below the two transitions. The depolarization ratio will approach $\rho = 0.33$ as excitation occurs close to resonance with either of the transitions (assuming the homogeneous linewidths are less than the energy difference between transitions). However, for excitation at energies between the transitions, the two Raman polarizability values will be of opposite sign,

leading to a peak in ρ which equals 0.75 for equal contributions. Obviously, peaks in the value of ρ can be used to signal the existence of electronic transitions underlying broad absorption bands.

The situation for our case is likely to be more complex since more than two transitions exist. For example, there is a deep UV transition which is already known to be important for the Am I vibration enhancement.[23] Further, for the ideal infinite α-helix the perpendicular exciton component is degenerate and should give rise to a resonance Raman ρ = 0.125.

For AP, the situation is even more complex, since the α-helix is of finite length and may include short α-helical segments. Further, we recently demonstrated that the AP α-helical state is actually composed of comparable amounts of α-helix, 3_{10} helix and π-bulge conformations.[14] Thus, the α-helix Raman excitation profile, as well as the depolarization ratios will derive from the weighted summed contributions from each of the underlying components, which we expect to be similar.

From 230 to 210 nm the α-helix resonance Raman depolarization ratios are centered around ρ~0.33, except for the $AmIII_1$ band. The AmI depolarization ratio measurement is complicated by overlap of the Arg band, and it is expected that ρ ≠0.33 because it is also expected to be strongly enhanced by a transition deep in the UV.[23]

At 204 nm excitation, ρ shows a maximum for all of the amide vibrations (ρ >0.5, Figure 4.9b, Table 4.3) indicating the contribution of at least two components to the Raman tensor with opposite signs. This is followed by a sharp dip in the Raman depolarization ratios of all of the amide bands at 202 nm. This dispersion must be signaling the existence of an electronic transition centered ~207 nm which coincides with the resonance Raman excitation profile shoulder (Figure 4.9). Probably these features result from the parallel component of the α-helix-like π→ π* transition.

Table 4.3 Depolarization Ratios of AP at 5 °C (α-helix).

	Wavelengths (nm)						
band	**198**	**202**	**204**	**206**	**210**	**218**	**229**
$AmIII_3$	0.30	0.23	0.53	0.46	0.28	0.41	0.49
$AmIII_2$	0.80	0.53	0.66	0.52	0.55	0.29	0.54
$AmIII_1$	0.73	0.27	0.79	0.74	0.48	0.5	0.79
AmII	0.51	0.40	0.55	0.38	0.39	0.39	0.44
AmI	0.32	0.19	0.73	0.30	0.34	0.23	0.51

4.3.5.2 PPII-like Conformation

The importance of excitonic interactions have not been clearly established for the PPII-like conformation. The lowest energy $\pi \rightarrow \pi^*$ electronic transition is expected at ~190 nm, while the weak $n \rightarrow \pi^*$ electronic transition occurs at 220 nm. The Raman excitation profiles and the Raman depolarization ratios of the PPII-like conformation are similar to those of the α-helix conformation with a shoulder at ~205 nm and a depolarization ratio peak at 204 nm (Figure 4.10, Table 4.4). The PPII-like Raman excitation profile maximum occurs at the same wavelength as the trough of the CD spectrum, affirming its assignment to the $\pi \rightarrow \pi^*$ transition.[46] The excitation profile shoulder (Figure 4.10a) coincides approximately with the values of ρ ~0.25 for all amide vibrations at ~205 nm (Figure 4.10b). This indicates the existence of an underlying electronic transition at ~205 nm for the PPII-like conformation of AP.

The similar enhancement patterns of the amide bands within the α-helical absorption spectrum indicates that the 207 nm transition is similar to the PPII ~190 nm π→π* transition. Thus, these components are probably excitonically split transition pairs. This is the first clear indication of exciton splitting in PPII-like conformations.

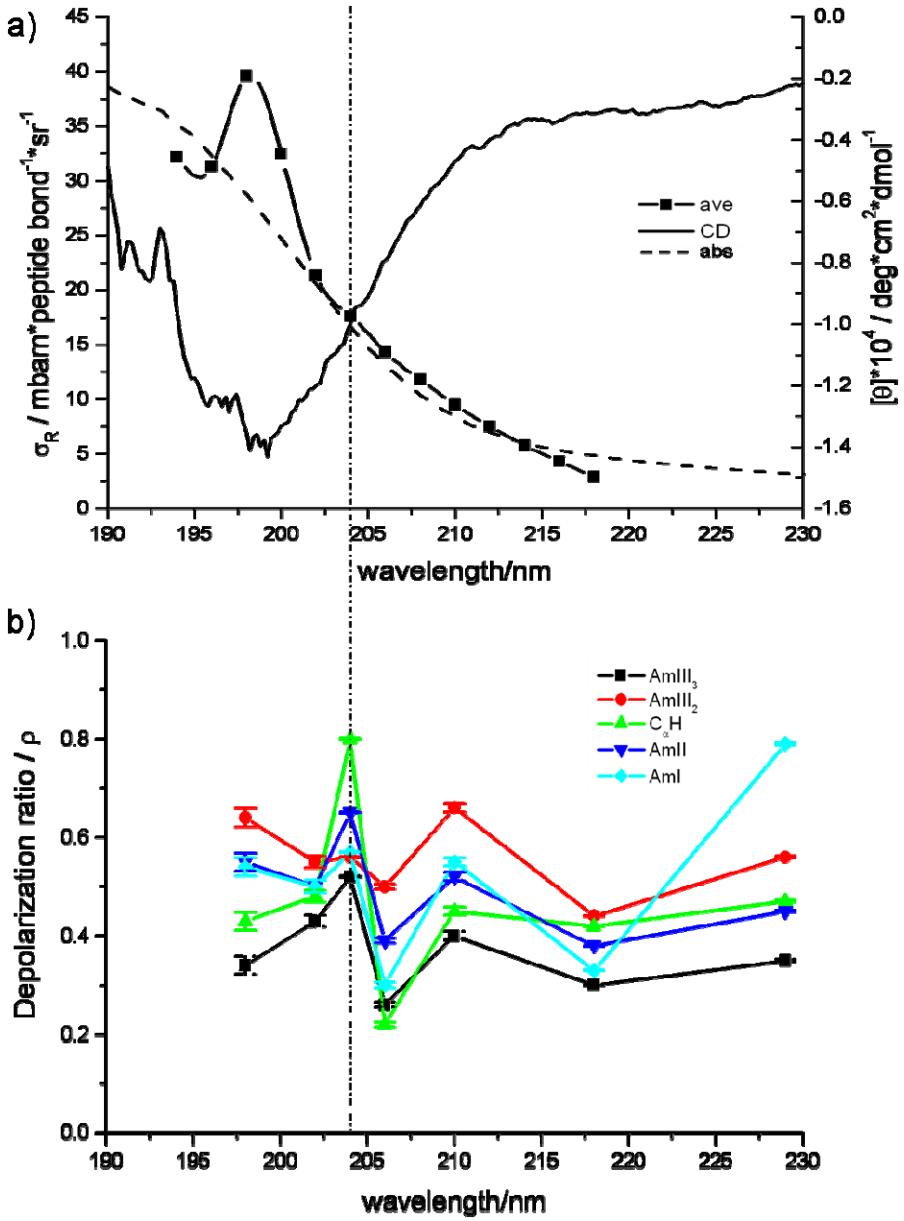

Figure 4.10 (a) The average amide band excitation profile for the PPII-like conformation, excluding the AmI cross section; CD spectrum of AP at 60 °C; absorption spectrum of AP at 60 °C. (b) Raman depolarization ratios of AP at 60 °C. The dashed line indicates the presence of the shoulder in the excitation profile.

Table 4.4 Depolarization Ratios of AP at 60° C (PPII-like).

	Wavelengths (nm)						
band	**198**	**202**	**204**	**206**	**210**	**218**	**229**
$AmIII_3$	0.34	0.43	0.52	0.26	0.40	0.30	0.35
$AmIII_2$	0.64	0.55	0.56	0.50	0.66	0.44	0.56
$C_\alpha H$	0.43	0.48	0.80	0.22	0.45	0.42	0.47
AmII	0.55	0.50	0.65	0.39	0.52	0.38	0.45
AmI	0.54	0.50	0.57	0.30	0.55	0.33	0.79

4.3.6 $AmIII_3$ Deconvolution

Recent theoretical[62-64] and experimental[20,65] studies indicate that the α-helix solution conformation actually contains contributions from 3_{10} helix[62] and π-bulge[63,64] as underlying defect structures at temperatures below 30 °C.[20] We recently demonstrated that these different α-helix-like conformations show separate underlying Raman bands.[14]

We deconvoluted our measured α-helical Raman $AmIII_3$ region with Gaussian bands to resolve the 3_{10} helix, π-bulge, and pure α-helix contributions (Figure 4.11) and calculated the individual Raman excitation profiles of these conformations (Figure 4.12). The excitation profiles of these conformations significantly differ. For example, the pure α-helix excitation profile shows the 207 nm shoulder and shows a maximum at ~197 nm. In contrast the 3_{10} helix

does not show the shoulder but only a peak at ~196 nm, possibly demonstrating a lack of excitonic interactions. In contrast, the π-bulge shows a large, broad feature between 200 and 210 nm with an excitation profile maximum deeper in the UV below 194 nm. We conclude that these different conformations within the α-helix basin have very different excitonic interactions.

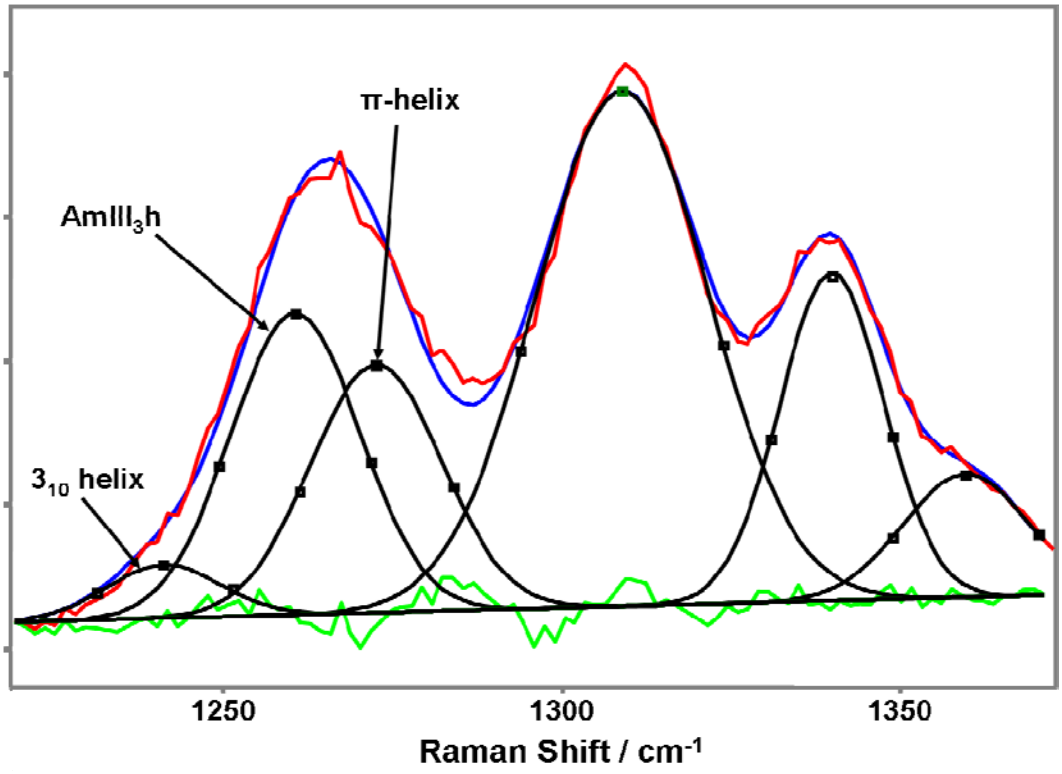

Figure 4.11 Spectral deconvolution of the $AmIII_3$ region of the α-helix-like conformations into Gaussian components. The measured and fitted Raman spectra are shown for the 3_{10} helix (1241 cm^{-1}), the pure α-helix (1261 cm^{-1}), and the π- bulge (1273 cm^{-1}) and the residual (green).

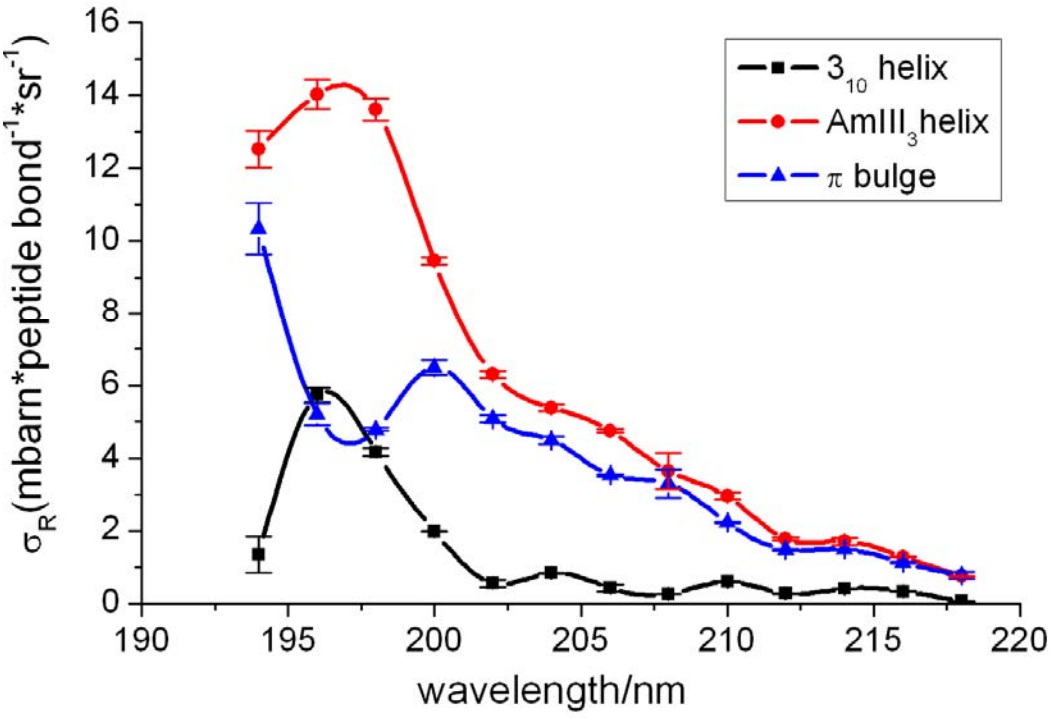

Figure 4.12 Raman excitation profiles of the $AmIII_3$ bands of the 3_{10} helix (1241 cm^{-1}), the pure α-helix (1261 cm^{-1}), and the π-bulge (1273 cm^{-1}).

4.4 CONCLUSIONS

We measured the UVRR excitation profiles and Raman depolarization ratio dispersions for the α-helix and PPII-like conformations of a 21 amino acid mainly ala peptide, AP. Both excitation profiles show a shoulder at ~205 nm. The PPII-like conformation shows a peak at ~198 nm. The α-helix like state shows shorter wavelength peak at ~194 nm. The Raman spectra and the depolarization ratios clearly signal that the 205-207 nm shoulders results from an underlying electronic transition similar to that of the shorter wavelength (~195 nm) $\pi \rightarrow \pi^*$ transitions. It is most likely that these transitions derive from the excitonically split amide $\pi \rightarrow \pi^*$ electronic

transitions. The α-helical 207 nm transition is clearly the parallel component of the excitonically split pair. The establishment of the existence of these underlying transitions will help advance the understanding of protein and peptide backbone electronic transitions. We also resolved the Raman excitation profiles of the pure α-helix, 3_{10} helix and π-bulge conformations.

Our excitation profiles of the pure α-helix, the 3_{10} helix, the π-bulge and the melted PPII-like conformations clearly indicate that different excitation wavelengths can be utilized to differentially enhance these different solution peptide conformations.

4.5 ACKNOWLEDGEMENTS

The authors thank Dr. Robert Woody and Dr. Nataliya Myshakina for useful discussions. We also thank the NIH, Grant #GM8R01EB002053

4.6 REFERENCES

1. Mix, G.; Schweitzer-Stenner, R.; Asher, S. A. *J. Am. Chem. Soc.* **2000,** *122*, 9028.
2. Ianoul, A.; Boyden, M. N.; Asher, S. A. *J. Am. Chem. Soc.* **2001,** *123*, 7433.
3. Asher, S. A.; Ianoul, A.; Mix, G.; Boyden, M. N.; Karnoup, A.; Diem, M.; Schweitzer-Stenner, R., *J. Am. Chem. Soc.* **2001,** *123*, 11775.
4. Chi, Z.; Chen, X. G.; Holtz, J. S. W.; Asher, S. A. *Biochemistry* **1998,** *37*, 2854.
5. Sieler, G.; Schweitzer-Stenner, R.; Holtz, J. S. W.; Pajcini, V.; Asher, S. A. *J. Phys. Chem. B* **1999,** *103*, 372.
6. Holtz, J. S. W.; Holtz, J. H.; Chi, Z.; Asher, S. A. *Biophys. J.* **1999,** *76*, 3227.

7. Ozdemir, A.; Lednev, I. K.; Asher, S. A. *Biochemistry* **2002,** *41*, 1893.

8. Holtz, J. S. W.; Lednev, I. K.; Asher, S. A. *Biopolymers* **2000,** *57*, 55.

9. Boyden, M. N.; Asher, S. A. *Biochemistry* **2001,** *40*, 13723-13727.

10. Chi, Z.; Asher, S. A., *J. Phys. Chem. B* **1998,** *102*, 9595.

11. Ianoul, A.; Mikhonin, A.; Lednev, I. K.; Asher, S. A. *J. Phys. Chem. A* **2002,** *106*, 3621.

12. Asher, S. A.; Mikhonin, A. V.; Bykov, S. *J. Am. Chem. Soc.* **2004,** *126*, 8433.

13. Mikhonin, A. V.; Ahmed, Z.; Ianoul, A.; Asher, S. A. *J. Phys. Chem. B* **2004,** *108*, 19020.

14. Mikhonin, A. V.; Bykov, S. V.; Myshakina, N. S.; Asher, S. A. *J. Phys. Chem. B* **2006,** *110*, 1928.

15. Mikhonin, A. V.; Myshakina, N. S.; Bykov, S. V.; Asher, S. A. *J. Am. Chem. Soc.* **2005,** *127*, 7712.

16. Cho, N.; Asher, S. A. *Biospectroscopy* **1996,** *2*, 71.

17. Asher, S. A. *Anal. Chem.* **1993,** *65*, 59A.

18. Chen, X. G.; Asher, S. A.; Schweitzer-Stenner, R.; Mirkin, N. G.; Krimm, S. *J. Am. Chem. Soc.* **1995,** *117*, 2884.

19. Beeler, J. A.; Yan, S.-Z.; Bykov, S.; Murza, A.; Asher, S.; Tang, W.-J. *Biochemistry* **2004,** *43*, 15463.

20. Mikhonin, A. V.; Asher, S. A. *J. Am. Chem. Soc.* **2006,** *128*, 13789.

21. Pimenov, K. V.; Bykov, S. V.; Mikhonin, A. V.; Asher, S. A. *J. Am. Chem. Soc.* **2005,** *127*, 2840

22. Dudik, J. M.; Johnson, C. R.; Asher, S. A. *J. Chem. Phys.* **1985,** *82*, 1732.

23. Asher, S. A.; Chi, Z.; Li, P., *J. Raman Spec.* **1998,** *29*, 927.

24. Chen, X. G.; Schweitzer-Stenner, R.; Asher, S. A.; Mirkin, N. G.; Krimm, S. *J. Phys. Chem.* **1995,** *99*, 3074.

25. Chen, X. G.; Schweitzer-Stenner, R.; Krimm, S.; Mirkin, N. G.; Asher, S. A. *J. Am. Chem. Soc.* **1994,** *116*, 11141.

26. Lednev, I. K.; Karnoup, A. S.; Sparrow, M. C.; Asher, S. A. *J. Am. Chem. Soc.* **1999,** *121*, 8074.

27. Chen, X. G.; Li, P.; Holtz, J. S. W.; Chi, Z.; Pajcini, V.; Asher, S. A.; Kelly, L. A. *J. Am. Chem. Soc.* **1996,** *118*, 9716.

28. Huang, C.-Y.; Balakrishnan, G.; Spiro, T. G. *J. Raman Spect.* **2006,** *37*, 277.

29. JiJi, R. D.; Balakrishnan, G.; Hu, Y.; Spiro, T. G. *Biochemistry* **2006,** *45*, 34.

30. Peterson, D. L.; Simpson, W. T. *J. Am. Chem. Soc.* **1957,** *79*, 2375.

31. Basch, H.; Robin, M. B.; Kuebler, N. A. *J. Chem. Phys.* **1967,** *47*, 1201.

32. Basch, H.; Robin, M. B.; Kuebler, N. A. *J. Chem. Phys.* **1968,** *49*, 5007.

33. Schellman, J. A.; Nielsen, E. B. *J. Phys. Chem.* **1967,** *71*, 3914.

34. Barnes, D. G.; Rhodes, W. *J. Chem. Phys.* **1968,** *48*, 817.

35. Serrano-Andres, L.; Fuelscher, M. P. *J. Am. Chem. Soc.* **1998,** *120*, 10912.

36. Serrano-Andres, L.; Fuelscher, M. P. *J. Phys. Chem. B* **2001,** *105*, 9323.

37. Clark, L. B. *J. Am. Chem. Soc.* **1995,** *117*, 7974.

38. Pajcini, V.; Asher, S. A. *J. Am. Chem. Soc.* **1999,** *121*, 10942.

39. Hunt, H. D.; Simpson, W. T. *J. Am. Chem. Soc.* **1953,** *75*, 4540.

40. Robin, M. B. *Higher Excited States of Polyatomic Molecules*, *vol. III;* Academic Press, Inc.:New York, 1985.

41. Moffitt, W. *J. Chem. Phys.* **1956,** *25*, 467.

42. Rosenheck, K.; Doty, P. *Proc. Natl. Acad. Sci. U.S.A.* **1961,** *47*, 1775.

43. Brahms, J.; Pilet, J.; Damany, H.; Chandrasekharan, V. *Proc. Natl. Acad. Sci. U.S.A.* **1968,** *60*, 1130.

44. Brahms, S.; Brahms, J. *J. Molec. Biol.* **1980,** *138*, 149.

45. Mandel, R.; Holzwarth, G. *J. Chem. Phys.* **1972,** *57*, 3469.

46. Woody, R. W. *Monatshefte fur Chemie* **2005,** *136*, 347.

47. Blanch, E. W.; Morozova-Roche, L. A.; Cochran, D. A. E.; Doig, A. J.; Hecht, L.; Barron, L. D. *J. Molec. Biol.* **2000,** *301*, 553.

48. Shi, Z.; Woody, R. W.; Kallenbach, N. R. *Adv. Prot. Chem.* **2002,** *62*, 163.

49. Ramakrishnan, V.; Ranbhor, R.; Durani, S. *J. Am. Chem. Soc.,* **2004,** *126,* 16332.

50. Asciutto, E. K.; Mikhonin, A. V.; Asher, S. A.; Madura, J. D. *Biochemistry*, **2008,** *47,* 2046.

51. Vila, J. A.; Baldoni, H. A.; Ripoll, D. R.; Ghosh, A.; Scheraga, H.A. *Biophys. J.* **2004,** *86*, 731.

52. Makowska, J.; Rodziewicz-Motowidlo, S.; Baginska, K; Makowski, M.; Vila, J. A.; Liwo, A.; Chmurzynski, L.; Scheraga, H.A. *Biophys. J.* **2007,** *92*, 2904.

53. Lednev, I. K.; Karnoup, A. S.; Sparrow, M. C.; Asher, S. A. *J. Am. Chem. Soc.* **2001,** *123*, 2388.

54. Bykov, S.; Lednev, I.; Ianoul, A.; Mikhonin, A.; Munro, C.; Asher, S. A. *Appl. Spect.* **2005,** *59*, 1541.

55. DeVito, V. L.; Cai, M. Z.; Asher, S. A.; Kehres, L. A.; Smith, K. M. *J. Phys. Chem.* **1992,** *96*, 6917.

56. Shriver, D. F.; Dunn, J. B. R. *Appl. Spect.* **1974,** *28*, 319.

57. Ludwig, M.; Asher, S. A. *Appl. Spect.* **1988,** *42*, 1458.

58. Lee, S.-H.; Krimm, S. *Biopolymers* **1998,** *46*, 283.

59. Imahori, K.; Tanaka, J. *J. Molec. Biol.* **1959,** *1*, 359.

60. Tinoco, Jr., I.; Halpern, A.; Simpson, W. T. In *Polyamino Acids, Polypeptides, and Proteins*; Stahmann, M.A. Ed.; University of Wisconsin Press: Madison, 1962; Chapter 13.

61. Long, D. A. *The Raman Effect: A Unified Treatment of the Theory of Raman Scattering by Molecules*; John Wiley & Sons: New York, 2002.

62. Sorin, E. J.; Rhee, Y. M.; Shirts, M. R.; Pande, V. S. *J. Mol. Biol.* **2006,** *356*, 248.

63. Cartailler, J.-P.; Luecke, H. *Structure,* **2004,** *12,* 133.

64. Ismer, L.; Ireta, J.; Neugebauer, J. *J. Phys. Chem. B*, **2008,** *112,* 4109.

65. Goetz, M.; Carlotti, C.; Bontems, F.; Dufourc, E.J. *Biochemistry,* **2001,** *40,* 6534.

5.0 UV RESONANCE RAMAN INVESTIGATION OF THE CONFORMATIONS AND LOWEST ENERGY ALLOWED ELECTRONIC EXCITED STATES OF TRI- AND TETRA-ALANINE: CHARGE TRANSFER TRANSITIONS

UV resonance Raman excitation profiles and Raman depolarization ratios were measured for trialanine and tetraalanine between 198 and 210 nm. Excitation within the $\pi \rightarrow \pi^*$ electronic transitions of the peptide bond results in UVRR spectra dominated by amide peptide bond vibrations. In addition to the resonance enhancement of the normal amide vibrations, we find enhancement of the symmetric terminal COO^- vibration. The Ala_3 UVRR $AmIII_3$ band frequencies indicate that poly-proline II and 2.5_1 helix conformations and Type II turns are present in solution. We also find that the conformation of the interior peptide bond of Ala_4 is predominantly poly-proline II-like. The Raman excitation profiles of both Ala_3 and Ala_4 reveal a charge transfer electronic transition at 202 nm, where electron transfer occurs from the terminal nonbonding carboxylate orbital to the adjacent peptide bond π^* orbital. Raman depolarization ratio measurements support this assignment. An additional electronic transition is found in Ala_4 at 206 nm. (This work was published in the *J. Phys. Chem. B* **2010**, 114, 6661-6668.)

5.1 INTRODUCTION

UV resonance Raman (UVRR) spectroscopy is recognized as a powerful technique for probing peptide and protein secondary structure.[1-14] UVRR spectroscopy also provides insight into the geometry of the excited states and electronic transitions through Raman excitation profiles and Raman depolarization ratios.[11-13] Excitation between 180 and 215 nm is in resonance with the amide $\pi \rightarrow \pi^*$ electronic transition of the peptide backbone, resulting in enhancement of amide vibrations.[1-13] In the work here, we use UVRR spectroscopy to examine the secondary structure conformations and underlying electronic transitions of both Ala_3 and Ala_4.

Alanine-based peptides are often used as theoretical and experimental models to study protein conformation and folding.[1, 2, 15-25] The folded state of longer alanine peptides is predominantly α-helix-like,[1-3, 19, 24, 25] while the conformation of the unfolded state has been established to be a polyproline II (PPII) helix-like structure,[9, 20-23, 26] (although there remains some controversy with this assignment.[27, 28]) Short alanine peptides, such as trialanine (Ala_3) and tetraalanine (Ala_4), are often used as models for the unfolded state of peptides and proteins. Although there have been numerous studies of Ala_3 and Ala_4 which have identified a number of equilibrium conformations, the conformational distributions are still not clear.[15, 29-43]

Most studies agree that the unfolded state for both peptides is populated mainly by the poly-proline II helix (PPII) conformation. [15, 29-36, 38, 41-43] There is, however, little agreement on the other conformations present in equilibrium. The reported conformational distributions include: only PPII [31, 39, 41, 42], PPII, with either an additional β structure [29, 30, 33] or a right-handed α-helix (α_R)43; and a β structure with α_R-helix.[15, 32, 35, 36, 40] Another study reported that the conformations in solution include PPII, a β-like structure, an α_R-helix, and a γ-turn.38 A few

studies that found only one conformation present assigned it to either a left-handed helix[34] or an extended β-helix-like structure,[37] both of which are similar to a PPII-like conformation.

In the study here we measured the UVRR excitation profiles and Raman depolarization ratios of aqueous solutions of Ala_3 and Ala_4 between 198 to 210 nm at 25 °C to determine the solution conformation(s) and electronic transitions of Ala_3 and Ala_4. We find that both Ala_3 and Ala_4 adopt three primary conformations: PPII-like, 2.5_1 helix-like, and Type II turns; and that Ala_4 may also adopt an additional unknown conformation. We observe the previously described charge transfer transition[12] at 202 nm in both peptides. We also observe a transition in Ala_4 at 206 nm, whose origin remains murky.

5.2 MATERIALS AND METHODS

5.2.1 Sample Preparation

Dialanine (Ala_2), trialanine (Ala_3) and tetra-alanine (Ala_4) were purchased from Bachem (Torrance, CA) and used as received. We used 6.6 mM, pH 7 solutions of Ala_3 and Ala_4 for the UVRRS measurements. Each sample contained sodium perchlorate (0.2 M) as an internal standard. The UVRR spectral measurements were taken at 25 °C ± 0.5 °C.

5.2.2 Raman Instrumentation

The UVRR instrumentation was previously described.[44] The laser source used was a Positive Light Co. Indigo-DUV Ti:Sapphire laser system (Coherent, Santa Clara, CA). The Indigo-DUV

system utilizes an intra-cavity frequency doubled, Q-switch pulsed Nd:YLF Evolution 15 laser (527 nm, 30 nsec pulse width, 5 kHz repetition rate, 10 W average power) to pump a Ti:Sapphire oscillator, which generates tunable radiation from 772 to 840 nm. Raman excitation in the deep UV is obtained by mixing the third harmonic with the fundamental, producing tunable radiation between 193 and 210 nm. The average powers in the deep UV vary between 2-5 mW.

The laser beam was focused into a temperature-controlled, circulating flow stream. The flow stream was purged with N_2 to eliminate Raman scattering from the O_2 band at 1555 cm^{-1}. Each 20-mL sample was irradiated for a maximum of 15 min. The scattered light was directed into a subtractive double monochromator[44] and the Raman scattered light was detected by a liquid nitrogen cooled CCD (Princeton Instruments, Spec-10:400B). The Raman intensities were normalized to that of the 932 cm^{-1} perchlorate (ClO_4^-) symmetric stretch vibration. The spectra were analyzed and deconvoluted using Grams/32 AI 8.0 software (Thermo Electron Corporation, Waltham, MA).

UV Raman depolarization ratios (ρ) were measured using a 180° back scattering geometry. The light collected from the sample was directed through a UV linear dichroic polarizer (Oriel Instruments, Stratford, CT) followed by a crystalline quartz polarization scrambler (Spex Industries, Edison, NJ) before the monochromator entrance slit. The depolarization ratio ρ was calculated as a ratio of the perpendicularly polarized light ($I_\perp$) to the parallel polarized light ($I_\parallel$):

$$\rho = \frac{I_\perp}{I_\parallel} \qquad \textbf{(5.1)}$$

The depolarization ratios of ClO_4^- and cyclohexane were used as standards[14] to verify the accuracy of the measured depolarization ratios.

5.2.3 Spectrometer Efficiency

The spectrometer used was a modified Spex 1401 double monochromator that operates over the 193-270 nm range. We corrected for the wavelength dependence of throughput efficiency by using previously determined spectrometer efficiencies. [44]

5.2.4 Absorption Measurements

The UV absorption spectra of Ala_2, Ala_3 and Ala_4 between 190 and 250 nm were measured using a Cary 5000 Varian UV-Vis-NIR spectrophotometer. The absorption measurements were taken with solution concentrations of 0.5 mM at pH 7 and pH 2 at room temperature (25 °C ± 0.5 °C).

5.3 RESULTS AND DISCUSSION

5.3.1 Absorption Spectra

The absorption spectra of Ala_2, Ala_3 and Ala_4 are shown in Figure 5.1. The molar absorptivities increase for all three peptides at both pH 7 and pH 2 as the wavelength decreases from 250 nm to 190 nm.

For Ala_2, the broad absorption band centered below ~190 nm derives from the amide $\pi \rightarrow \pi^*$ NV_1 electronic transition for both pH 7 and pH 2 (Figure 5.1a). The absorption maximum of the pH 2 spectrum, where the carboxylate group is protonated, appears to be blue-shifted

compared with the pH 7 spectrum. The pH difference spectrum for Ala_2 indicates the presence of an underlying transition in the pH 7 absorption spectrum at ~202 nm, which disappears at pH 2. The absorption difference spectra for each peptide can be well fit with two Gaussian bands (Figure 5.2a-c). For Ala_2, the Gaussian bands are centered at 180 nm (not shown) and 203 nm (Figure 5.2a). The 180 nm band is assigned to the amide NV_1 $\pi \rightarrow \pi^*$ electronic transition, and we assign the ~203 nm band to a charge transfer transition, similar to those previously found in Gly dipeptides.[12] Chen et al. [12] previously demonstrated that a charge transfer transition occurs at ~ 200 nm in short Gly peptides. The transition involves transfer of charge from the nonbonding carboxylate orbital to the amide π^* orbital (Figure 5.3). This charge transfer band disappears in the low pH protonated species.

For Ala_3 (Figure 5.1b) and Ala_4 (Figure 5.1c), the broad absorption band centered below ~190 nm derives from the amide $\pi \rightarrow \pi^*$ NV_1 electronic transitions at both pH 7 and pH 2. The Ala_3 and Ala_4 pH 7 spectra are broader and absorb more than the pH 2 spectra.

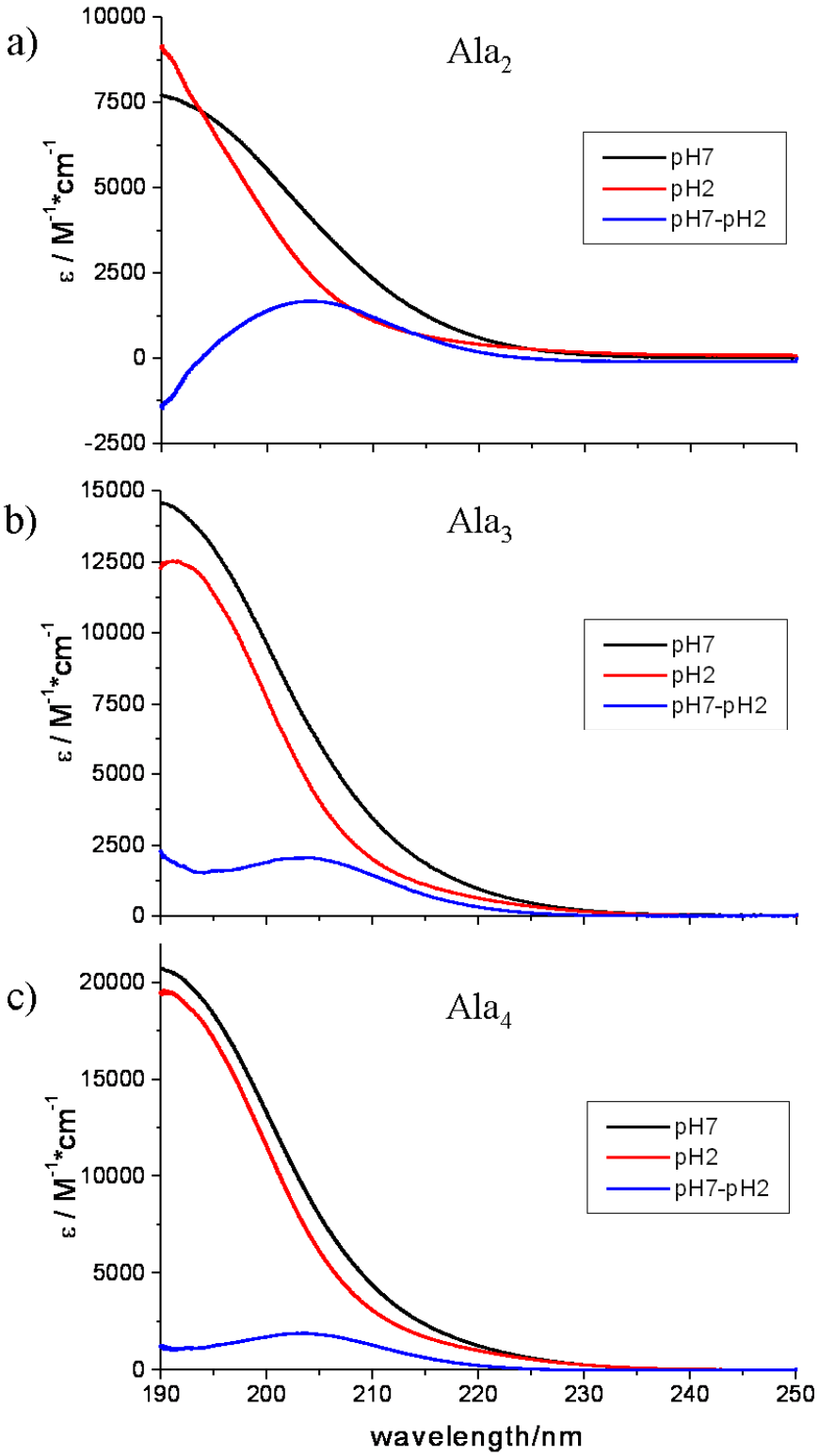

Figure 5.1 UV absorption spectra at pH 7 (black), pH 2 (red), and the pH absorption difference spectra (blue) for (a) Ala_2, (b) Ala_3, and (c) Ala_4. All absorption measurements were taken of 0.5 mM peptide solutions at 25 °C.

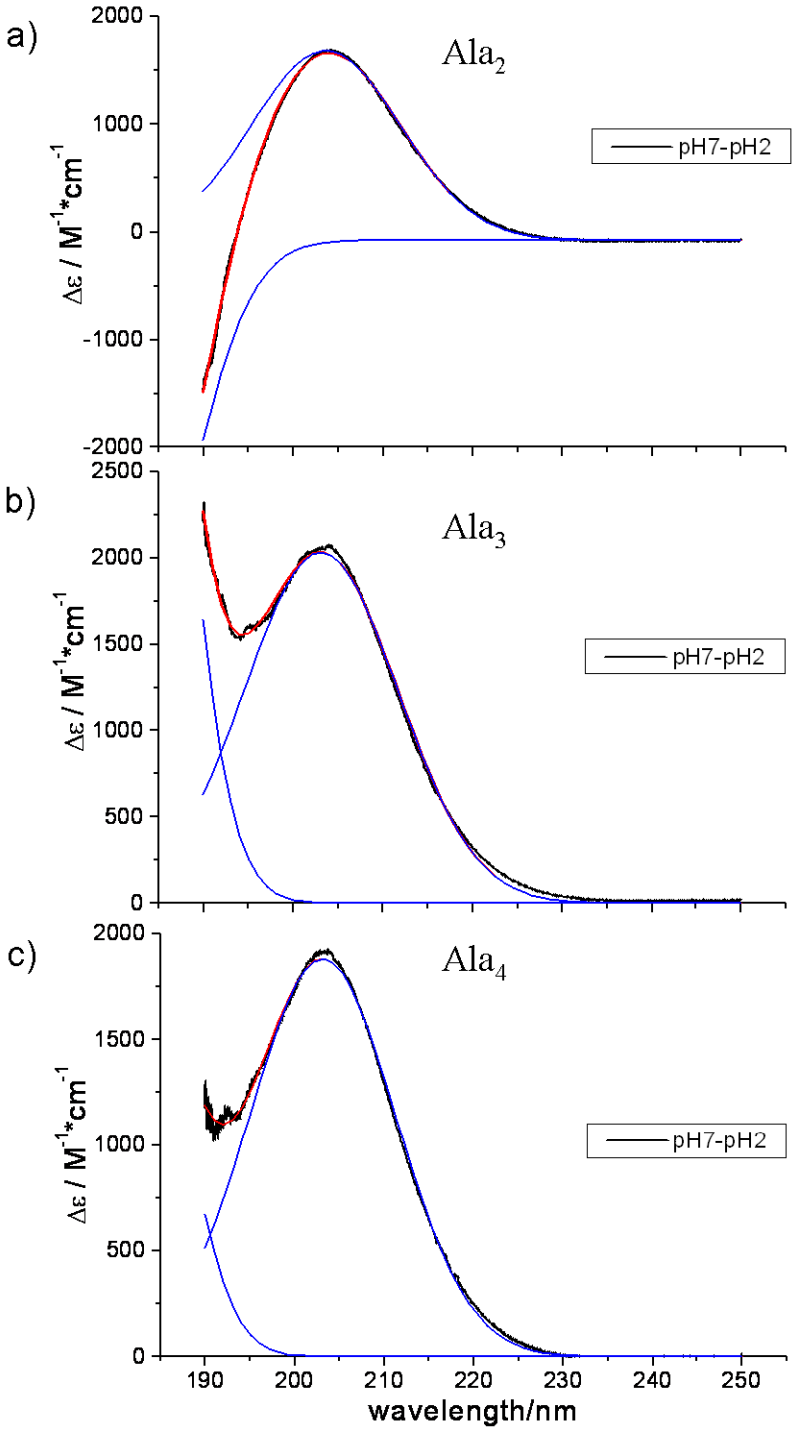

Figure 5.2 Deconvolution of absorption spectra. The pH7-pH2 difference spectra (black) are fit with two Gaussian bands (blue), the resulting fit curve (red) matches the experimental curve remarkably well. (a) Ala_2, (b) Ala_3, (c) Ala_4.

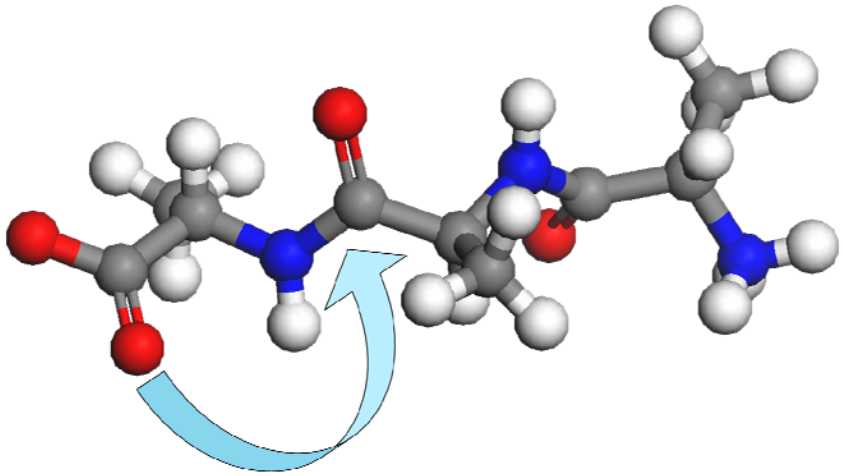

Figure 5.3 Ala_3 zwitterion in an extended β conformation. The electron density charge transfer from carboxylate to amide is indicated by the blue arrow. (Picture courtesy of Nataliya Myshakina).

5.3.2 UVRR Spectra

The UVRR spectra for Ala_3 and Ala_4 at 25 °C excited between 198 and 210 nm are shown in Figure 5.4 and Figure 5.5, respectively. All spectra were normalized to the symmetric perchlorate stretch (932 cm^{-1}).

Vibrations enhanced in both Ala_3 and Ala_4 include the Amide I (AmI) vibration at ~1655 cm^{-1}, which is primarily a C=O stretching vibration (st). The enhanced Amide II (AmII) vibration involve C-N stretching (st), coupled with N-H bending (b) at ~ 1550 cm^{-1}. The symmetric stretching of the carboxylate appears at ~1400 cm^{-1} but is overlapped by other bands. The symmetric b vibrations of the CH_3 and C_α-H groups occur at 1371 cm^{-1} and 1332 cm^{-1}, respectively. There is an additional vibration present at 1391 cm^{-1} assigned as CH_3 + C_α-H bending, which most strongly overlaps the symmetric carboxylate stretch. The Amide III (AmIII) region is broad and spans the 1200 - 1300 cm^{-1} range. The bands in the AmIII region

result primarily from vibrations composed of C-N st coupled to N-H b, but can also include C_α-C st, N-C st, C-N st, and some C_α-H b.[9] Both peptides show the highest relative band intensities for 202 nm excitation. The relative band intensities within the spectra are similar across the range of excitation wavelengths, indicating that similar or identical electronic transitions are involved in the enhancement.

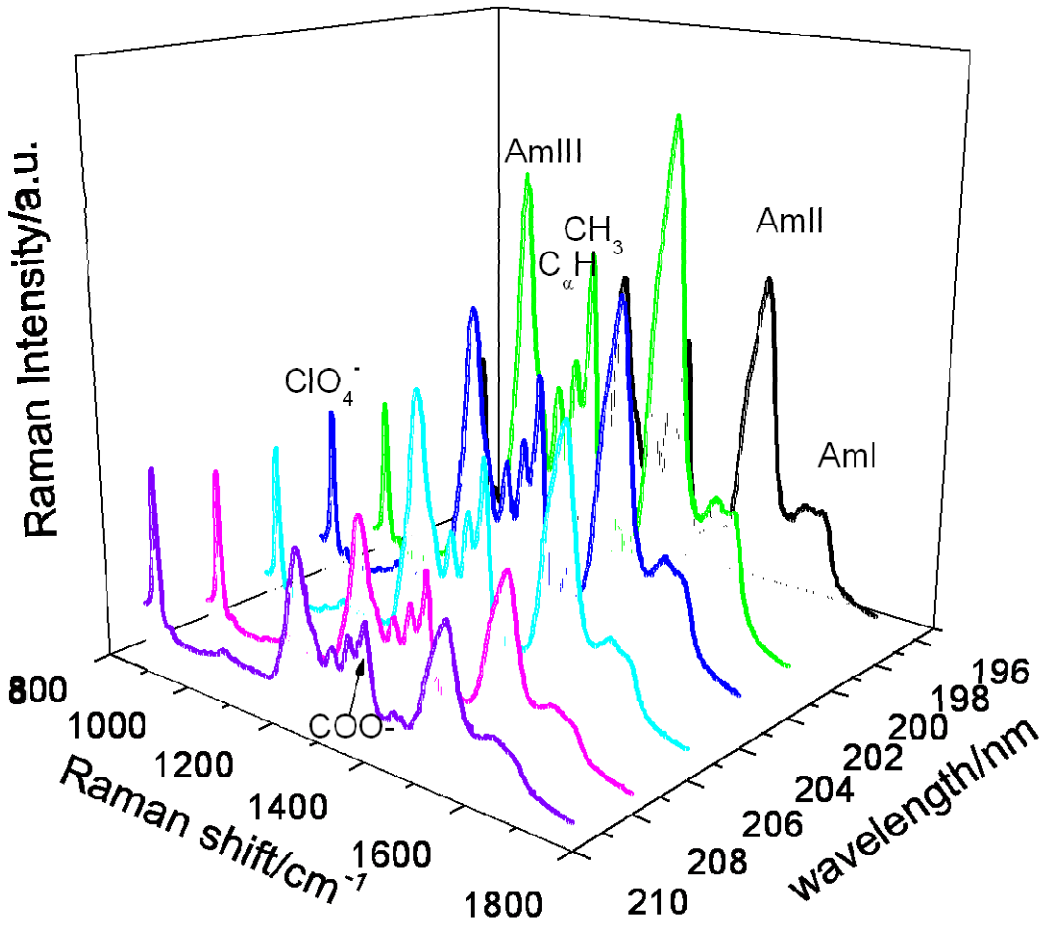

Figure 5.4 UVRR spectra of Ala_3 (6.6×10^{-3} M) at 25 °C excited between 198 and 210 nm. Spectra were collected for 15 min each. The spectral resolution is ~ 5 cm^{-1}. Spectra were not corrected for self-absorption or spectrometer throughput efficiency.

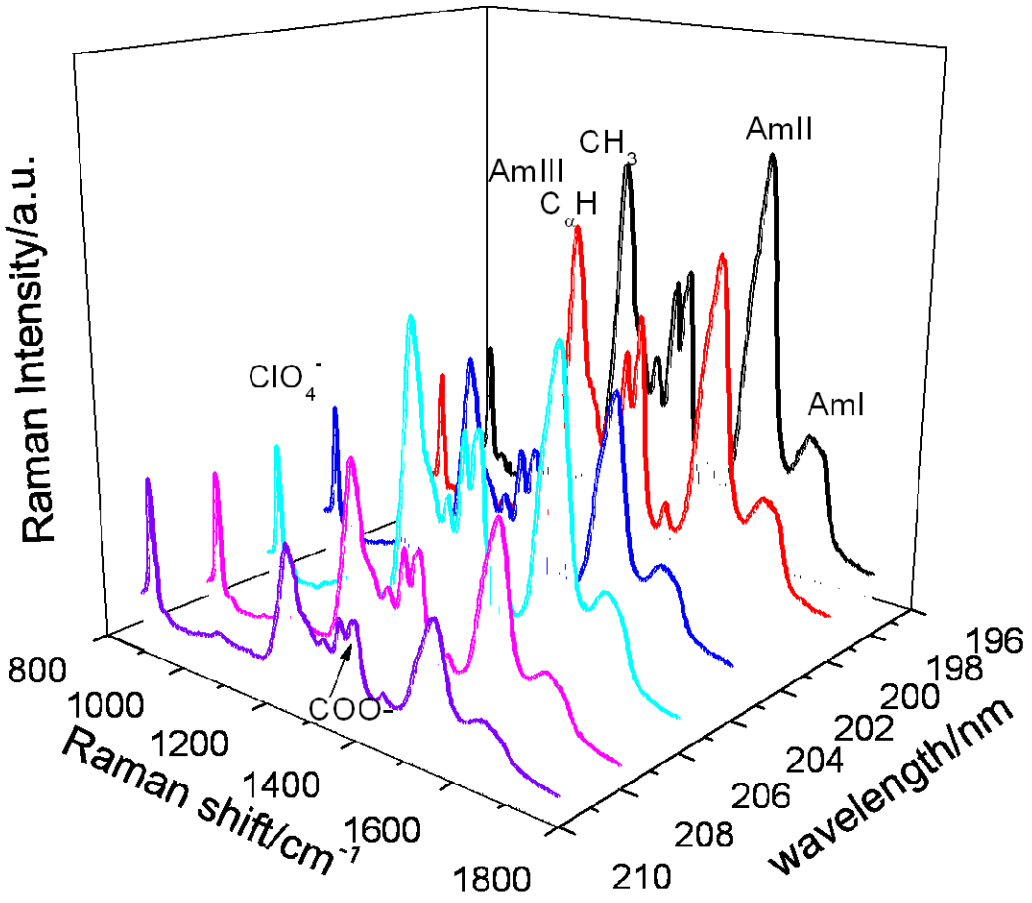

Figure 5.5 UVRR spectra of Ala_4 (6.6×10^{-3} M) at 25 °C excited between 198 and 210 nm. Spectra were collected for 15 min each. The spectral resolution is ~ 5 cm^{-1}. Spectra were not corrected for self-absorption or spectrometer throughput efficiency.

Our group has previously shown that for a 21-residue, primarily Ala peptide in mixtures of H_2O/D_2O, the spectra of the partially deuterated chains can be modeled as a statistically weighted linear sum of the deuterated and protonated segments of the peptide.[10, 45] This result indicates that the peptide bond vibrations are localized within the individual peptide bonds. More recently, we also showed that for short Gly peptides, there is also a lack of coupling between adjacent peptide bond vibrations.[46] These results allow for accurate modeling of the

Raman spectra of peptides in solution because the spectra are simply a linear sum of the terminal and internal peptide bonds. The spectra for the terminal and internal peptide bonds significantly differ. [46] We showed that the spectrum of a three residue peptide approximates the spectrum of the two terminal peptide bonds of an oligopeptide, while the difference spectrum between a six residue peptide and a five residue peptide accurately models the spectra of an internal peptide bond. We use this methodology to resolve the spectra of the COO^- vibration for both Ala_3 and Ala_4.

To resolve the COO^- vibration in Ala_3 we assume that UVRR spectrum of the Ala_3 NH_3^+ end peptide bond is similar to that of the interior peptide bond of Ala_4, which we model as that resulting from subtraction of the $Ala_4 - Ala_3$ UVRR (Figure 5.12). The underlying reasoning is that this peptide bond has the standard peptide bond $\pi \rightarrow \pi^*$ transition as the internal peptide bonds, without the charge transfer band of the carboxylate terminal peptide bonds.

We then model the Ala_3 UVRR spectra of the carboxylate end peptide bond as resulting from the UVRR spectral subtraction Ala_3-(Ala_4-Ala_3) = 2*Ala_3-Ala_4, where the NH_3^+ end peptide bond UVRR (interior Ala_4 peptide bond spectrum) is subtracted from the Ala_3 spectrum (Figure 5.6a). This spectral subtraction is obtained using the perchlorate internal standard intensity. This spectrum clearly shows the strong enhancement of the 1405 cm^{-1} carboxylate stretching vibration due to excitation within the charge transfer absorption spectrum.

Identically we can resolve the Ala_4 COO^- band by the UVRR subtraction $Ala_4 - 2^*$ ($Ala_4 - Ala_3$) = 2*Ala_3-Ala_4, where we assume that the UVRR spectrum of the Ala_3 NH_3^+ end peptide bond is similar to that of the interior Ala_4 peptide bond, which we model as that resulting from subtraction of the $Ala_4 - Ala_3$ UVRR (Figure 5.6b). The resulting spectrum identically shows

the strong Ala_4 enhancement of the 1405 cm^{-1} carboxylate stretching vibration due to excitation within the charge transfer absorption spectrum.

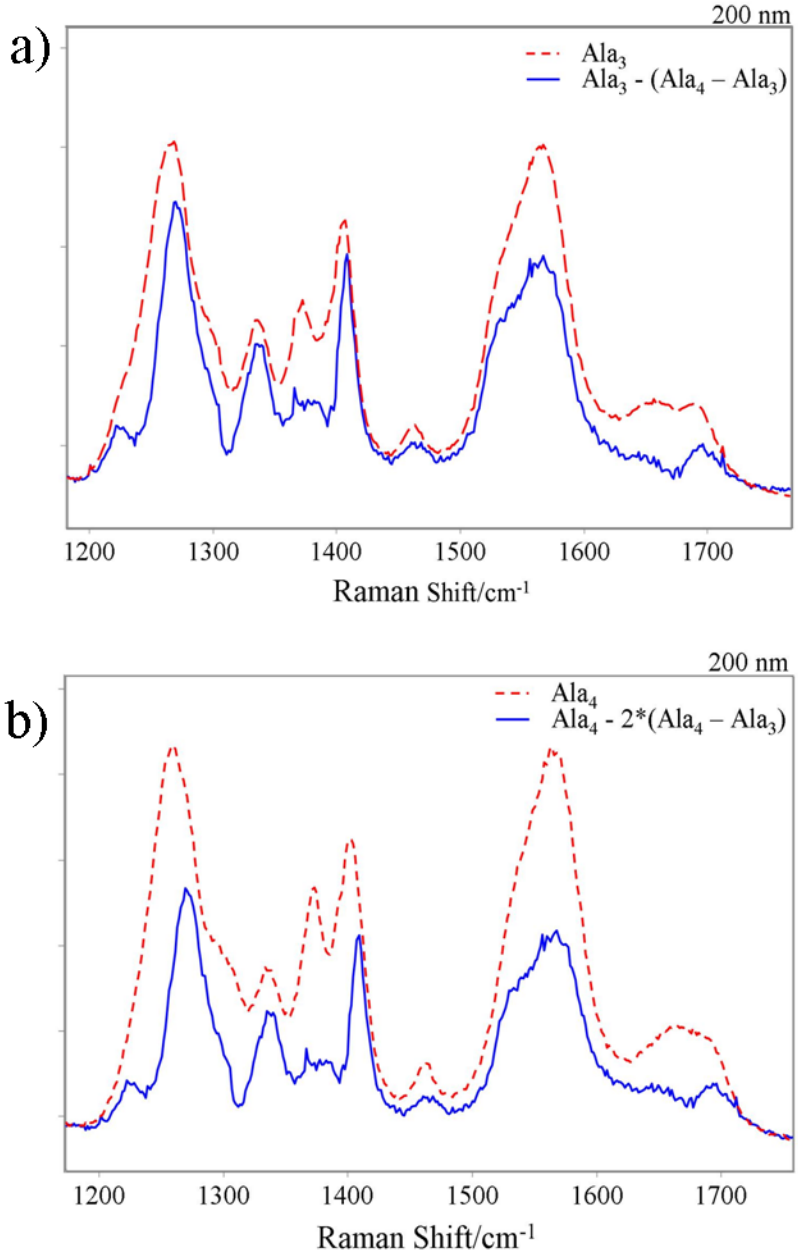

Figure 5.6 Resolving the carboxylate stretching vibration in 200 nm excited (a) Ala_3: measured spectrum (red) and Ala_3 - (Ala_4 – Ala_3) difference spectra (blue) at showing COO^- vibration enhanced in COO^- end peptide bond. (b) Ala_4: measured spectrum (red) and Ala_4 – 2*(Ala_4 – Ala_3) difference spectra (blue) showing COO^- vibration enhanced in COO^- end peptide bond.

5.3.3 Absolute Raman Cross Sections

To quantitatively compare the spectra across the range of excitation wavelengths, we calculated the Raman cross sections for each amide band at each wavelength, using ClO_4^- as the internal standard. It has been shown that the ClO_4^- symmetric stretching band has an Albrecht A-term frequency dependence for excitation wavelengths from the visible to the UV (to 220 nm).[47] We extrapolated the ClO_4^- cross sections to 198 nm.

The absolute Raman cross sections (with a correction factor for self absorption) were calculated from:

$$\sigma_{peptide} = \frac{I_{band} \cdot k(\lambda_{ClO4}) \cdot C_{ClO4} \cdot \sigma_{ClO4}}{I_{ClO4} \cdot k(\lambda_{band}) \cdot C_{peptide} \cdot n_A} \cdot \left[\frac{\varepsilon_s + \varepsilon_o}{\varepsilon_r + \varepsilon_o} \right] \qquad \textbf{(5.2)}$$

where I_{band} and I_{ClO4} are the relative intensities of the amide and ClO_4^- bands, respectively;[4, 47] $k(\lambda_{band})$ and $k(\lambda_{ClO4})$ are the spectrometer efficiencies at the wavelengths of the Raman bands; $C_{peptide}$ and C_{ClO4} are the concentrations (M) of the individual Ala peptides and perchlorate; σ_{ClO4} is the calculated ClO_4^- cross section at the band wavelength; n_A is the number of amide bonds in the peptide; ε_o is the molar absorptivity of the peptide at the laser excitation frequency; ε_s is the molar absorptivity of the peptide at the Raman band wavelength; and ε_r is the molar absorptivity at the ClO_4^- band wavelength. The expression in the brackets corrects the measured Raman intensities for self absorption.[48, 49]

These Raman cross sections of the AmI, AmII, AmIII, the C_α-H and CH_3 bends are actually the summed Raman cross sections of each of these Raman bands over all of the peptide bonds, which as we have shown previously scatter independently[46] (except for the AmI band of the α-helix conformation). In contrast, only the terminal COO^- peptide bond gives rise to

enhancement of the symmetric COO^- stretch. Thus, we evaluated its cross section from the difference spectra obtained as shown in Figure 5.6.

5.3.4 Excitation Profiles

The excitation profiles for Ala_3 shown in Figure 5.7 indicate that the Raman cross sections increase as the excitation wavelength decreases from 210 nm to maxima at 202 nm. It is well-established that the NV_1 $\pi \rightarrow \pi^*$ electronic transitions in short peptides occur at or below 190 nm (Figure 5.1).[50-52] The excitation profile maxima at 202 nm occur close to the maximum wavelength of the charge transfer transition found in the pH difference absorption spectrum of Ala_3.

Examination of the Figure 5.7 Ala_3 excitation profiles indicates that the largest cross sections occur for the AmII vibration, which is mainly a C-N st coupled to an N-H b. A similar maximal AmII band enhancement is also seen in the longer, 21 – residue alanine peptide (AP).[4] The next largest cross section occurs for the AmIII vibration, which is also composed of a C-N st and N-H b. The AmIII cross section in AP was also found to be less than that of the AmII.[4] Normal mode calculations of polyalanine indicate that C-N motion contributes twice as much to the AmII vibration than to the AmIII vibration.[53] The COO^- symmetric stretch shows the next largest excitation profile cross section.[12] The COO^- symmetric st is selectively enhanced by the ~202 nm charge transfer transition. [12]

All of the excitation profiles are much narrower than the charge transfer absorption difference spectra. The resonance Raman cross sections of CH_3, $C_\alpha H$, and the AmI vibrations are significantly smaller with only a modest charge transfer enhancement.

The Raman excitation profiles for Ala_4 shown in Figure 5.8 differ significantly from those of Ala_3 in that they show two distinct maxima. There are two peptide bonds in Ala_3, whereas Ala_4 contains three. The AmII and AmIII vibrations once again have the largest cross sections, with the AmIII vibration having a significantly larger relative cross section than in Ala_3. The AmI band cross section per peptide bond at 202 nm is approximately twice that in Ala_3.

As the excitation wavelength decreases from 210 to 198 nm, a small excitation profile maximum is observed at 206 nm, followed by a larger maximum at 202 nm. The excitation profile maximum at 202 nm for Ala_4 is assumed to be due to the charge transfer transition in the pH difference absorption spectrum (Figure 5.1c and Figure 5.2c), while understanding the origin of the 206 nm maximum will require additional information. It is important to note that the cross sections per peptide bond are roughly similar between Ala_3 and Ala_4 (except for the AmI) but the peak values are smaller in Ala_4 while the excitation profiles appear broader than those of Ala_3.

The lowest order theory[54] indicates that the resonance Raman excitation profiles will scale as the square of the absorbance band molar absorptivity. Figure 5.7 and Figure 5.8 also compare the excitation profiles of Ala_3 and Ala_4 to the squares of their absorption difference spectra. This comparison shows more similar bandwidths.

The COO^- symmetric st is clearly visible for short peptides such as Ala_3 and Ala_4. However, the COO^- symmetric st will be less evident in longer peptides such as AP, where the peptide bond NV_1 $\pi \rightarrow \pi^*$ transitions dominate the excitation profile resulting in a small relative enhancement of the COO^- symmetric st.

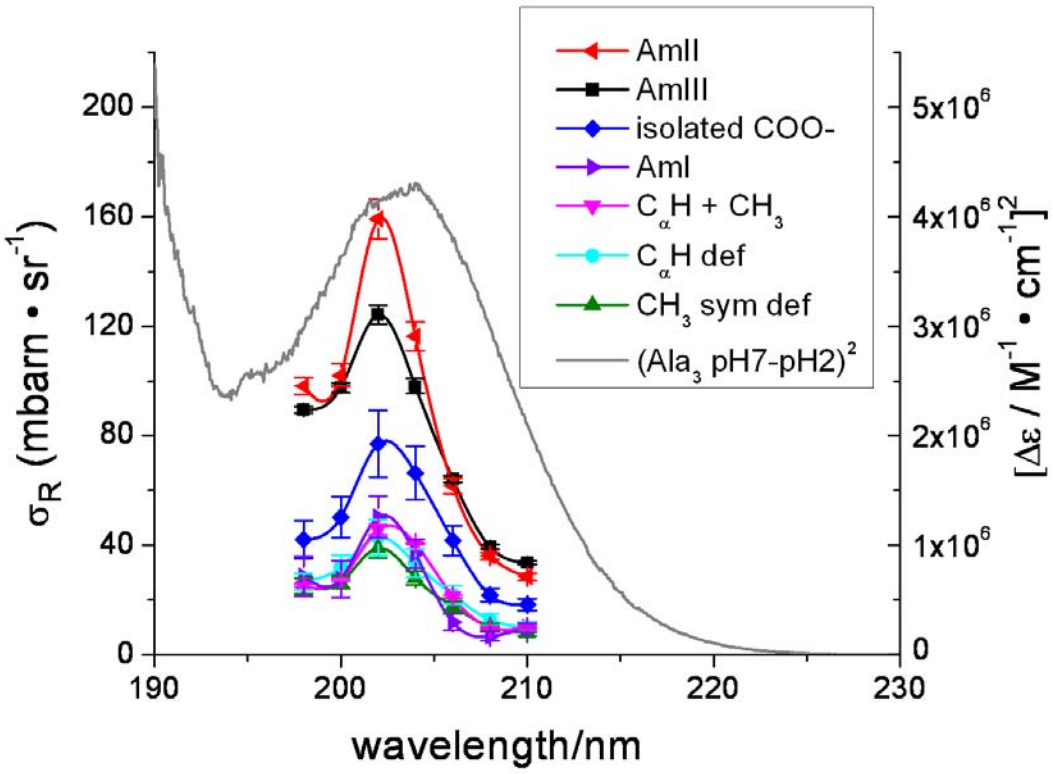

Figure 5.7 Absolute Raman cross section excitation profiles of Ala_3 (mbarn/sr) between 198 and 210 nm. See text for details. Also shown is the squared pH absorption difference spectrum from Figure 5.2. The isolated COO^- profile was calculated using the $Ala_3 – (Ala_4 – Ala_3)$ difference spectra shown in Figure 5.6.

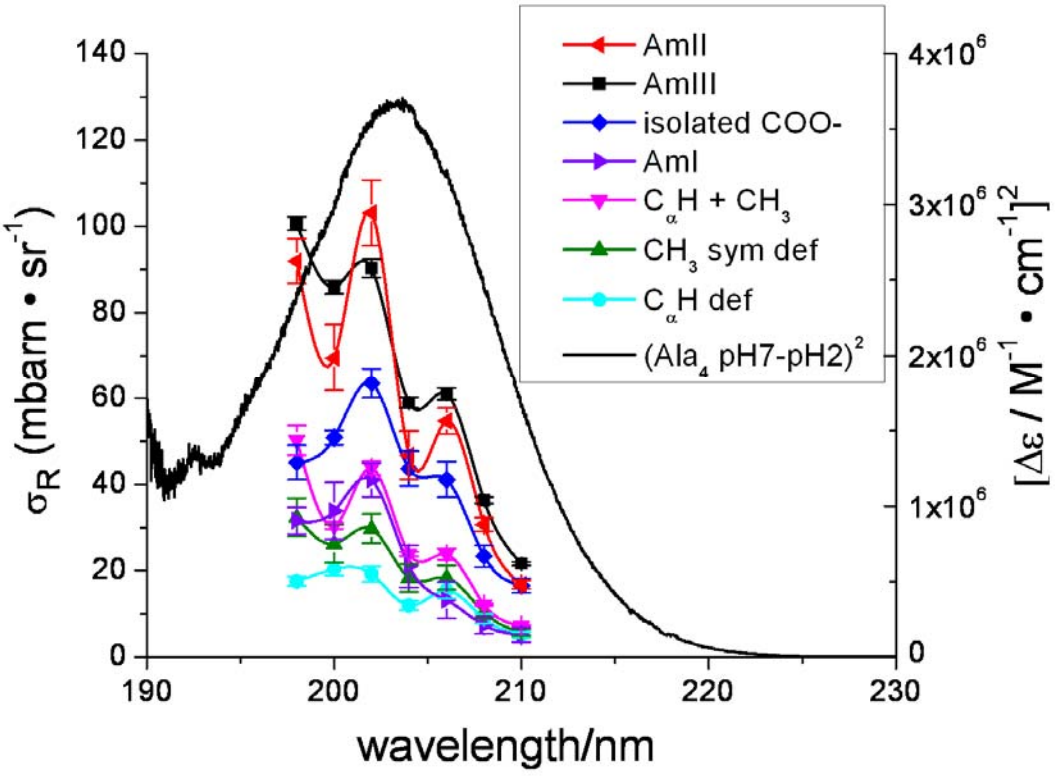

Figure 5.8 Absolute Raman cross section excitation profiles of Ala_4 (mbarn/sr) between 198 and 210 nm. See text for details. Also shown is the squared pH absorption difference spectrum from Figure 5.2. The isolated COO- profile was calculated using the $Ala_4 - 2*(Ala_4 - Ala_3)$ difference spectra shown in Figure 5.6.

5.3.5 Raman Depolarization Ratios, Excitation Profiles, and Absorption Spectra

In order to gain insight into the origin of the excitation profiles, we measured the dispersions of the resonance Raman depolarization ratios. Figure 5.9 compares the Ala_3 absorption difference spectrum, the Raman excitation profile averaged over the enhanced vibrations and the Raman depolarization ratios. The excitation profile is slightly blue shifted and much narrower than the absorption difference spectrum.

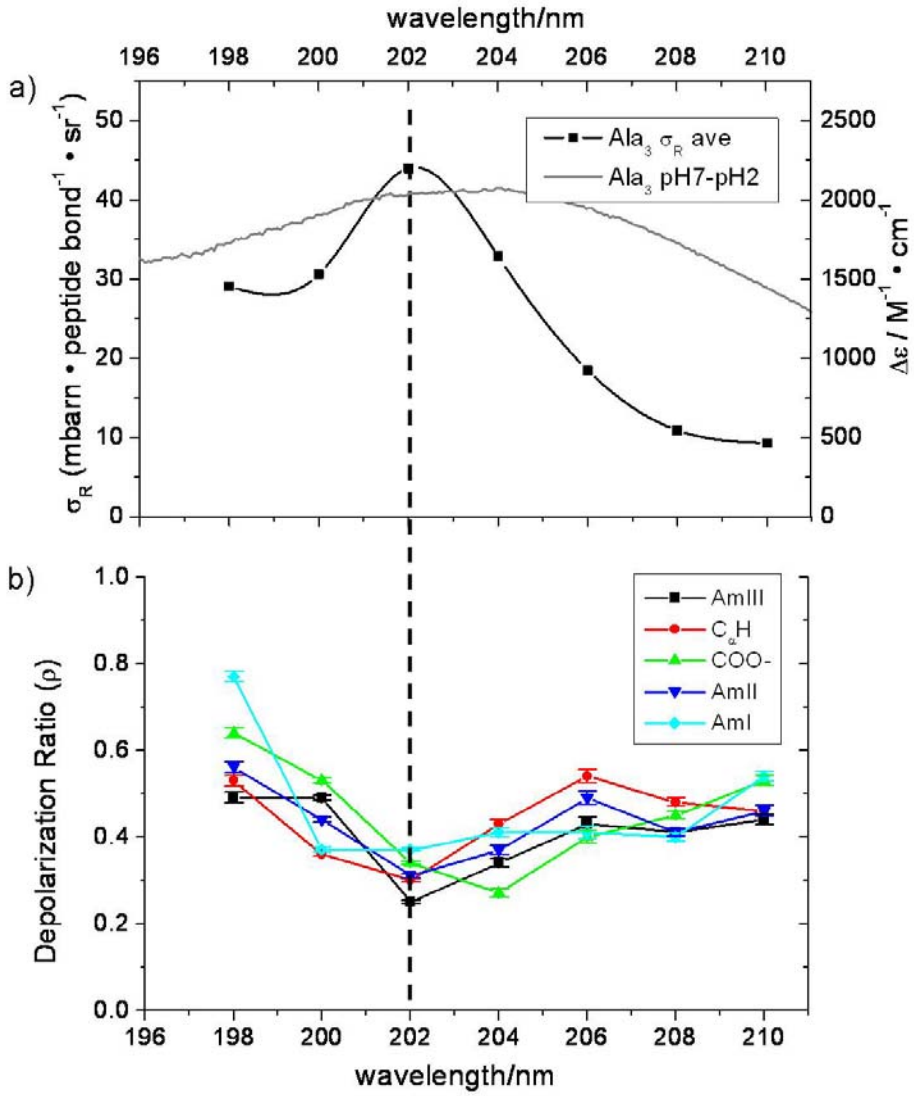

Figure 5.9 (a) The average Raman excitation profile for the Ala_3 amide bands at 25 °C between 198 to 210 nm and the pH 7-pH 2 absorption difference spectrum of Ala_3 at 25 °C between 190 to 250 nm. (b) Raman depolarization ratios of Ala_3 at 25 °C. The dashed line indicates the coincidence between the excitation maximum of the excitation profile, the pH absorption difference spectrum, and the depolarization ratio minimum with $\rho \approx 0.33$ at 202 nm.

The Ala_3 depolarization ratio shows a minimum of ρ~0.33 at the excitation profile maximum, indicating that a single nondegenerate electronic transition, presumably the charge transfer transition, dominates the resonance Raman enhancement at 202 nm.[4,12,13,55] At excitation wavelengths above and below the excitation profile maximum ρ>0.33, indicating

contributions of additional electronic transitions.[4,12,13,55] This excitation profile behavior, where $\rho>0.33$ for preresonance excitation and also $\rho>0.33$ values from 201 to 198 nm, between the charge transfer transition and the NV_1 transition, are not possible if the 202 nm transition and the NV_1 are the only transitions involved in enhancement. There is a hint of another transition at 206 nm evidenced by the skewed Raman excitation profile.

Figure 5.10 shows the Ala_4 pH absorption difference spectrum, the average resonance Raman excitation profile and the depolarization ratio dispersion measurements. The Ala_4 excitation profile shows a second maximum at 206 nm, ~1000 cm^{-1} lower in frequency than that of the ~202 nm charge transfer transition. As observed for Ala_3, a global depolarization minimum occurs with $\rho\sim0.33$ at the charge transfer excitation profile maximum at 202 nm. Also, as for Ala_3, $\rho>0.33$ from 201 to 198 nm, between the charge transfer transition and the NV_1 transition at ~190 nm. In contrast to Ala_3, a local depolarization ratio maximum occurs at the 206 nm second excitation profile maximum ($\rho\sim0.5$). $\rho > 0.33$ in preresonance with all of these transitions for the carboxylate stretch and the AmII and III bands (although less so than for Ala_3).

We do not, as yet, have a simple explanation for these results. One possibility would require two charge transfer transitions close in energy that give rise to the two excitation profile peaks in Ala_4 and the very weak 206 nm shoulder in Ala_3. These charge transfer transitions would involve two different sets of carboxylate non-bonding electrons undergoing a transition to the adjacent peptide bond π^* orbital. The weakness of the 206 nm excitation profile maximum in Ala_3 could result from destructive interference between the contributions from these two charge transfer transitions and the NV_1 transition. Although, the observed 206 nm Raman

intensities could be dramatically attenuated by the destructive interference, the 206 nm transition could still significantly increase ρ in the wings of the excitation profile maxima.

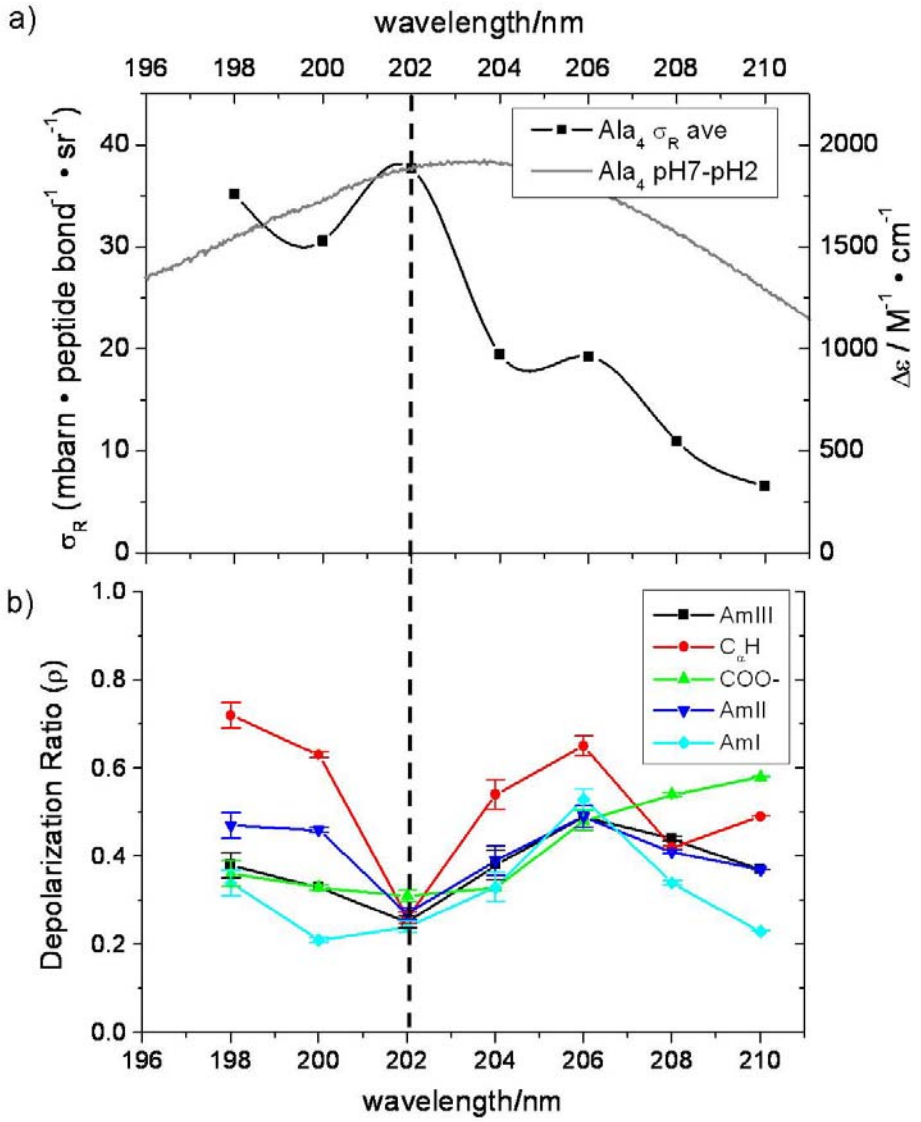

Figure 5.10 (a) The averaged Raman excitation profile for Ala_4 at 25 °C between 198 to 210 nm and the pH7 – pH2 absorption difference spectrum of Ala_4 at 25 °C from 190 to 250 nm. (b) Raman depolarization ratios of Ala_4 at 25 °C. The dashed line indicates the coincidence between the maximum of the excitation profile, the pH absorption difference spectrum, and the depolarization ratio minimum with $\rho \approx 0.33$ at 202 nm.

The dispersion of ρ can be understood if the contribution to the polarizability of the NV_1 transition and the 202 nm charge transfer transition were of the same sign and the 206 nm transition contribution were of opposite sign. This would yield the dispersion observed with ρ>0.33 between 201 to 198 nm, if the NV_1 transition and the 202 nm charge transfer transition dominated in this spectral region and the NV_1 transition and the 202 nm charge transfer transition contributed similarly to that of the 206 nm transition.

The alternative explanation would assign the 206 and 202 nm transitions to the 0-0 and 0-1 vibronic components of the charge transfer transition. The ~1000 cm^{-1} difference in the peak maxima would indicate a decreased excited state carboxylate frequency. A detailed theoretical calculation would be required to understand the dispersion of the depolarization ratios around the 206 nm transition.[56]

Another possible origin of the 206 nm band is that second conformation of the Ala_4 peptide occurs in solution, which has its charge transfer transition shifted to 206 nm. To search for evidence for this additional conformation, we examined the AmIII region, which is sensitive to the peptide bond conformations.[7]

5.3.6 Deconvolution of the AmIII Region

We deconvoluted the $AmIII_3$ region in both Ala_3 and Ala_4 (Figure 5.11) and found that the $AmIII_3$ region could be well fit with three Gaussian bands, at ~1226 cm^{-1}, 1249 cm^{-1}, and 1268 cm^{-1}. We utilized the methodology of Mikhonin et al. [7] which correlates Raman $AmIII_3$ frequency to Ψ angle, specifically using their equation 6A which is applicable to peptide bonds fully exposed to water, such as in poly-proline II (PPII) helix, 2.5_1 helix, extended β-strand conformations, and certain turn structures. The deconvoluted peak positions correlate to the

following Ψ angles: ~ +120°, ~ +150°, ~ +170°, which most likely derive from Type II turns, PPII helix-like, and 2.5_1 helix-like conformations, respectively. The Ψ angle of 120° is also found for Type VIa and Type VIII turns, however these are less likely structures to occur. Also, note that the Raman frequencies correspond only to Ψ angle values, with no information about the Φ angle. Thus, there are structures with Type II turn Ψ angles, but it is possible that a significant Φ angle variation could be present. Comparing Figure 5.11a and Figure 5.11b, assuming identical Raman cross sections for these species, we find that the relative contribution of the 2.5_1 helix-like structure in Ala_4 is less than in Ala_3, and conversely, the PPII-helix-like contribution is larger in Ala_4 than in Ala_3.

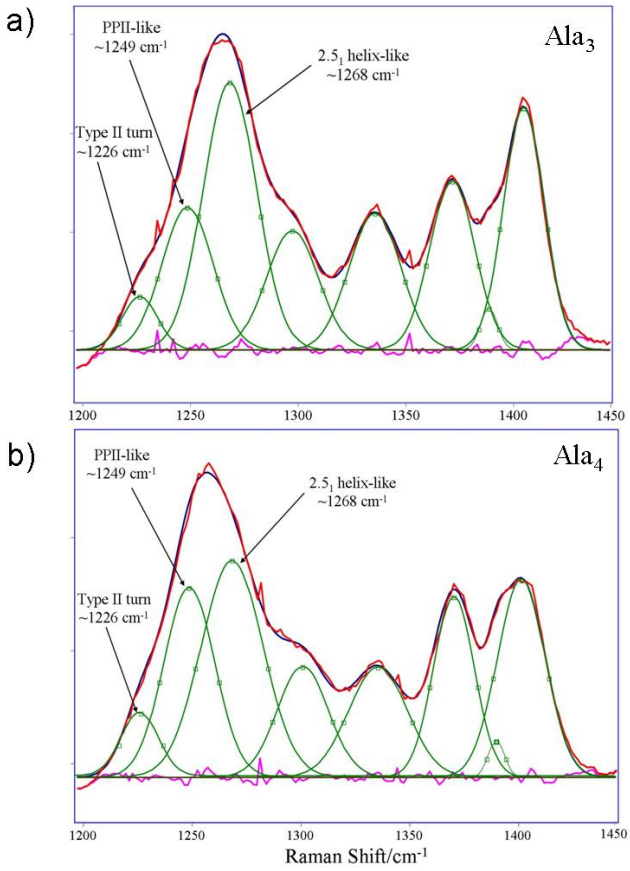

Figure 5.11 (a) Deconvolution of Ala_3 $AmIII_3$ region excited at 204 nm with three Gaussian bands. (b) Deconvolution of Ala_4 $AmIII_3$ region excited at 204 nm, also with three Gaussian bands. Different conformational distributions are present. There is excellent agreement between the modeled peaks and the observed data (R^2>99%).

Assuming identical Raman cross sections per peptide bond for each conformation, we can roughly estimate the population distributions from the $AmIII_3$ bands of both peptides. We find that the relative population distributions of both peptides are independent of wavelength. For Ala_3, the Type II turn has the lowest relative contribution (~8%), the PPII-like conformation contribution is ~ 29%, and the 2.5_1 helix contribution is ~63%.

Although there have been numerous theoretical and experimental studies performed on Ala_3 using a variety of techniques, there is no existing consensus on the conformational distribution for Ala_3 in solution. Most studies agree that Ala_3 occurs in a PPII-like conformation.[15, 29-36, 38, 41-43] Other possible conformations include β-sheet-like,[29] β-strand, [15, 30] β structures,[32, 33, 35, 36, 38, 43] right-handed α-helix, [15, 33, 35, 36, 38, 43] and γ-turn. [38] No previous study identified the 2.5_1 helix conformation, although there is a suggestion of an extended β-strand-like conformation with a similar Ψ angle (~ 170°).[15, 37]

For Ala_4, the conformations found are similar to those in Ala_3, although the distribution is different. There is a larger contribution from the PPII-helix-like structure (39%). The type II turn contribution is similar (8.5%), while the 2.5_1 helix contribution is less than that in Ala_3 (52%). Garcia[57] determined that four consecutive amino acid residues are required to form a water stabilized PPII structure, lending support to the result that Ala_4 should show a larger contribution from PPII-like structures than Ala_3. Again, there is little consensus on the conformational distribution in Ala_4, although there is agreement that the peptide adopts both PPII-like and β-like structure,[39,40] with a small amount of a right-handed α-helix-like conformation. [40] We assign the 202 nm excitation maximum as the charge transfer transition for all three conformations of Ala_4. None of these conformations should obviously give rise to a shifted 206 nm charge transfer band.

5.3.7 Ala_3 and Ala_4 Difference Spectra

To differentiate the conformational distribution of the internal versus terminal peptide bonds of Ala_4 we examined the $Ala_4 - Ala_3$ difference spectrum (Figure 5.12a), which models the internal Ala_4 peptide bond UVRR by removing the contribution of the terminal carboxylate and amine groups. We note that the COO^- symmetric stretching vibration is absent in the difference spectra. The contributions of the carboxyl end group of both peptides were removed by this subtraction. The relative intensities and frequencies of the bands within each spectrum are similar across the range of excitation wavelengths, once again indicating similar enhancement of the bands.

We calculated the Raman cross sections of the $AmIII_3$ bands (Figure 5.12b). We find that the internal residue of Ala_4 is predominantly PPII-like (~72%), with smaller contributions from 2.5_1 helix (19%) and Type II turn structures (~9%). A previous MD simulation study on the middle residue of Ala_3 found that it was ~ 85% PPII-like,[31] which closely agrees with our findings here. We can also infer that the 2.5_1 helix-like conformation is largely found at the peptide ends, which could be representative of a less compact structure at the peptide terminal ends.

An interesting feature in the excitation profiles of $Ala_4 - Ala_3$ is that the 202 nm and 206 nm excitation profile maxima are present for both the PPII-like and 2.5_1 helix conformation profiles, but less evident in the Type II turn profiles. Thus, as expected, we see less contribution from the charge transfer enhancement in the estimated excitation profile of the internal peptide bond. This residual enhancement may result because our assumption that the difference spectrum results completely from the Ala_4 internal peptide bond is not completely accurate.

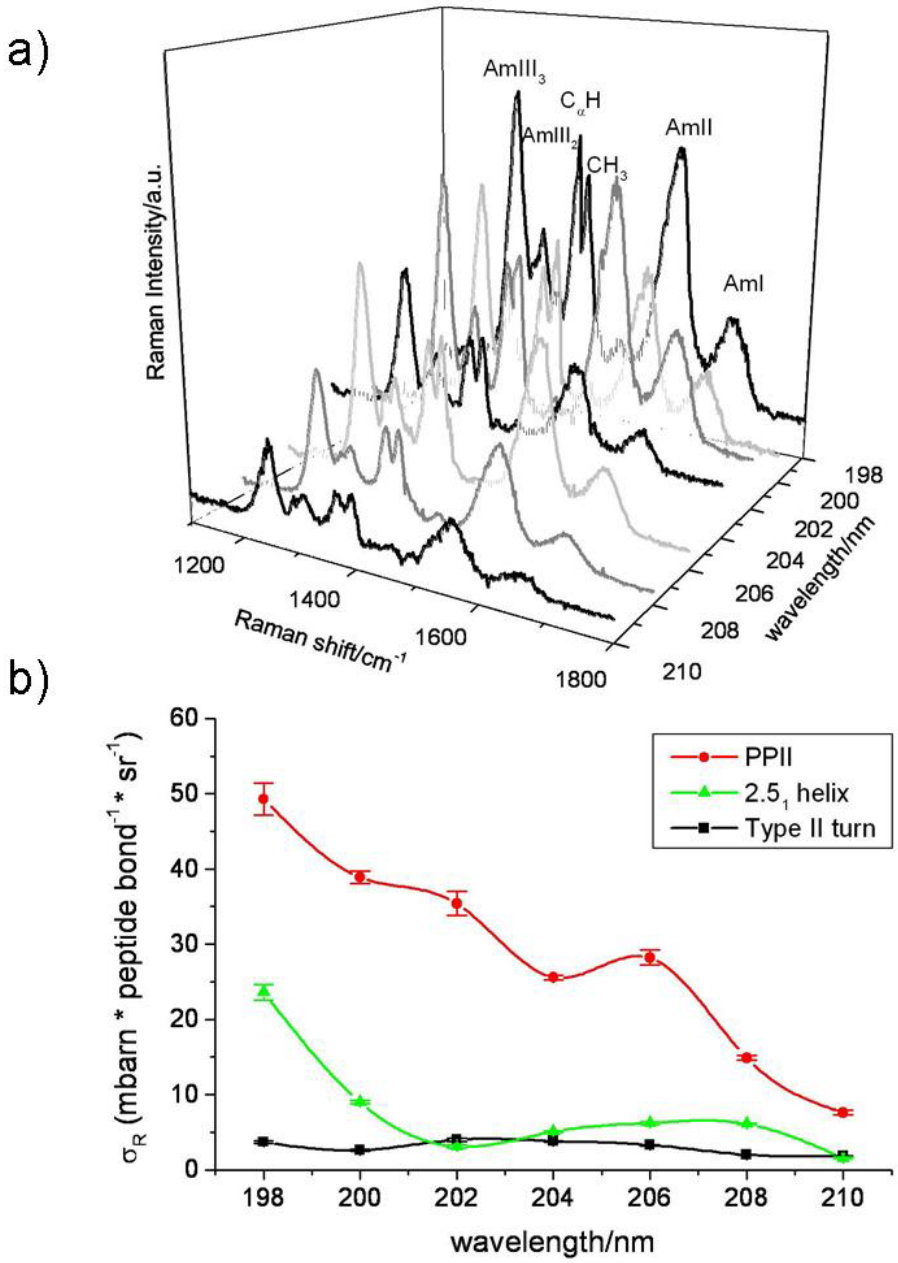

Figure 5.12 (a) Ala4 – Ala3 difference spectra, from 198 to 210 nm. (b) The AmIII3 band Raman cross sections of the three conformations (Type II turn, PPII-helix-like, 2.51 helix) in the Ala4 – Ala3 difference spectra.

5.4 CONCLUSIONS

We measured the Raman excitation profiles and depolarization ratios for both Ala_3 and Ala_4. Both peptides show excitation profile maxima at 202 nm, which we assign to charge transfer transitions of the carboxylate terminated peptide bonds clearly observed in the pH absorption difference spectra. Ala_4 shows an additional smaller excitation profile maximum at 206 nm whose origin remains unclear.

We correlated the $AmIII_3$ band Raman frequencies to the Ψ angle of both Ala_3 and Ala_4 to determine the conformational distribution of these peptides. We found Type II turns, as well as PPII-like and 2.5_1 helix-like conformations in solution. The Ala_4 – Ala_3 Raman difference spectra, allowed us to separately study the interior peptide bond of Ala_4, which is found to be predominantly PPII-like.

We assign the charge transfer transition at 202 nm to the three β-type structures deconvoluted from the Raman spectra. We are also able to resolve the COO^- vibration for both Ala_3 and Ala_4. We find a shoulder in the Ala_4 excitation profile at 206 nm, but are unable at this time to definitively assign its origin.

5.5 ACKNOWLEDGEMENTS

We would like to thank Prof. John A. Shelnutt for a very helpful discussion and Dr. Nataliya Myshakina for providing the image for Figure 5.3. We thank the NIH for funding, Grants # 5R01EB002053 and #1R01EB009089.

5.6 REFERENCES

1. Ianoul, A.; Mikhonin, A.; Lednev, I. K.; Asher, S. A. *J. Phys. Chem.* **2002,** *106*, 3621.

2. Lednev, I. K.; Karnoup, A. S.; Sparrow, M. C.; Asher, S. A. *J. Am. Chem. Soc.* **1999,** *121*, 8074.

3. Mikhonin, A. V.; Asher, S. A. *J. Am. Chem. Soc* **2006,** *128*, 13789.

4. Sharma, B.; Bykov, S. V.; Asher, S. A. *J. Phys. Chem. B* **2008,** *112*, 11762.

5. Myshakina, N. S.; Ahmed, Z.; Asher, S. A. *J. Phys. Chem. B* **2008,** *112*, 11873.

6. Efremov, E. V.; Ariese, F.; Gooijer, C. *Anal. Chim. Acta* **2008,** *606*, 119.

7. Mikhonin, A. V.; Bykov, S. V.; Myshakina, N. S.; Asher, S. A. *J. Phys. Chem. B* **2006,** *110*, 1928-1943.

8. Mikhonin, A. V.; Myshakina, N. S.; Bykov, S. V.; Asher, S. A. *J. Am. Chem. Soc.* **2005,** *127*, 7712.

9. Mikhonin, A. V.; Ahmed, Z.; Ianoul, A.; Asher, S. A. *J. Phys. Chem. B* **2004,** *108*, 19020.

10. Mix, G.; Schweitzer-Stenner, R.; Asher, S. A. *J. Am. Chem. Soc.* **2000,** *122*, 9028.

11. Pajcini, V.; Asher, S. A. *J. Am. Chem. Soc.* **1999,** *121*, 10942.

12. Chen, X. G.; Li, P.; Holtz, J. S. W.; Chi, Z.; Pajcini, V.; Asher, S. A.; Kelly, L. A. *J. Am. Chem. Soc.* **1996,** *118*, 9705.

13. Chen, X. G.; Asher, S. A.; Schweitzer-Stenner, R.; Mirkin, N. G.; Krimm, S. *J. Am. Chem. Soc* **1995,** *117*, 2884.

14. DeVito, V. L.; Cai, M. Z.; Asher, S. A.; Kehres, L. A.; Smith, K. M. *J. Phys. Chem.* **1992,** *96*, 6917.

15. Tsai, M.; Xu, Y.; Dannenberg, J. J. *J. Phys. Chem. B* **2009,** *113*, 309-318.

16. Imamura, H.; Kato, M. *Proteins: Struct., Funct., Bioinf.* **2009,** *75*, 911.

17. Wang, W.-Z.; Lin, T.; Sun, Y.-C. *J. Phys. Chem. B* **2007,** *111*, 3508.

18. Quapp, W *J. Comput. Chem.* **2007,** *28*, 1834.

19. Morozov, A. N.; Lin, S. H. *J. Phys. Chem. B* **2006,** *110*, 20555.

20. Zagrovic, B.; Lipfert, J.; Sorin, E. J.; Millett, I. S.; van Gunsteren, W. F.; Doniach, S.; Pande, V. S. *Proc. Natl. Acad. Sci. U. S. A.* **2005,** *102*, 11698.

21. Chen, K.; Liu, Z.; Zhou, C.; Shi, Z.; Kallenbach, N. R. *J. Am. Chem. Soc.* **2005,** *127*, 10146.

22. Ramakrishnan, V.; Ranbhor, R.; Durani, S. *J. Am. Chem. Soc.* **2004,** *126*, 16332.

23. McColl, I. H.; Blanch, E. W.; Hecht, L.; Kallenbach, N. R.; Barron, L. D. *J. Am. Chem. Soc.* **2004,** *126*, 5076.

24. Huang, C.-Y.; Klemke, J. W.; Getahun, Z.; DeGrado, W. F.; Gai, F. *J. Am. Chem. Soc.* **2001,** *123*, 9235.

25. Thompson, P. A.; Eaton, W. A.; Hofrichter, J. *Biochemistry* **1997,** *36*, 9200.

26. Gnanakaran, S.; Garcia, A. E. *Proteins: Struct., Funct., Bioinf.* **2005,** *59*, 773.

27. Vila, J. A.; Baldoni, H. A.; Ripoll, D. R.; Ghosh, A.; Scheraga, H.A. *Biophys. J.* **2004,** *86*, 731.

28. Makowska, J.; Rodziewicz-Motowidlo, S.; Baginska, K; Makowski, M.; Vila, J. A.; Liwo, A.; Chmurzynski, L.; Scheraga, H.A. *Biophys. J.* **2007,** *92*, 2904

29. Eker, F.; Cao, X.; Nafie, L.; Schweitzer-Stenner, R. *J. Am. Chem. Soc.* **2002,** *124*, 14330.

30. Eker, F.; Griebenow, K.; Schweitzer-Stenner, R.. *J. Am. Chem. Soc.* **2003,** *125*, 8178.

31. Gnanakaran, S.; Garcia, A. E. *J. Phys. Chem. B* **2003,** *107*, 12555.

32. Gorbunov, R. D.; Nguyen, P. H.; Kobus, M.; Stock, G. *J. Chem. Phys.* **2007,** *126*, 054509/1.

33. Graf, J.; Nguyen, P. H.; Stock, G.; Schwalbe, H. *J. Am. Chem. Soc.* **2007,** *129*, 1179.

34. Lee, O.; Roberts, G. M.; Diem, M. *Biopolymers* **1989,** *28*, 1759.

35. Mu, Y.; Kosov, D. S.; Stock, G. *J. Phys. Chem. B* **2003,** *107*, 5064.

36. Mu, Y.; Stock, G. *J. Phys. Chem. B* **2002,** *106*, 5294.

37. Schweitzer-Stenner, R. *Biophys. J.* **2002,** *83*, 523.

38. Schweitzer-Stenner, R. *J Phys Chem B* **2009,** *113*, 2922.

39. Schweitzer-Stenner, R.; Eker, F.; Griebenow, K.; Cao, X.; Nafie, L. A. *J. Am. Chem. Soc.* **2004,** *126*, 2768.

40. Torii, H. *J. Phys. Chem. B* **2007,** *111*, 5434.

41. Woutersen, S.; Hamm, P. *J. Phys. Chem. B* **2000,** *104*, 11316.

42. Woutersen, S.; Hamm, P. *J. Chem. Phys.* **2001,** *114*, 2727.

43. Woutersen, S.; Pfister, R.; Hamm, P.; Mu, Y.; Kosov, D. S.; Stock, G. *J. Chem. Phys.* **2002,** *117*, 6833.

44. Bykov, S.; Lednev, I.; Ianoul, A.; Mikhonin, A.; Munro, C.; Asher, S. A. *Appl. Spectrosc.* **2005,** *59*, 1541.

45. Mikhonin, A. V.; Asher, S. A. *J. Phys. Chem. B* **2005**, *109*, 3047.

46. Dudik, J. M.; Johnson, C. R.; Asher, S. A. *J. Chem. Phys.* **1985,** *82*, 1732.

47. Ludwig, M.; Asher, S. A. *Appl. Spectrosc.* **1988,** *42*, 1458.

48. Shriver, D. F.; Dunn, J. B. R. *Appl. Spectrosc.* **1974,** *28*, 319.

49. Bykov, S. V.; Asher, S. A. *J. Phys. Chem. Lett.* **2010**, 1, 269.

50. Basch, H.; Robin, M. B.; Kuebler, N. A. *J. Chem. Phys.* **1967,** *47*, 1201.

51. Peterson, D. L.; Simpson, W. T. *J. Am. Chem. Soc.* **1957,** *79*, 2375.

52. Schellman, J. A.; Nielsen, E. B. *J. Phys. Chem.* **1967,** *71*, 3914.

53. Lee, S.-H.; Krimm, S. *Biopolymers* **1998,** *46*, 283.

54. Myers, A. B.; Mathies, R. A., in *Biological Applications of Raman Spectroscopy, vol. 2: Resonance Raman Spectra of Polyenes and Aromatics* (ed. T. G. Spiro); John Wiley & Sons, 1987, pp.1-58.

55. Long, D. A., *The Raman Effect: A Unified Treatment of the Theory of Raman Scattering by Molecules*; John Wiley & Sons: New York, 2001.

56. Shelnutt, J. A.; O'Shea, D. C. *J. Chem. Phys.* **1978**, *69*, 5361.

57. Garcia, A. E. *Polymer* **2004,** *45*, 669.

6.0 UV RESONANCE RAMAN FINDS PEPTIDE BOND – ARG SIDE CHAIN ELECTRONIC INTERACTIONS

We measured the UV resonance Raman excitation profiles and Raman depolarization ratios of the arginine (Arg) vibrations of the amino acid monomer, as well as, Arg in the 21-residue predominantly alanine peptide, $AAAAA(AAARA)_3A$ (AP) between 194 and 218 nm. Excitation within the $\pi \rightarrow \pi^*$ peptide bond electronic transitions result in UVRR spectra dominated by amide peptide bond vibrations. The Raman cross sections and excitation profiles indicate that the Arg side chain electronic transitions mix with the AP peptide bond electronic transitions. The Arg Raman bands in AP exhibit Raman excitation profiles similar to those of the amide bands in AP which are conformation specific. These Arg excitation profiles distinctly differ from the Arg monomer. The Raman depolarization ratio of Arg in monomeric solution are quite simple with $\rho=0.33$ indicating enhancement by a single electronic transition. In contrast, we see very complex depolarization ratios of Arg in AP that indicate that the Arg residues are resonance enhanced by multiple electronic transitions. (This work has been accepted for publication in *J. Phys. Chem. B.*, **2011**)

6.1 INTRODUCTION

There is little understanding of the electronic transitions of peptides and proteins.[1-10] It is generally assumed that peptide and protein electronic transitions result from the summation of the electronic transitions of the constituent chromophores. The peptide bond $\pi \rightarrow \pi^*$ transitions have been characterized to a limited extent, as have been the transitions of the different isolated side chain chromophores.[1-13] However, there has been little attention paid to the potential coupling of the peptide bond transitions to the side chain electronic transitions or to coupling between side chain transitions. Coupling of side chain – peptide bond transitions could be important in areas such as electron transport, for example.

In the work here, we use UV resonance Raman (UVRR) spectroscopy[14-28] to probe the electronic transitions of Arg side chains in a predominantly poly-Ala peptide. UVRR spectroscopy is unique in its ability to provide insight into the electronic excited state geometry and the localization of electronic transitions through measurements of Raman excitation profiles and Raman depolarization ratios.[24,25,29-37]

We examined the excitation profiles of the three Arg residues within a 21-residue, primarily poly-Ala peptide (AP), which has been well characterized and used as a model for α-helix conformations and α-helix melting. AP has previously been shown to be in an α-helical conformation at low temperatures that melts to a predominantly poly-proline II-like (PPII) conformation at high temperatures.[15,19,21,22,25] Excitation between 180 and 215 nm occurs in resonance with the peptide bond $\pi \rightarrow \pi^*$ electronic transitions, resulting in enhancement of amide vibrations.[14-17,19-22,24,25,28-38] We show here that the electronic transitions of the Arg side chains strongly couple to the $\pi \rightarrow \pi^*$ peptide bond electronic transitions.

6.2 MATERIALS AND METHODS

6.2.1 Sample Preparation

The 21-residue poly-alanine peptide AAAAA(AAARA)$_3$A (AP) was prepared by AnaSpec (San Jose, CA) using solid-state peptide synthesis (HPLC pure). We used 2 mg/ml (1.13 mM) AP solutions that contained sodium perchlorate (0.2 M) as an internal standard for the UVRRS measurements. The Arg HCl (Arg) (Sigma; St. Louis, MO) UVRRS measurements used 2 mg/ml (9.7 x 10^{-3} M) solutions with sodium perchlorate (0.2 M) as an internal standard. The UVRR spectral measurements of Arg were taken at 25 ^{o}C ± 0.5 ^{o}C. The AP UVRR spectral measurements were measured at both 5 ^{o}C ± 0.5 ^{o}C (where AP is a mixture of α-helical and PPII conformations) and at 60 ^{o}C ± 0.5 ^{o}C (where the PPII-like conformation dominates) (Figure 6.1). All UVRRS and absorption spectra of AP and Arg were measured at pH 7.

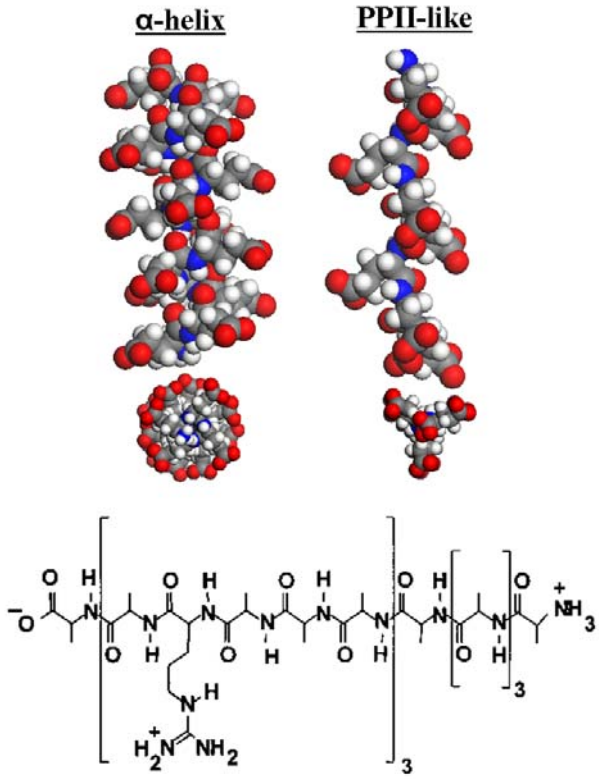

Figure 6.1 AP conformations (upper panel) and structure (lower panel). AP is predominantly α-helical at low temperatures, and PPII-like at high temperatures.

6.2.2 Raman Instrumentation

The UVRR instrumentation was previously described in detail.[39] The excitation profile measurements utilize two Coherent Indigo-S Ti:Sapphire laser systems to span the spectral region of interest. Both lasers utilize intra-cavity frequency doubled, Q-switch pulsed Nd:YLF Evolution 15 lasers (527 nm wavelength, 5 kHz repetition rate, 10 W average power) to pump Ti:Sapphire oscillators generating tunable radiation from 772 to 840 nm and 840 to 960 nm. These tunable Ti:Sapphire lasers are frequency quadrupled and mixed, utilizing two different harmonic generation approaches. The first laser uses two successive frequency doublers to

convert the fundamental wavelengths (840-960 nm) to the deep UV (210-240 nm). The second harmonic generation process mixes the third harmonic with the fundamental to produce tunable radiation between 193 and 210 nm. The average powers in the UV are between 2-5 mW (193-210 nm) and 2-10 mW (210-220 nm).

The laser beam is focused into a temperature-controlled, circulating flow stream which was surrounded by a N_2 gas environment, thereby eliminating Raman scattering from the O_2 Raman band at 1555 cm^{-1}. Each 20-mL sample of AP or Arg was irradiated for a maximum of 15 min. The scattered light was directed into a subtractive double monochromator[39] and the Raman scattered light was detected by a liquid nitrogen cooled CCD (Princeton Instruments, Spec-10:400B). The Raman intensities were normalized to the 932 cm^{-1} perchlorate ClO_4^- symmetric stretch vibration. The spectra were analyzed and deconvoluted using Grams/32 AI 8.0 software (Thermo Electron Corporation, Waltham, MA).

UV Raman depolarization ratios (ρ) were measured by using a backscattering geometry. The light scattered from the sample was directed through a UV linear dichroic polarizer (Oriel Instruments, Stratford, CT) and a crystalline quartz scrambler (Spex Industries, Edison, NJ) placed directly before the monochromator entrance slit. The depolarization ratios were measured between 198 to 218 nm and at 229 nm. The incident beams were highly polarized. ρ was calculated as the ratio of the perpendicularly polarized ($I_\perp$) to the parallel polarized scattered light (I||):

$$\rho = \frac{I_\perp}{I_\parallel} \qquad \textbf{(6.1)}$$

The depolarization ratios were calibrated by using the depolarization ratios of ClO4- and cyclohexane as standards.[35]

6.2.3 Spectrometer Efficiency

The spectrometer used is a modified Spex 1401 double monochromator that operates in the 193-270 nm range. The throughput efficiency of the spectrometer varies over this range. We corrected for the differences in throughput by using previously determined efficiency measurements. [39]

6.2.4 Absorption Measurement

The UV absorbance spectra between 190 and 260 nm were measured by using a Cary 5000 Varian UV-Vis-NIR spectrophotometer. The Arg solution concentration used for the absorbance measurements was 3.4×10^{-4} M. The absorbance measurements for the Arg samples were taken at 25 ^{o}C ± 0.5 ^{o}C. The AP absorption measurements used 0.15 mM concentrations at temperatures of 5 ^{o}C ± 0.5 ^{o}C and 60 ^{o}C ± 0.5 ^{o}C.

6.3 RESULTS AND DISCUSSION

6.3.1 Absorption Spectra

Figure 6.2 shows the absorption spectra of AP and Arg. The broad bands at 190 nm of the AP samples derive from the peptide bond $\pi \rightarrow \pi^*$ transitions, while the band from Arg monomer derives from the two lowest $\pi \rightarrow \pi^*$ transitions of the guanidinium group.[40] These guanidinium electronic transitions have been calculated to be at 199 and 185 nm by Sension et al. [40] These

authors, however, have further stated that the calculated energy values are probably too low by 3000-6000 cm^{-1}, and the transitions are more likely to be at 177-188 nm and 166-175 nm. The Figure 6.2 absorption spectrum does not show discrete peaks for the transitions, presumably because it does not go to short enough wavelengths. We previously showed that AP at both low and high temperatures show excitonic interactions between the peptide bond NV_1 $\pi \rightarrow \pi^*$ transitions and higher energy transitions that impact the peptide bond absorption band.[25]

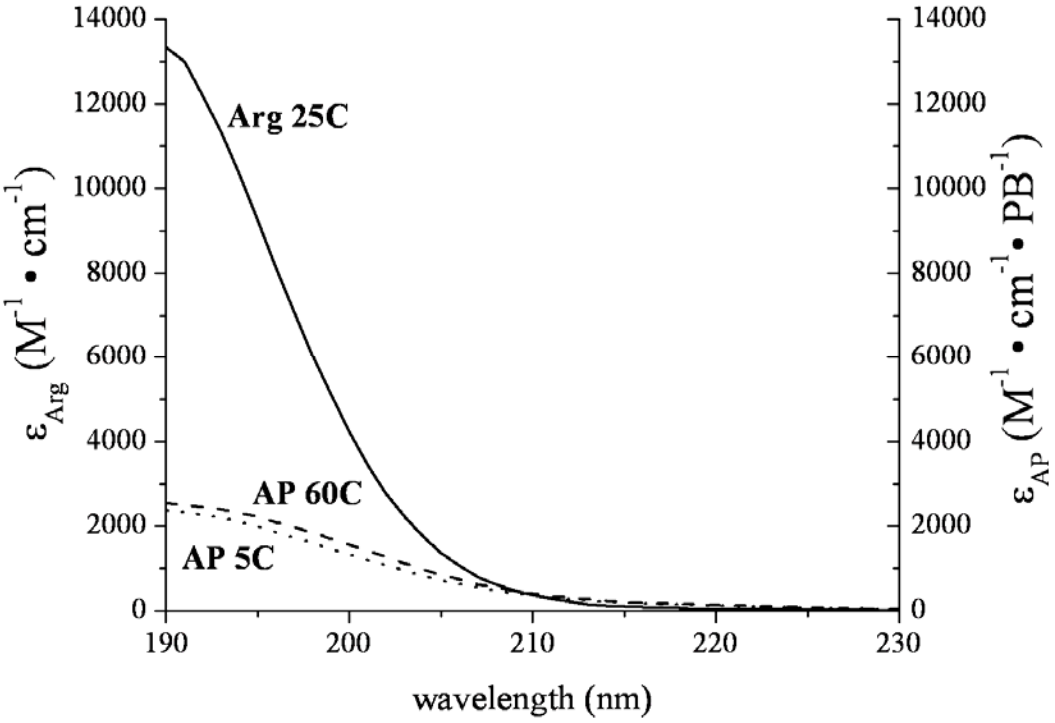

Figure 6.2 UV absorption spectra per Arg residue at pH 7 of Arg at 25 °C; AP at 5 °C, where it is predominantly α-helical, and at 60 °C, where it is predominantly in a PPII-like conformation.

6.3.2 UVRR Spectra of Arg

The UVRRS of Arg at 25 °C excited between 218 to 194 nm are shown in Figure 6.3. The spectra are normalized with respect to the 932 cm^{-1} ClO_4^- band (not shown), but are not corrected

for self absorption or spectrometer efficiency. The UV Raman enhanced Arg vibrations include the guanidinium group overlapping 1669 and 1633 cm^{-1} bands, which arise primarily from CN stretching (st), NH_2 scissoring (sci), and NH bending (b) vibrations.[41-44] The 1565 cm^{-1} band is due to NH_2 sci, and is only present in spectra excited below 200 nm.[40] The 1454 cm^{-1} band is due to CH2 sci.[42,43] The 1176 cm^{-1} band results from CH_2 twisting (tw), CH b, and NH_2 tw of the guanidinium group.[42,43,45] The 1091 cm^{-1} band is due primarily to a NH_2 rocking (rock) vibration of the guanidinium group with NH_2 wagging (w), CH_2 w, and CH b.[42,43,45]

The relative intensities of the UVRR bands of Arg increase as the excitation wavelength decreases from 218 to 196 nm (Figure 6.3), but the intensity decreases for 194 nm excitation.

The 204 nm UVRR spectra of AP in the PPII-like and α-helix conformations are shown in Figure 6.4 with the Arg bands labeled. The UVRR spectra of the PPII-like and α-helical AP conformations significantly differ, as do their excitation profiles.[25] The Arg bands at 1091, 1176, and 1454 cm^{-1} are clearly evident. The 1600-1670 cm^{-1} region Arg bands underlie the amide I band, but by modeling can be resolved.

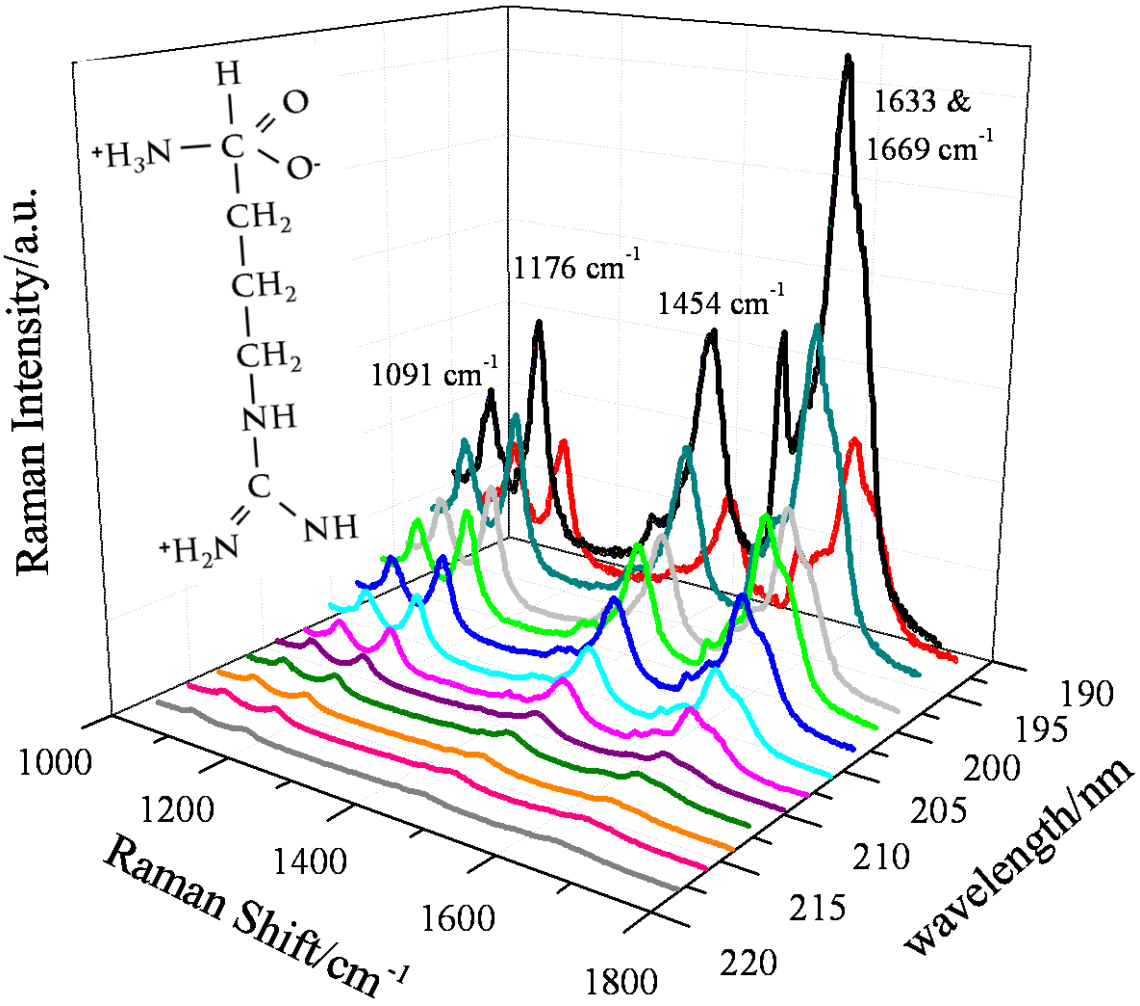

Figure 6.3 UVRR spectra of Arg at 25° C between 218 and 194 nm. The spectra were collected for 15 min at each excitation wavelength. The spectral resolution varies between 5.9 cm^{-1} at 218 nm and 7 cm^{-1} at 194 nm. All spectra were normalized to the ClO_4^- internal standard (not shown). Inset: Arg structure.

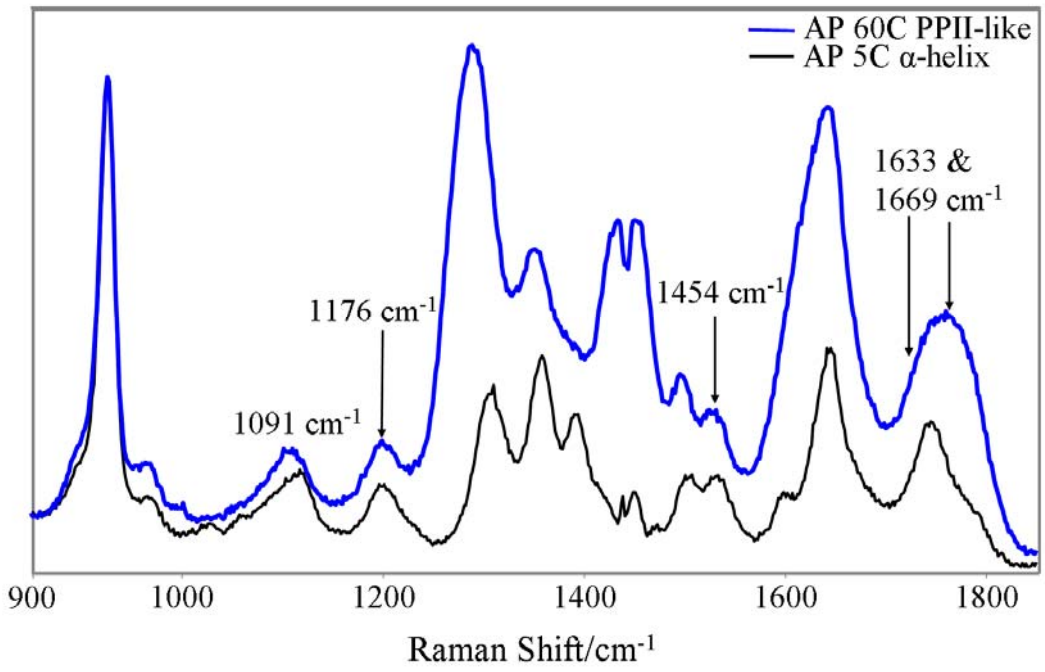

Figure 6.4 UVRR spectra of AP (pH 7) at 60 °C and 5 °C excited at 204 nm. The spectra were collected for 15 min at each excitation wavelength. The Arg bands in the AP spectra are labeled.

6.3.3 Absolute Raman Cross Sections

We calculated the Raman cross sections of the Arg bands in solution and the Arg bands in AP by using ClO_4^- as an internal standard. We previously showed that the ClO_4^- Raman cross section dependence on excitation wavelength is well modeled by an Albrecht A-term frequency dependence for excitation wavelengths from the visible to the UV to 220 nm:[18]

$$\sigma_R = K_2 \nu_o \left(\nu_o - \nu_{mn}\right)^3 \left[\frac{\nu_e^2 + \nu_o^2}{\nu_e^2 - \nu_o^2}\right]^2 \qquad \textbf{(6.2)}$$

where K_2 is a constant equal to 2.34 x 10^{-26} $cm^2/mol \cdot sr$, ν_o is the incident laser excitation frequency (cm^{-1}), ν_{mn} is the frequency of the Raman vibrational mode (cm^{-1}), and ν_e is the

frequency of the transition to the resonant excited state (1.28 x 10^5 cm^{-1}). We assume this cross section frequency dependence occurs down to 194 nm.[24,25]

We normalized all of the UVRR spectra to the integrated intensity of the ClO_4^- 932 cm^{-1} band. The absolute Raman cross sections (with correction for self absorption) of the Arg bands in both conformations of AP and for pure Arg in solution were calculated as:

$$\sigma_R = \frac{I_{band} \cdot k(\lambda_{ClO4}) \cdot C_{ClO4} \cdot \sigma_{ClO4}}{I_{ClO4} \cdot k(\lambda_{band}) \cdot C_{sample} \cdot n_{Arg}} \cdot \left[\frac{\varepsilon_s + \varepsilon_o}{\varepsilon_r + \varepsilon_o} \right] \qquad \textbf{(6.3)}$$

where I_{band} and I_{ClO4} are the observed integrated intensities of the Arg and ClO_4^- bands, respectively; $k(\lambda_{band})$ and $k(\lambda_{ClO4})$ are the spectrometer efficiencies at the specific wavelengths of the Raman bands; C_{sample} and C_{ClO4} are the concentrations (M) of the AP or Arg samples and perchlorate; σ_{ClO4} is the calculated ClO_4^- cross section at the excitation wavelength; n_{Arg} is the number of Arg residues in AP; ε_o is the extinction coefficient for AP at the excitation frequency; ε_s is the extinction coefficient for AP at each Raman band wavelength; and ε_r is the extinction coefficient for ClO_4^- band at each excitation wavelength. The expression in the brackets corrects the Raman intensities for self absorption.[24,25,46,47]

6.3.4 Excitation Profiles of Arg in Solution

Figure 6.5a shows the Raman excitation profile cross sections of Arg in solution. The excitation profile cross sections increase from 218 to 194 nm, reaching a maximum at 196 nm and then decrease. The excitation profiles are all significantly narrower than is the Arg absorption spectrum (Figure 6.5). These Arg monomer excitation profile maxima, which should signal a guanidinium group $\pi \rightarrow \pi^*$ transition appear at lower energy than the calculated lowest energy

transitions for the guanidinium group (< 188 nm).[40] Thus, our Raman excitation profile data are not consistent with Sension et al.'s calculations and indicate that the lowest $\pi \rightarrow \pi^*$ transition of Arg occurs at 196 nm. The 1091 (NH_2 rock; NH_2 w, CH_2 w, and CH b), 1176 (CH_2 twist, CH b, and NH_2 tw), 1454 (CH_2 sci), and 1633 (CN st, NH_2 sci, NH b) cm^{-1} vibrations have similar excitation profiles between 198 and 218 nm. There appears to be a shoulder between 200 and 210 nm in the Arg excitation profiles.

Recent studies by our group on the absorption spectrum of ethylguanidinium, that has the same local guanidinium group symmetry and the same vibrational spectra above ~ 1000 cm^{-1} as the Arg side chain, indicates the existence of a broad underlying transition centered between 200 and 210 nm.[48]

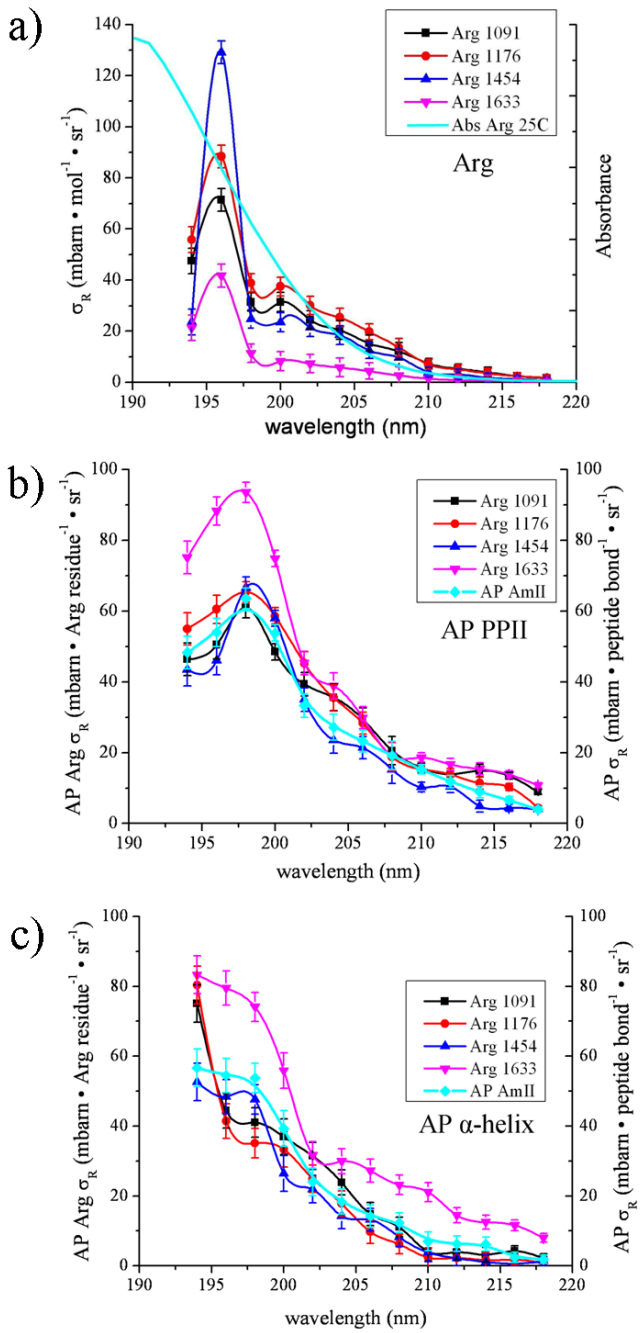

Figure 6.5 a) Absolute Raman cross section (mbarn·mol^{-1}·sr^{-1}) excitation profiles between 194 to 218 nm of Arg in solution at 25 °C. Also shown is the Arg absorption spectrum. b) Absolute Raman cross section excitation profiles (mbarn·Arg residue^{-1}·sr^{-1}) of Arg vibrations in the PPII-like conformation of AP, and the AP AmII Raman cross section excitation profile (mbarn·peptide bond^{-1}·sr^{-1}) of the PPII-like conformation. c) Absolute Raman cross section excitation profiles (mbarn·Arg residue^{-1}·sr^{-1}) of the Arg vibrations of the α-helix conformation of AP, and the α-helix conformation AP peptide bond AmII Raman cross section excitation profile (mbarn·peptide bond^{-1}·sr^{-1}).

6.3.5 Excitation Profiles of Arg in AP

Figure 6.5b and Figure 6.5c show the Raman cross section excitation profiles of the 1091, 1176, 1454, and 1633 cm^{-1} Arg bands observed in the UVRR spectra of AP in both the PPII and α-helix conformations, along with the AP peptide bond AmII vibration which has an excitation profile similar to those of other peptide bond amide vibrations.

The excitation profiles of the Arg residues in both conformations of AP (Figure 6.5b and Figure 6.5c) significantly differ from the excitation profiles of pure Arg in solution (Figure 6.5a). **Remarkably, and quite unexpectedly, the AP PPII Arg and the α-helix Arg bands have the same excitation profiles as the peptide bonds in both the AP PPII-like and α-helix conformations.** The cross sections of the AP Arg bands (per Arg residue) are similar to those of the AmII vibration (per peptide bond; Figure 6.5b and Figure 6.5c). This is most clearly evident in Figure 6.6.

The essentially identical Raman excitation profiles of the Arg and peptide bond vibrations in AP clearly indicates mixing between the overlapping Arg guanidinium group electronic transitions and those of the peptide backbone.

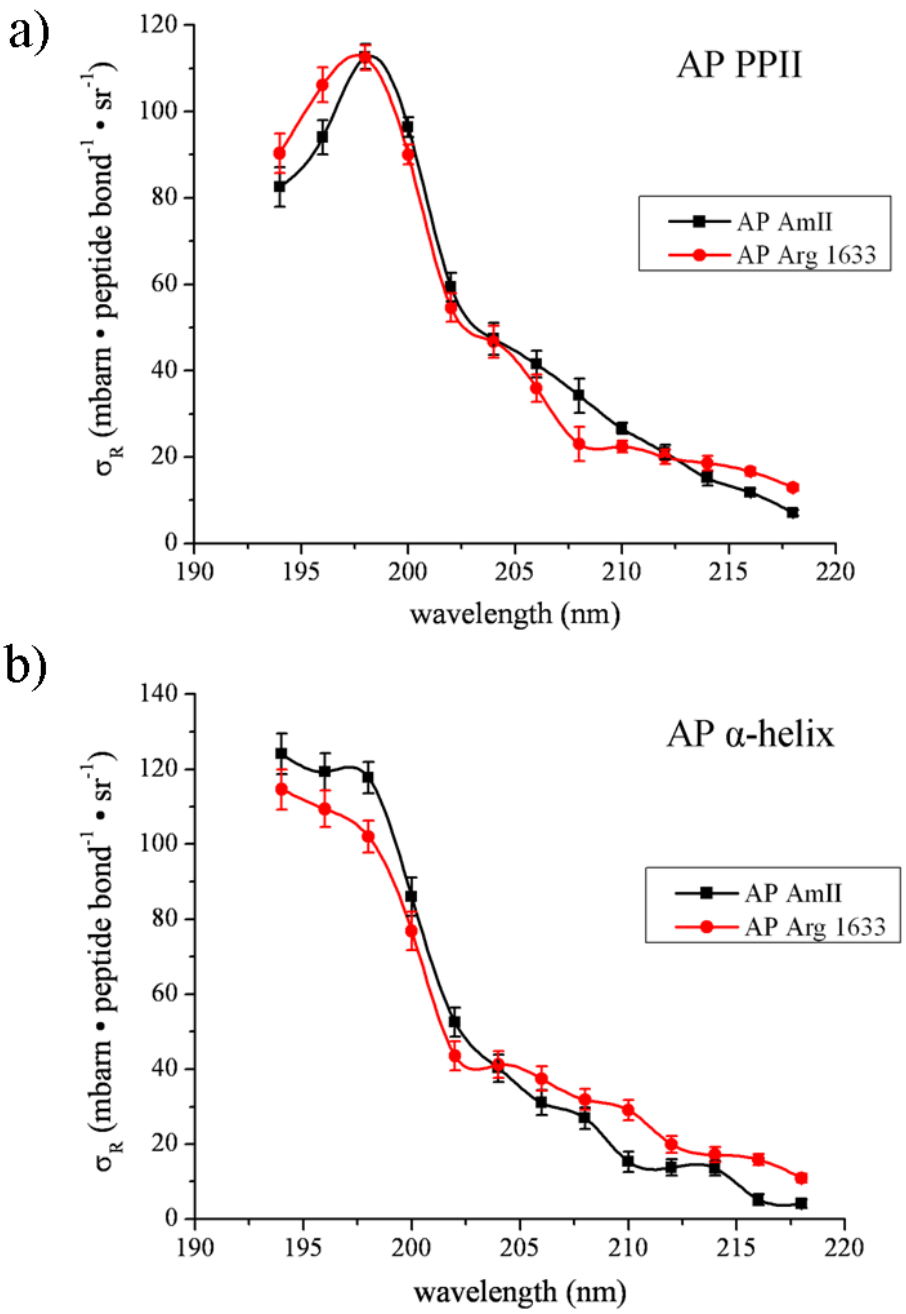

Figure 6.6 Overlapped (mbarn · peptide bond^{-1} · sr^{-1}) cross sections of (a) the AP AmII vibration and Arg 1633 cm^{-1} band in AP PPII-like conformation; (b) AP AmII vibration and Arg 1633 cm^{-1} band in AP α-helix conformation.

6.3.6 Depolarization Ratios

To further explore the electronic interactions between the AP peptide backbone and Arg side chains, we measured the dispersions of the UVRR depolarization ratios of the Arg bands in AP. The value of ρ can be used to signal the existence of electronic transitions underlying broad absorption bands. A resonance Raman depolarization ratio of $\rho = 0.33$ indicates that only a single, non-degenerate electronic transition contributes to the resonance Raman tensor elements.[24,25,31,32,49] When $\rho \neq 0.33$ the resonance enhancement arises from at least two electronic transitions contributing to the Raman tensor. If $\rho > 0.33$, and if there are only two diagonal elements of the Raman tensor, they must be of opposite sign. For $\rho < 0.33$, where only two diagonal elements contribute, the two diagonal elements must be of the same sign.[24,25,31,32,49] Thus, $\rho \neq 0.33$ requires the contribution of at least two electronic transitions.

In resonance Raman, $\rho = 0.75$ indicates a totally non-symmetric vibration, while $\rho = 0.125$ indicates two identical Raman tensor elements that could result from a doubly degenerate resonant electronic transition.[49]

For Arg in solution, with $\rho = 0.33$ the excitation wavelength independence of the depolarization ratios indicates that a single electronic transition dominates the enhancement for this excitation frequency region (Figure 6.7). This presumably is the lower energy ~ 200 nm $\pi \rightarrow \pi^*$ transition of the substituted guanidinium group. This alkyl guanidinium substitution breaks the symmetry of the normally degenerate guanidinium group $\pi \rightarrow \pi^*$ symmetry, splitting the transition.[40]

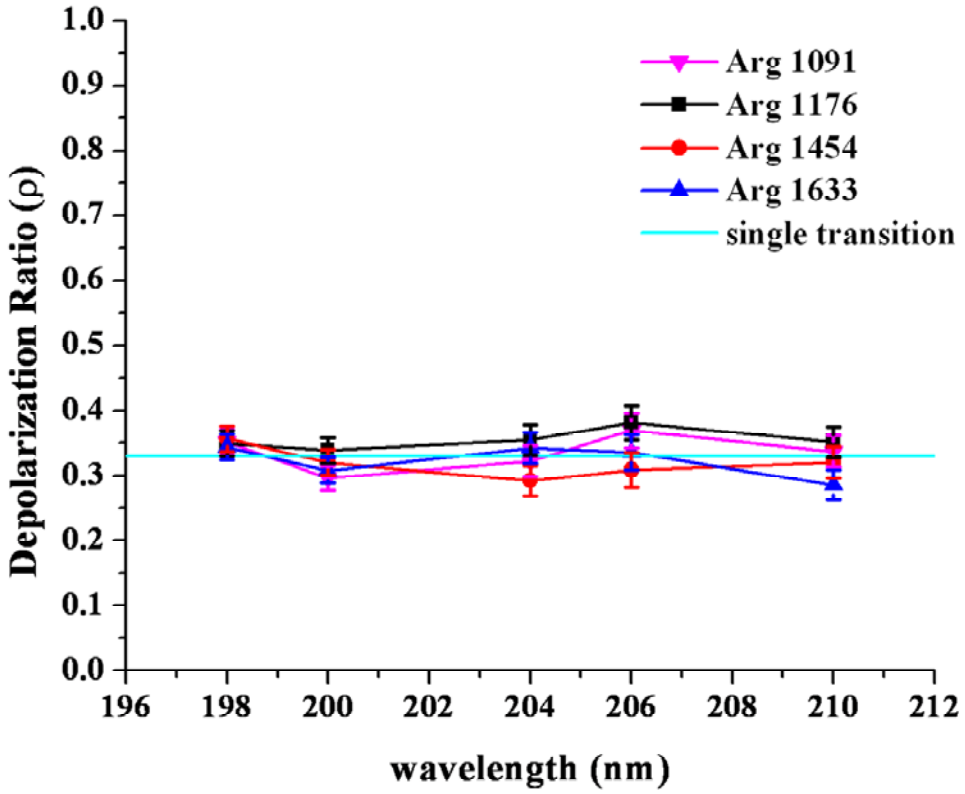

Figure 6.7 Depolarization ratios of Arg in water. These ρ = 0.33 values indicate the occurrence of a single electronic transition.

Figure 6.8 and Figure 6.9 show the depolarization ratios of the 1178, 1454, and 1633 cm^{-1} AP Arg bands, as well as two amide peptide bond vibrations of the $AmIII_3$ and AmII in the PPII-like (Figure 6.8) and the α-helix (Figure 6.9) conformations. For both conformations we find that the there is a complex dispersion of the depolarization ratio with variation in the excitation wavelength. For the PPII-like conformation (Figure 6.8) we see that although both the AP AmIII[3] and AmII vibrations have depolarization ratios above ρ = 0.33, the ratios do not go above ρ = 0.65, with four of the AmII ρ values at or below ρ = 0.33 (at λ_{ex} = 198, 206, 218 and 229 nm). The AP Arg vibrations however reach values of both ρ = 0.125 and ρ = 0.75 for several wavelengths.

These depolarization values indicate contributions of multiple electronic transitions. For the α-helix conformation (Figure 6.9), we see a similar depolarization ratio pattern for the Arg vibrations. Further, the UV resonance Raman excitation profiles and Raman depolarization ratios indicate that the electronic transitions of the Arg side chains in the peptide AP distinctly differ for those of pure Arg in solution. The results clearly show that the Arg side chains in AP undergo electronic interactions with the overlapping peptide bond $\pi \rightarrow \pi^*$ electronic transitions of the peptide backbone.

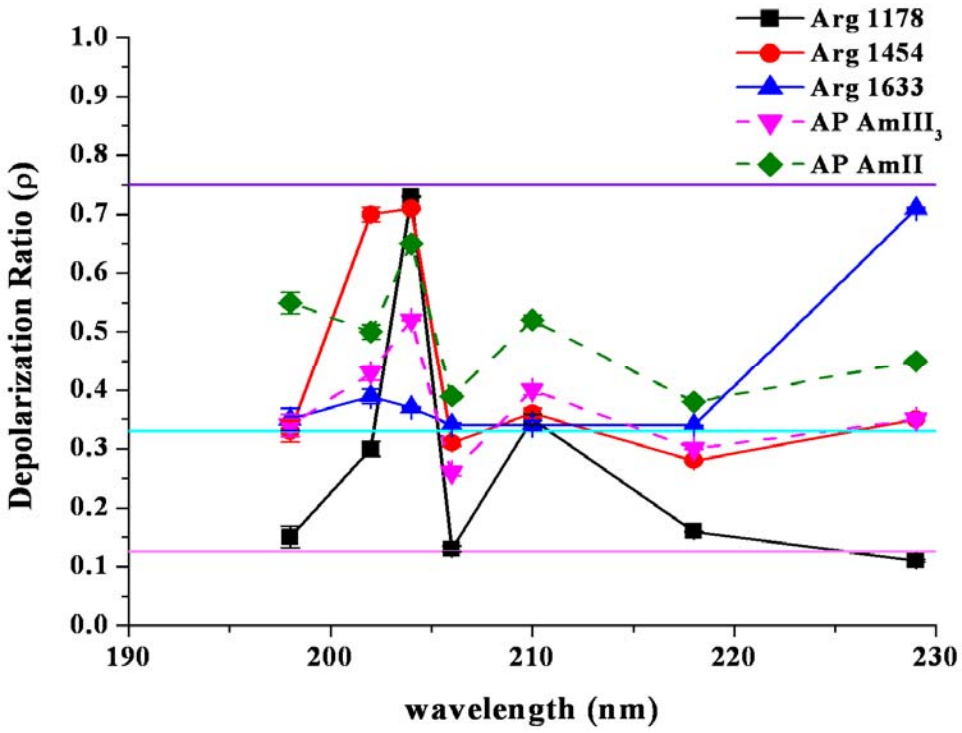

Figure 6.8 Depolarization ratios of the Arg vibrations and of two AP amide vibrations in the PPII-like conformation of AP. Single electronic transitions ρ = 0.33 (aqua), totally non-symmetric transitions ρ = 0.75 (purple) and totally symmetric transitions, ρ = 0.125 (pink) ρ values are indicated by solid lines.

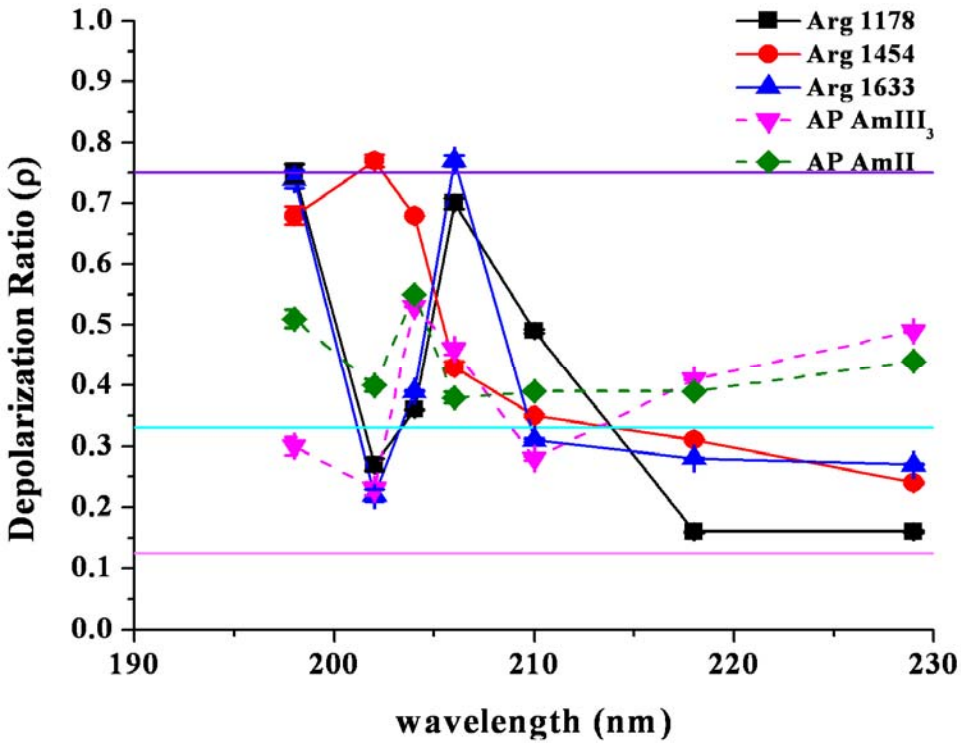

Figure 6.9 Depolarization ratios for the Arg vibrations and for two AP amide vibrations in the α-helix conformation of AP. Single electronic transitions ρ = 0.33 (aqua), totally non-symmetric transitions ρ = 0.75 (purple) and doubly degenerate symmetric transitions, ρ = 0.125 (pink) are indicated by solid lines.

6.4 CONCLUSIONS

We measured the UV resonance Raman excitation profiles and depolarization ratios for the Arg residues attached to the peptide AP and for Arg in solution. We find that the resonance Raman excitation profiles of the Arg in both the α-helix and PPII-like conformations of AP are essentially identical to those of the amide peptide bond bands. These excitation profiles are distinctly different from the excitation profiles of the monomeric Arg amino acid in solution. The excitation profiles similarities must result from interactions of the Arg side chain electronic transitions with the peptide backbone amide $\pi \rightarrow \pi^*$ transition.

We show that the depolarization ratios of the Arg monomer amino acid in water indicate that a single electronic transition dominates for excitation between 198 and 210 nm. In complete contradiction, we show the depolarization ratios of the Arg residues in AP indicate contributions of multiple electronic transitions.

This must be due to the mixing of higher electronic transitions with the peptide bond NV_1 $\pi \rightarrow \pi^*$ transition in AP and with the overlapping broad transition of the guanidinium group at ~ 204 nm. Excitation in this spectral region drives both electronic transitions. This may have important consequences on understanding electron transport in peptides and proteins.

6.5 ACKNOWLEDGMENTS

We thank Dr. Nataliya Myshakina, Zhenmin Hong, and Jonathan Wert for useful discussions. We also thank the NIH for funding, Grant #1R01EB009089.

6.6 REFERENCES

1. Barnes, D. G.; Rhodes, W. *J. Chim. Phys.* **1968**, *48*, 817.
2. Basch, H.; Robin, M. B.; Kuebler, N. A. *J. Chem. Phys.* **1967**, *47*, 1201.
3. Basch, H.; Robin, M. B.; Kuebler, N. A. *J. Chem. Phys.* **1968**, *49*, 5007.
4. Johnson, W. C., Jr.; Simpson, W. T. *J. Chem. Phys.* **1968**, *48*, 2168.
5. Kaya, K.; Nagakura, S. *Theor. Chim. Acta* **1967**, *7*, 117.
6. Moffitt, W. *Proc. Natl. Acad. Sci. U.S.* **1956**, *42*, 736.
7. Moffitt, W. *J. Chem. Phys.* **1956**, *25*, 467.
8. Nagakura, S. *Mol. Phys.* **1960**, *3*, 105.
9. Peterson, D. L.; Simpson, W. T. *J. Am. Chem. Soc.* **1957**, *79*, 2375.
10. Schellman, J. A.; Nielsen, E. B. *J. Phys. Chem.* **1967**, *71*, 3914.
11. Woody, R. W. *Monatsh. Chem.* **2005**, *136*, 347.
12. Woody, R. W. *J. Am. Chem. Soc.* **2009**, *131*, 8234.
13. Woody, R. W. *Chirality* **2010**, *22*, E22.
14. Asher, S. A.; Ianoul, A.; Mix, G.; Boyden, M. N.; Karnoup, A.; Diem, M.; Schweitzer-Stenner, R. *J. Am. Chem. Soc.* **2001**, *123*, 11775.
15. Asher, S. A.; Mikhonin, A. V.; Bykov, S. *J. Am. Chem. Soc.* **2004**, *126*, 8433.

16. Bykov, S.; Asher, S. *J Phys Chem B* **2010**, *114*, 6636.

17. Bykov, S. V.; Asher, S. A. *J. Phys. Chem. Lett.* **2010**, *1*, 269.

18. Dudik, J. M.; Johnson, C. R.; Asher, S. A. *J. Chem. Phys.* **1985**, *82*, 1732.

19. Lednev, I. K.; Karnoup, A. S.; Sparrow, M. C.; Asher, S. A. *J. Am. Chem. Soc.* **1999**, *121*, 8074.

20. Ma, L.; Ahmed, Z.; Mikhonin, A. V.; Asher, S. A. *J. Phys. Chem. B* **2007**, *111*, 7675.

21. Mikhonin, A. V.; Ahmed, Z.; Ianoul, A.; Asher, S. A. *J. Phys. Chem. B* **2004**, *108*, 19020.

22. Mikhonin, A. V.; Bykov, S. V.; Myshakina, N. S.; Asher, S. A. *J. Phys. Chem. B* **2006**, *110*, 1928.

23. Shafaat, H. S.; Sanchez, K. M.; Neary, T. J.; Kim, J. E. *J. Raman Spectrosc.* **2009**, *40*, 1060.

24. Sharma, B.; Asher, S. A. *J. Phys. Chem. B* **2010**, *114*, 6661.

25. Sharma, B.; Bykov Sergei, V.; Asher Sanford, A. *J Phys Chem B* **2008**, *112*, 11762.

26. Shi, Z.; Olson, C. A.; Bell, A. J., Jr.; Kallenbach, N. R. *Biopolymers* **2001**, *60*, 366.

27. Topilina, N. I.; Ermolenkov, V. V.; Sikirzhytski, V.; Higashiya, S.; Lednev, I. K.; Welch, J. T. *Biopolymers* **2010**, *93*, 607.

28. Xiong, K.; Asciutto, E. K.; Madura, J. D.; Asher, S. A. *Biochemistry* **2009**, *48*, 10818.

29. Asher, S. A.; Chi, Z.; Li, P. *J. Raman Spectrosc.* **1998**, *29*, 927.

30. Asher, S. A.; Ludwig, M.; Johnson, C. R. *J. Am. Chem. Soc.* **1986**, *108*, 3186.

31. Chen, X. G.; Asher, S. A.; Schweitzer-Stenner, R.; Mirkin, N. G.; Krimm, S. *J. Am. Chem. Soc.* **1995**, *117*, 2884.

32. Chen, X. G.; Li, P.; Holtz, J. S. W.; Chi, Z.; Pajcini, V.; Asher, S. A.; Kelly, L. A. *J. Am. Chem. Soc.* **1996**, *118*, 9716.

33. Chen, X. G.; Schweitzer-Stenner, R.; Krimm, S.; Mirkin, N. G.; Asher, S. A. *J. Am. Chem. Soc.* **1994**, *116*, 11141.

34. Cho, N.; Asher, S. A. *Biospectroscopy* **1996**, *2*, 71.

35. DeVito, V. L.; Cai, M. Z.; Asher, S. A.; Kehres, L. A.; Smith, K. M. *J. Phys. Chem.* **1992**, *96*, 6917.

36. Harmon, P. A.; Asher, S. A. *J. Chem. Phys.* **1990**, *93*, 3094.

37. Sweeney, J. A.; Asher, S. A. *J. Phys. Chem.* **1990**, *94*, 4784.

38. Balakrishnan, G.; Weeks, C. L.; Ibrahim, M.; Soldatova, A. V.; Spiro, T. G. *Curr. Opin. Struct. Biol.* **2008**, *18*, 623.

39. Bykov, S.; Lednev, I.; Ianoul, A.; Mikhonin, A.; Munro, C.; Asher, S. A. *Appl. Spectrosc.* **2005**, *59*, 1541.

40. Sension, R. J.; Hudson, B.; Callis, P. R. *J. Phys. Chem.* **1990**, *94*, 4015.

41. Garfinkel, D. *J. Am. Chem. Soc.* **1958**, *80*, 3827.

42. Hernandez, B.; Pfluger, F.; Derbel, N.; De Coninck, J.; Ghomi, M. *J. Phys. Chem. B* **2010**, *114*, 1077.

43. Hildebrandt, P.; Czernuszewicz, R. S.; Grygon, C. A.; Spiro, T. G. *J. Raman Spectrosc.* **1989**, *20*, 645.

44. Kalaiselvi, D.; Kumar, R. M.; Jayavel, R. *Cryst. Res. Technol.* **2008**, *43*, 851.

45. Lima, R. J. C.; Freire, P. T. C.; Sasaki, J. M.; Melo, F. E. A.; Mendes Filho, J. *J. Raman Spectrosc.* **2002**, *33*, 625.

46. Ludwig, M.; Asher, S. A. *Appl. Spectrosc.* **1988**, *42*, 1458.

47. Shriver, D. F.; Dunn, J. B. R. *Appl. Spectrosc.* **1974**, *28*, 319.

48. Hong, Z.; Wert, J.; Asher, S. A. in preparation.

49. Long, D. A. The Raman Effect: A Unified Treatment of the Theory of Raman Scattering by Molecules, John Wiley & Sons: New York, 2001.

7.0 DISSERTATION SUMMARY

We showed that UV resonance Raman excitation profiles and Raman depolarization ratios are incisive tools for examining electronic transitions that underlie the broad peptide absorption bands. We can use UVRR excitation profiles and Raman depolarization ratios to discover exciton splitting of the $\pi \rightarrow \pi^*$ electronic transition, charge transfer transitions, and interactions between the electronic transitions of the peptide backbone and the individual amino acid side chains in that peptide.

We measured the UVRR excitation profiles and Raman depolarization ratio dispersions for the α-helix and PPII-like conformations of a 21 amino acid poly-ala peptide, AP. The excitation maximum for the PPII-like conformation shows a peak at ~198 nm and α-helix like state shows shorter wavelength peak at ~194 nm. Both excitation profiles show a shoulder at ~205 nm. The Raman spectra and the depolarization ratios clearly signal that the 205-207 nm shoulders results from an underlying electronic transition similar to that of the shorter wavelength (~195 nm) $\pi \rightarrow \pi^*$ transitions. It is most likely that these transitions derive from the excitonically split amide $\pi \rightarrow \pi^*$ electronic transitions. The α-helical 207 nm transition is clearly the parallel component of the excitonically split pair. The establishment of the existence of these underlying transitions will help advance the understanding of protein and peptide backbone electronic transitions.

We also resolved the Raman excitation profiles of the pure α-helix, 3_{10} helix and π-bulge conformations. These excitation profiles along with that of the melted PPII-like conformation clearly indicate that different excitation wavelengths can be utilized to differentially enhance these different solution peptide conformations.

We measured the Raman excitation profiles and depolarization ratios for both Ala_3 and Ala_4. Both peptides show excitation profile maxima at 202 nm, which we assigned to charge transfer transitions of the carboxylate terminated peptide bonds clearly observed in the pH absorption difference spectra.

We correlated the $AmIII_3$ band Raman frequencies to the Ψ angle of both Ala_3 and Ala_4 to determine the conformational distribution of these peptides. We found Type II turns, as well as PPII-like and 2.5_1 helix-like conformations in solution. We assigned the charge transfer transition at 202 nm to the three β-type structures deconvoluted from the Raman spectra.

The $Ala_4 - Ala_3$ Raman difference spectra allowed us to separately study the interior peptide bond of Ala_4, which is found to be predominantly PPII-like. We were also able to resolve the COO^- vibration for both Ala_3 and Ala_4. We find a shoulder in the Ala_4 excitation profile at 206 nm, but are unable at this time to definitively assign its origin.

Finally, we measured the UV resonance Raman excitation profiles and depolarization ratios for the Arg residues in AP and for Arg amino acid in solution. We found that the resonance Raman excitation profiles of the Arg residues in both the α-helix and PPII-like conformations of AP show similar excitation profiles as the whole peptide, and are distinctly different from the excitation profiles of the Arg amino acid in solution. We attributed this similarity in excitation profiles to result from the interaction of the Arg side chain with the

peptide backbone, allowing for interactions between the electronic transitions of the peptide bond with the electronic transitions of the guanidinium group of Arg.

We showed that the depolarization ratios of the monomeric Arg amino acid in water indicate that a single electronic transition occurs over the wavelength range examined. The depolarization ratios of the Arg residues in AP, however, indicate that multiple electronic transitions occur. This is believed to be due to the mixing of higher electronic transitions with the peptide bond $\pi \rightarrow \pi^*$ transition in AP, along with a broad underlying transition of the guanidinium group at ~ 204 nm.

The combined results from the UV resonance Raman excitation profiles and the Raman depolarization ratios support the hypothesis that the Arg residues in AP interact with the peptide backbone, and that the electronic transitions of the guanidinium group of Arg interact with the dominant peptide bond $\pi \rightarrow \pi^*$ transition, resulting in the similar peptide bond and Arg residue excitation profiles for AP and depolarization ratios which indicate multiple transitions.

8.0 FUTURE WORK

As stated in the introduction, UV resonance Raman (UVRR) spectroscopy is a powerful technique for interrogating peptide and protein secondary structure. In this work, it has been shown that UVRR excitation profiles and depolarization ratios provide insight not only about secondary structure, but also about the electronic transitions that occur within the peptide backbone. Although we have discovered underlying electronic transitions, there is still much that is not well understood.

After more than 50 years of experimental and theoretical research on the electronic structure of peptide bonds, the classical model of peptide bond electronic transitions remains the standard. The classical model refers to only the major peptide bond electronic transitions (NV_1, NV_2, $n\rightarrow\pi^*$) and rarely addresses any possible additional transitions. We have developed a sensitive methodology for identifying the presence of additional transitions of the peptide backbone; we are, however, unable to determine from where these transitions arise due to a lack of available information.

At the present time, electronic structure theory is not incisive enough to determine the excited state of large polyatomic molecules. One of the most recent electronic structure studies available examines the $n\rightarrow\pi^*$ and the $\pi\rightarrow\pi^*$ in the small peptide model N-methylacetamide (NMA), and then applies exciton Hamiltonian of NMA to larger proteins. As of today, electronic structure theory remains unable to accurately model even the $n\rightarrow\pi^*$ and the $\pi\rightarrow\pi^*$

electronic transitions in large polyatomic molecules. If it is not possible to accurately model these well-studied electronic transitions, the progress on identifying additional electronic transitions may be limited. Some of the responsibility for this lack of theoretical knowledge falls on experimentalists who have not characterized these additional transitions. This results in a lack of data available for the development of the electronic structure theory. Theoreticians currently do not have the tools available that would allow them to solve these multi-electron systems.

The proposed future work will provide more experimental data about the peptide backbone electronic transitions. These data along with the results presented in this work should provide electronic structure theoreticians with the groundwork necessary to develop models that can answer questions such as, what are these transitions and where do they come from.

8.1.1 Peptide Bond Interactions

The data presented in this work indicates that the peptide bond electronic excited states are far more complex than previously thought. Future work should continue to explore and determine the electronic transitions that occur in short peptides and that underlie the stronger NV_1, NV_2, and $n \rightarrow \pi^*$ electronic transitions.

For short peptides (less than 5 residues), it has been shown that besides the classical transitions, there is a dominating charge transfer transition, which results from the transfer of an electron from the carboxylate nonbonding orbital to the amide π^* orbital. The charge transfer transition may confound studies that look for the presence of additional transitions in the peptide. To isolate these additional transitions, the UV resonance Raman excitation profiles and Raman depolarization ratios for small peptides with both the N- and C-terminal ends blocked should be

measured. This will effectively remove the charge transfer from the carboxylate to the peptide bond, allowing other underlying transitions to dominate the spectra.

8.1.2 Side Chains

Peptide bond electronic transitions are also able to interact with the electronic transitions of adjacent amino acid side chains present in the peptide. To eliminate spectral effects due to interaction of the peptide bond transitions with side chain transitions, the UV resonance Raman excitation profiles and depolarization ratios for $(Gly)_3$ and $(Gly)_4$, which have no side chains, should be measured. These peptides should also be examined with blocked terminal ends. The blocked Gly peptides will be the simplest peptide models available, essentially allowing for the peptide bond electronic transitions to be characterized. The unblocked peptides will include the peptide bond transitions, along with charge transfer transitions. Using spectral subtraction, if the spectrum of the blocked peptide is subtracted from the spectrum of the unblocked peptide, information will be gained about the charge transfer transitions, along with any additional transitions. These studies will give insight into the role of side chains in the complexity of the peptide bond interactions, as well as help to identify underlying transitions in the simplest peptide models.

Further studies should explore the interactions between the side chain and peptide bond electronic transitions by examining amino acids with chromophoric side chains similar to Arg. The resonance Raman excitation profiles and Raman depolarization ratios of AP-like peptides, with the Arg residues replaced by amino acids such as his, asn, gln, and lys, should be measured. Also measurements of the excitation profiles and depolarization ratios of the monomeric amino

acids should be made. By comparing the peptide and amino acid Raman excitation profiles and depolarization ratios, it will be possible to determine the impact of the interaction of the side chain electronic transitions with the peptide bond electronic transitions.

8.1.3 Proteins

The UVRR spectra of proteins can sometimes be difficult to interpret because the secondary structures which compose the protein result in spectra with overlapping bands. The observed UVRR spectrum of a protein can be viewed as the sum of the spectra of the resonantly enhanced individual secondary structures.

We have shown that different secondary structures, such as α-helix and β-type (i.e., PPII) conformations, have distinctly different excitation profiles and maxima. A methodology can be developed using the unique excitation profiles of each secondary structure to identify the various secondary structures present in a protein UVRR spectrum, including major structures such as α-helix and PPII and minor structures such as 3_{10}-helix, π-bulge, turns, etc. Spectral subtraction of different excitation Raman spectra of a protein can be used to isolate individual structures, and deconvolute additional species.